Aus dem Institut für Schlaganfall- und Demenzforschung

Klinikum der Universität München, Großhadern

Vorstand: Prof Dr. Martin Dichgans

Modulation of Neuroinflammation and Stroke Outcome by the COP9 Signalosome

Dissertation

zum Erwerb des Doctor of Philosophy (Ph.D.)

an der Medizinischen Fakultät der

Ludwig-Maximilians-Universität München

vorgelegt von

Yuan Tian

aus

Beijing, China

Jahr

2022

Mit Genehmigung der Medizinischen Fakultät
der Ludwig-Maximilians-Universität zu München

First evaluator:	Prof. Dr. Jürgen Bernhagen
Second evaluator:	Prof. Dr. Christian Behrends Priv.
Third evaluator:	Doz. Dr. Johann Szecsi
Fourth evaluator:	Prof. Dr. Dr. Markus Kipp
Dean:	Prof. Dr. med. Thomas Gudermann
Datum der Verteidigung:	08.09.2022

LMU LUDWIG-MAXIMILIANS-UNIVERSITÄT MÜNCHEN

Dekanat Medizinische Fakultät
Promotionsbüro

Affidavit

Tian, Yuan

Surname, first name

Address

I hereby declare, that the submitted thesis entitled

Modulation of Neuroinflammation and Stroke Outcome by the COP9 Signalosome

is my own work. I have only used the sources indicated and have not made unauthorised use of services of a third party. Where the work of others has been quoted or reproduced, the source is always given.

I further declare that the submitted thesis or parts thereof have not been presented as part of an examination degree to any other university.

ISD, Munich, 08.09.2022
Place, Date

Yuan Tian
Signature doctoral candidate

LMU LUDWIG-MAXIMILIANS-UNIVERSITÄT MÜNCHEN

Dekanat Medizinische Fakultät
Promotionsbüro

Confimation of congruency between printed and electronic version of the doctoral thesis

Doctoral Candidate: Yuan Tian

Address:

I hereby declare that the electronic version of the submitted thesis, entitled

Modulation of Neuroinflammation and Stroke Outcome by the COP9 Signalosome

is congruent with the printed version both in content and format.

ISD, Munich, 08.09.2022 — Yuan Tian

Place, Date — Signature doctoral candidate

Congruency of submitted versions — Date: 18.03.2022

Table of Contents

List of Figures

Abbreviations

Aβ	Amyloidβ
ABCA1	ATP-binding cassette transporters A1
AD	Alzheimer's disease
AJ	Adherens junction
AMPA	α-Amino-3-hydroxy-5-methyl-4-isoxazolepropionic acid
APC/C	Anaphase promoting complex/cyclosome
APP	Amyloid precursor protein
APS	Ammonium persulfate
Arg1	Arginase 1
BBB	Blood brain barrier
BMDM	Bone marrow-derived macrophages
BMI	Body mass index
Brn-2	Brain-2
BSA	Bovine serum albumin
c-FLIP	cellular FLICE-inhibitory protein
CAND1	Cullin-associated NEDD8-dissociated protein 1

CCL2	CC-chemokine ligand 2
CGN	Cerebellar granule neuron
Chil3/Ym1	Chitinase-like 3
CNS	Central nervous system
COP9	Constitutive photomorphogenesis 9
COPS, CSN	COP9 signalosome
CRL	Cullin-RING ligase
Ct	Cycle time
CUL	Cullin
DAB	3,3'-diaminobenzidine
DCN1	Defective in cullin neddlylation protein 1
DCs	Dendritic cells
DIV	Day in vitro
DMEM	Dulbecco's modified eagle medium
DMSO	Dimethylsulfoxide
DPBS	Dulbecco's phosphate-buffered saline
DTT	DL-Dithiothreitol
ECAR	Extracellular acidification rate
EDTA	Ethylenediaminetetraacetic acid
EGFR	Epidermal growth factor receptor

eIF3	Translation initiation factor 3
ER	Endoplasmic reticulum
ET(A)R	Endothelin type A receptor
FBS	Fetal bovine serum
HAoECs	Human aortic endothelial cells
HBSS	Hank's balanced salt solution
hCMEC/D3	Human cerebral microvascular endothelial
HDL	High-density lipoproteins
HF	Heart failure
HUVECs	Human umbilical vein endothelial cells
IFN-β	Interferon-β
IHC	Immunohistochemistry
IHD	Ischemic heart disease
IKK	IkappaB kinase
IL	Interleukin
iNOS	Inducible nitric oxide synthase
IPC	Ischemic preconditioning
IRF	Interferon regulatory transcription factor
ITPK1	Inositol 1, 3, 4-trisphosphate 5/6-kinase
JNK	c-Jun N-terminal kinase

LDL	Ligh-density lipoproteins
LPS	Lipopolysaccharide
LY	Lucifer yellow
Maf	Musculo-aponeurotic fibrosarcoma
MAoECs	Mouse aortic endothelial cells
MAPK	Mitogen-activated protein kinase
MEM	Minimum Eesential medium
MI	Myocardial infarction
MIF	Macrophage migration inhibitory factor
MLKL	Mixed lineage kinase-like
MMP	Matrix metalloproteinase
MPN	Mov34-and-Pad1p N-terminal
NAE1	NEDD8-activating enzyme
NEDD8	Neural precursor cell-expressed developmentally downregulated 8
NF-κB	Nuclear factor-κB
NF1	Neurofibromatosis 1
NMDA	N-methyl-D-aspartate
OBSC	Organotypic brain slice culture
OGD	Oxygen glucose deprivation
OxLDL	Oxidized low-density lipoprotein

P/S	Penicillin/Streptomycin
PAGE	polyacrylamide gel electrophoresis
PBS	Phosphate-buffered saline
PCI/PINT	Proteasome-COP9-initiation factor 3
PD	Parkinson's disease
PFA	Paraformaldehyd
PI	Propidium iodide
PI3Ks	Phosphoinositide 3-kinases
PKM2	Pyruvate kinase M2
PVDF	Polyvinylidene difluoride
RA	Rheumatoid arthritis
Rbf	retinoblastoma binding factor
RIPK	Receptor-interacting protein kinase
ROS	Reactive oxygen species
RPMI	Roswell Park Memorial Institute
RPMI1640	Roswell ark Memorial Institute 1640
scRNA	Single cell RNAseq
SD	Standard deviation
SDS	Sodium dodecyl sulfate
SKP	S phase kinase-associated protein

SOCS3	Suppressor of cytokine signaling 3
SP	Sodium pyruvate
SRA	Scavenger receptor class A
t-SNE	t-Distributed stochastic neighbor-embedding analysis
TEER	Transendothelial electrical resistance
TEMED	Tetramethylethylenediamine
TGF-β	Transforming the growth factor-beta
TJ	Tight junction
tMCAo	Transient middle cerebral artery occlusion
TNF-α	Tumor necrosis factor alpha
TRAIL	TNF-related apoptosis-inducing ligand
TREM2	Triggering receptor expressed on myeloid cell-2
Tris	Tris-(hydroxymethyl)-aminomethan
Tris-HCl	Tris-hydrochloride
UBE2M	Ubiquitin conjugating enzyme E2 M
USP	Ubiquitin-specific protease
VE-cadherin	Vascular endothelial cadherin
VEGF	Vascular endothelial growth factor
WM	White matter

List of Publications

- Milic J, **Tian Y** & Bernhagen J (2019). Role of the COP9 Signalosome (CSN) in cardiovascular diseases. *Biomolecules*, 9(6), 217.
- Wang S, El Bounkari O, Zan C, **Tian Y**, Gao Y & Bernhagen J. (2021). Classical chemokines, atypical chemokines, and MIF proteins in ischemic stroke: effects, mechanisms and roles in conditoning. *Cond Med*, 4, 39-57.
- Hofmann E, Soppert J, Ruhl T, Gousopoulos E, Gerra S, Storti G, **Tian Y**, Brandhofer M, Schweizer R, Song S Y, Lindenblatt N, Pallua N, Bernhagen J & Kim B S (2021). The role of macrophage migration inhibitory factor in the proliferation of adipose-derived stem cells under hypoxia. *Front Physiol*, 12, 1068.
- Taş K, Volta BD, Lindner C, El Bounkari O, Hille K, **Tian Y**, Puig-Bosch X, Ballmann M, Hornung S, Ortner M, Prem S, Meier L, Rammes G, Haslbeck M, Weber C, Megens RTA, Bernhagen J, Kapurniotu A (2022). Designed peptides as nanomolar cross-amyloid inhibitors acting via supramolecular nanofiber co-assembly. *Nat Commun*, 2022 Aug 25;13(1):5004.

1 Introduction

1.1 Stroke: A Brief Outline

Stroke constitutes one of the most common reasons for death or people suffering from disabilities [1]. Strokes can be broadly categorized into two groups, ischemic stroke and hemorrhagic stroke. Among them, ischemic stroke makes up 80% of all strokes which are caused by arterial occlusion in the brain, spinal cord or retina. Hemorrhagic stroke happens when a blood vessel is ruptured, which leads to bleeding in the brain. The symptoms of stroke vary from person to person, but the most typical symptom starts from abrupt weakness of face, arm or leg, most of the time on one side of the body. Other signs or symptoms include confusion, difficulty speaking, understanding, seeing, walking, dizziness, severe headache, and fainting [2].

In 2019, the number of incident and prevalent cases of stroke was 12.2 million and 101 million, respectively, causing a total of approximately 6.55 million deaths and 143 million disabilities due to stroke worldwide. Stroke ranks as the second-leading cause of death, and this accounts for 11.6% of total amount death. Among the deaths, stroke has a global epidemiology which with up to 86% of deaths in countries with low and low to middle income economies. Despite the advanced genetic discoveries of stroke in clinical studies, which have already been helping with risk prediction and prevention over the past few years [3], the number of incident strokes has gone up by 70% compared to 1990 [4]. In addition, the costs of stroke have increased significantly as well. From 2003 to 2017, the total care costs of stroke patients for 25 countries forming the European

Union rose from 34 billion euros to 55 billion euros [5]. The enhanced number of cases was not only due to the population growth and aging, but also associated with a variety of risk factors, including high body mass index (BMI), increased fasting plasma glucose and blood pressure, ambient particulate matter air pollution exposure, low physical activity, as well as excessive alcohol consumption [6].

The therapeutic goal for cerebral ischemia is to rapidly restore the blood flow and minimize the infarct volume of cerebral tissue. Currently, the only employed therapy of acute ischemic stroke is reperfusion using thrombolysis, including intravenous tissue plasminogen activator or/and endovascular thrombectomy, but both are highly time-critical. In addition, intravenous alteplase (rtPA) is the only pharmaceutical agent which has been approved and it has a limitation due to short administration time window, with a maximum of up to 4.5 h after symptom onset [7]. Therefore, due to the few treatments and narrow therapeutic time window, merely a minority of stroke patients is able to receive these treatment options, and the majority of stroke patients presents with a poor outcome with different neurological symptoms such as paralysis, dementia and depression. This leads to both an enormous medical and economic burden. Although over a thousand of translation stroke studies that focused on neuroprotection has been conducted in the past a few decades, only 10% of the compounds reached clinical trials. Notably, the small amount of drugs which have been used in the clinical trials did improve the stroke patients' condition [8]. Taken together, novel strategies for treatment of post-stroke pathophysiology are urgently needed.

1.1.1 Neuroinflammation and Inflammation After Stroke

Neuroinflammation is an underlying and associated component of multiple acute and chronic central nervous system (CNS) disorders, such as stroke, Parkinson's disease (PD) and Alzheimer's disease (AD). This inflammation is regulated by a great number of factors including cytokines, chemokines, as well as reactive oxygen species [9], and these factors are mainly produced by the brain resident cells including microglia,

astrocytes, microvascular endothelial cells as well as peripherally derived macrophages. There are, however, both positive and negative aspects of the consequences of mediator-driven neuroinflammation. For instance, a sequence of events usually occurs during the inflammatory process. As a result, sometimes inflammation leads to the recruitment of immune cells and tissue damage, but in other cases, inflammation may lead to tissue repair and adaption. In this thesis, the focus is on neuroinflammation and inflammation after stroke.

Brain injury following transient or permanent ischemic stroke is caused by a series of cellular and molecular events induced by the cerebral blood flow impairment. Neurons are more vulnerable than other cells, and in the ischemic core, they become dysfunctional and die rapidly due to the reduction of oxygen and glucose. The main mechanism of the cell death is that neurons cannot generate enough ATP for the ionic pumps to maintain the ionic gradient across the membrane, leading to K^+ loss and membrane depolarization [10]. During this period, Na^+ and Ca^{2+} cytoplasmic accumulation encourages glutamate release, which causes organelle swelling and membrane integrity loss, at the end leading to necrotic cell death. In the peri-infarct, the major event is the extracellular accumulation of glutamate, which overstimulates post synaptic excitatory receptors, including α-Amino-3-hydroxy-5-methyl-4-isoxazolepropionic acid (AMPA), N-methyl-D-aspartate (also known as NMDA) and kainite, allowing influx of Ca^{2+} [10, 11]. Consequently, massive Ca^{2+} activates proteolytic enzymes and forces free-radicals and cytochrome C from mitochondria. This cellular toxicity triggers necrosis and/or apoptosis, and these injured neurons secret a “danger signal” which activates microglia and other immune cells. Overall, these events take place in the acute phase of ischemic stroke which only ends after several minutes or even hours [10].

Following the acute phase of stroke, within the sub-acute phase, immunity and inflammation are the key drivers for the ischemic brain pathobiology. Inflammation exerts a deleterious role on promoting neuronal cell damage by releasing immune

mediators or beneficial effects on providing the anti-inflammatory signals to help with wound repairing. It has been widely studied that inflammation is initiated along with the pathological features of ischemic stroke including necrotic cells, impaired tissues, as well as reactive species (ROS), which can activate resident microglia, astrocytes, and attract leukocytes infiltration [12]. Moreover, the inflammatory response is a multiphasic cascade including an early phase of inflammation and a chronic inflammation (Figure1). In order to understanding the role of this multiphasic immune response after stroke, two of the important cells, microglia and endothelial cells, will be introduced in the following chapters.

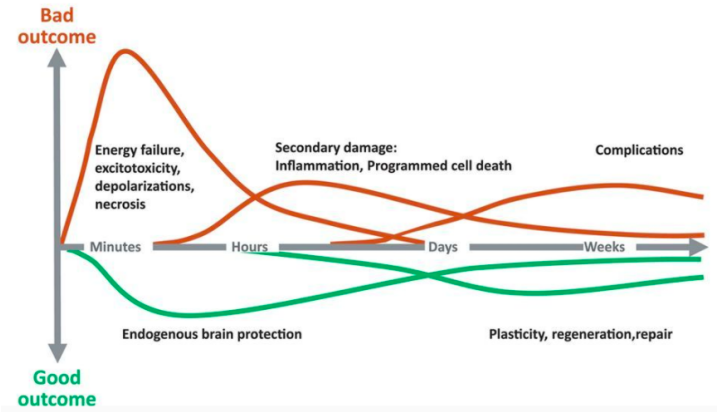

Figure 1: Inflammation after stroke. Cascade of destructive and protective or restorative mechanisms in stroke. Figure taken from [13].

1.1.2 Microglia

When there are stimuli acting on the brain, the “resident macrophages” microglial cells are considered to be the forefront defense of the innate immune system [14]. Representing about 10% of the total cell population in the brain [15], microglia develop from the embryonic yolk sac around embryonic day 8.5, and increase continuously in the first two postnatal weeks, which identifies microglia as a distinct population from other macrophages [16]. In homeostatic state, microglia with a ramified morphology are all over the CNS while constantly surveying the brain environment. Once a certain cue such as pathogen invasion or brain injury is recognized, microglia rapidly switch

to an activated state. They transform their morphology from the ramified state into an ameboid phenotype and migrate towards injured tissue [17]. For an illustration of changing microglia morphology, please refer to figure 2. Other profiles of microglia are simultaneously changing along with the altering morphology, and this provide microglia with a crucial role of the communication between the nervous and immune system. For instance, microglia become the "activated" state upon an infection, and they rapidly alter their transcriptional profile while secreting pro-inflammatory cytokines and chemokines, including tumor necrosis factor alpha (TNF-α), Interleukin (IL) 6, IL-1β and CC-chemokine ligand 2 (CCL2) [18]. These cytokines and chemokines can further promote leukocytes recruitment and interfere with the brain [19]. In addition, these cytoskeletal and profile alterations allow microglia to increase the phagocytosis activity and migrate to the injured tissue [20]. Besides exaggerating in inflammation, microglia activation can offer protection from brain damage to the brain in the different stages of inflammation, and the dual function of microglia activation under inflammation after ischemic stroke will be discussed in more detail below.

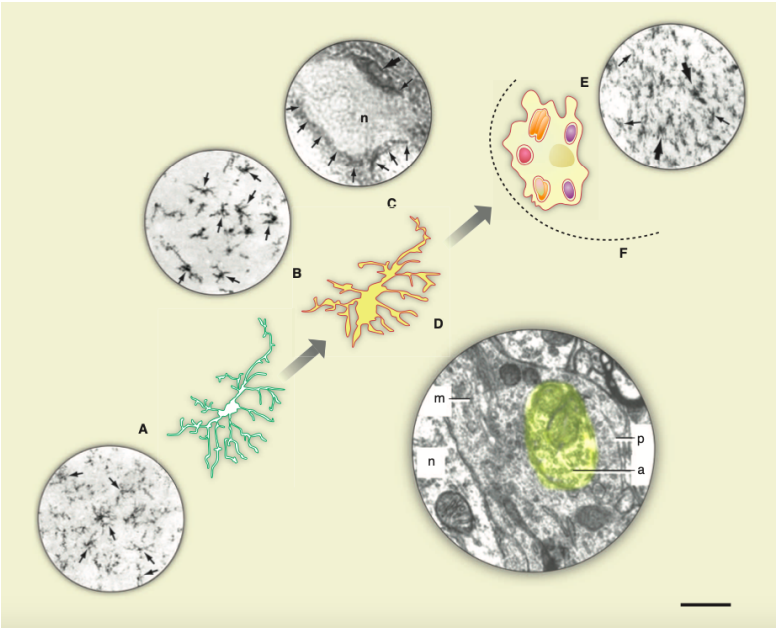

Figure 2: Cascade of microglia activation associated with plastic phenotypes associated. (A) Ramified microglia (resting microglia) in normal rat facial nucleus. (B) Activated microglia which are still of ramified type within 24 h of facial nerve axotomy. (C,D) Microglia are next to a regenerating facial motor neuron 4 days after facial nerve axotomy. (E, F) Ameboid phenotype and phagocytic microglia. Figure taken from [17].

As discussed in the last paragraph, microglia are one of the first-line responders to the injury. They rapidly migrate to the injured brain site after ischemia. The activation status of microglia has frequently been described in terms of a binary classification as pro-inflammatory (M1, also called classically activated) and predominantly anti-inflammatory (M2, also named alternatively activated) types. The concept of M1-type microglia is by high expression of pro-inflammatory regulators including inducible nitric oxide synthase (iNOS), IL-1β, IL-6, TNF-α and matrix metalloproteinase (MMP) [21, 22]. Of note, theses mediators trigger neuronal apoptosis and degrade extracellular matrix resulting in blood brain barrier (BBB) disruption. Conversely, M2-type microglia are characterized by their high production of chitinase-like 3 (Chil3, also named Ym1), IL-10, vascular endothelial growth factor (VEGF), transforming the growth factor-beta (TGF-β), as well as arginase 1 (Arg1), [23].

However, this classification of microglia is over-simplified, as microglia appear at numerous overlapping states during the post-stroke phase, so the binary classification is not adequate. Within 6h of transient middle cerebral artery occlusion (tMCAo) in the mouse brain, CD11b, a constitutive marker of microglia and macrophages has been detected increased and remained elevated for at least till 7 days [24]. In the ischemic core, CD32, CD16, M1 markers are upregulated from day 3 on until at least day 14, whereas, CD206, Arg1, M2 markers have appeared at day 1-3 and peaked by day 3-5 [25]. In the peri-infarct area, microglial activation, proliferation and migration persist weeks after MCAo. Additionally, a marker of active phagocytosis, CD68 expressed in both ramified and globular microglia is confirmed in the peri-infarct area at the early time but increased in the core at 7 days [24, 26]. These microglia with a high phagocytic capacity can contribute to cell debris removal and this process is essential to resolve the inflammation and promote the remodeling [27, 28]. Nevertheless, this phagocytosis in the poststroke phase remains controversial, wherein phagocytosis contributes to the pathology by attacking the viable neurons [29].

1.1.3 Blood Brain Barrier

Another key event in the development of neurological dysfunction after stroke is the disruption of the BBB. As a part of the neurovascular unit formed by microvascular endothelial cells, accompanied by astrocytes, pericytes and other cells, the BBB is a unique physical and biochemical barrier that controls the molecules, ions, fluid and cells between the CNS and the blood [30]. For an illustration of BBB composition, please refer to figure 3. This gatekeeper role of the brain is accomplished by the BBB tight junction integrity, and following stroke, the increase of tight junction permeability can lead to vasogenic edema, hemorrhagic transformation and worsened outcome [31, 32]. Additionally, the factors contributing to BBB breakdown in ischemic stroke are various, including MMPs, VEGF, proinflammatory cytokines and chemokines, adhesion molecules, nitrosative stress, as well as oxidative stress [33]. Interestingly, MMPs were found to be significantly increased in ischemic stroke in both clinical studies and experimental studies [34, 35]. Moreover, MMP activation can be triggered by multiple factors in stroke, and this includes TNF-α inducing MMP-9 and MMP-3, hypoxia-inducible factor-1α (HIF-1α) promoting MMP2 [36, 37]. Further evidence for MMPs regulating BBB comes from some studies showing that inhibition of MMP benefits neurovascular remodeling from cerebral ischemia [38, 39]. However the mechanism is not fully investigated yet.

To understand the BBB dysfunction in pathologies, a hallmark of BBB disruption, the alternative expression of tight junction (TJ) protein complexes has been revealed. TJ protein occludin degradation was detected in the ischemic cerebral microvessels due to the mediation by MMP2, and claudin-5 improper localisation was associated with caveolin-1 [40, 41]. The reduced expression of zonula occludens (ZO-1) has also been identified under oxygen-glucose deprivation/reoxygenation (OGD/RO) [42, 43]. Another important component of the cell-cell interactions, adherens junctions (AJ), are formed by cadherins and associated proteins are able to be linked into actin filaments [44]. In this case, endothelial cells presents vascular endothelial cadherin (VE-cadherin), and the deletion of VE-cadherin in mice can directly induce the disruption of TJ proteins

via mis-localised Rac and activated atypical protein kinase C [45]. Therefore, regulating TJ and AJ proteins is a critical strategy for the BBB dysfunction in ischemic stroke.

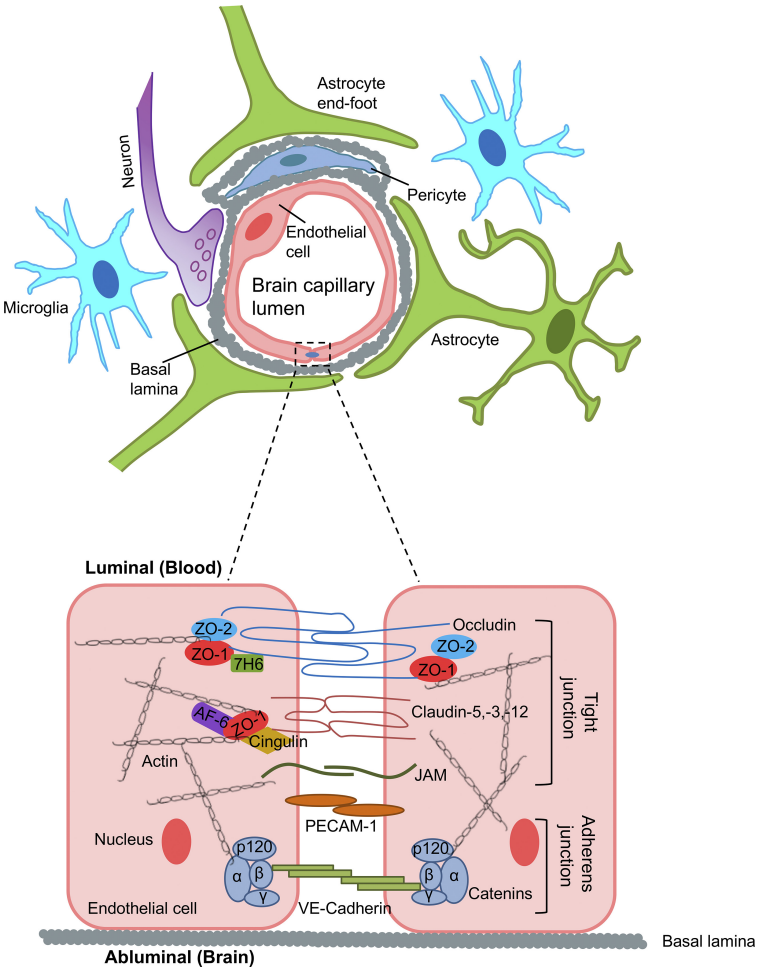

Figure 3: Schematic diagram of the BBB. The BBB is formed by the microvascular endothelial cells which contact with astrocytes, pericytes, neurons, perivascular microglia and basal lamina. The permeability of the BBB is controlled by the tight junction and adherent junction proteins which form a matrix of multiprotein complexes interacted to the actin cytoskeleton. Figure taken from [33].

1.2 The COP9 Signalosome: A Short Introduction

The constitutive photomorphogenesis 9 (COP9) signalosome (CSN, also known as COPS) is a conserved multiprotein complex. In 1992, CSN was identified and characterized as a light-regulatory locus of Arabidopsis (4). It was termed COP9 since its mutation results in similar phenotypes as COP1 which functions as a repressor of dark-grown

growth pattern [46]. Following the first purification of the COP9 signalosome from cauliflower, mammalian CSN was purified as an ortholog of Arabidopsis COP9 complex or signalosome [47–50]. The core CSN in mammals is constituted by eight subunits designated CSN1 to CSN8 and enumerated by their molecular size, the largest, CSN1 and the smallest, CSN8 [51]. The CSN has architectural homologies to the 19S lid sub-complex of the 26S proteasome lid and the translation initiation factor 3 (eIF3). Six subunits (CSN1, CSN2, CSN3, CSN4, CSN7 and CSN8) include a proteasome-COP9-initiation factor 3 (PCI) domain (also known as PINT) and two subunits (CSN5 and CSN6) contain a Mov34-and-Pad1p N-terminal (MPN) domain [52, 53]. Since CSN was discovered in Arabidopsis, it was identified in all different eukaryotes. In this chapter, the biochemical function and the structure of the CSN is discussed in detail.

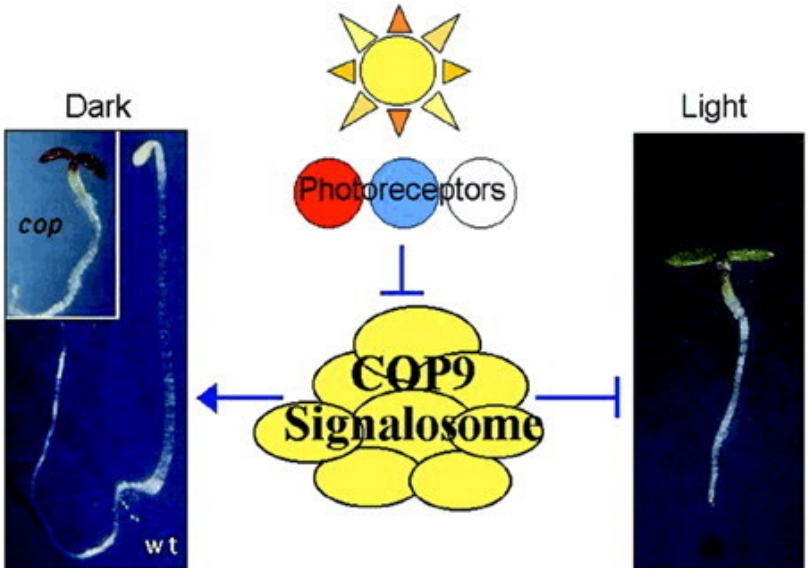

Figure 4: Model of CSN activity in photomorphogenesis. The CSN inhibits photomorphogenesis resulting in dark-grown growth patterns, when the light signals are absent (wt, left). Figure taken from [54].

1.2.1 Cullin-RING Ligase Regulation by the CSN

Protein stability is mediated under the control of the ubiquitin-proteasome system, which is a three step cascade of enzyme (E1-E3) for marking substrates by ubiquitylation in order to be degraded by proteasome. In mammals, Cullin-RING ligases (CRLs) compose

the largest multi-unit E3 ligase family with more than 200 acknowledged members which are responsible for over 20% of protein degradation through the ubiquitin system [55]. They are usually composed of four parts: one of the elongate C-shaped cullin protein which functions as the scaffold, an embedded RING finger protein which recruits E2 binding and offers ubiquitin transfer activity, an adaptor and a substrate receptor which is able to recognize the specific ubiquitylation target [56]. Hence, CRLs are able to engage substrates and catalyze ubiquitin transfer. To date, eight cullins (CUL1, CUL2, CUL3, CUL4A, CUL4B CUL5, CUL7, CUL9) have been identified to form eight subfamilies of CRLs. Additionally, anaphase promoting complex/cyclosome (APC/C) is a cullin related ligase which is also included in the CRL subfamily due to its ligases using a RING protein to recognize E2 [57]. Each of the CRLs (except CRL7 and 9) encompasses different substrate receptors, and each substrate receptor contains approximately 30-70 proteins [58]. For instance, CRL1, also known as the S phase kinase-associated protein 1 (SKP1) – cullin1 (CUL1) – F-box protein (SCF) complexes contains at least 60 F-box proteins for recruitment of its own substrates [59]. Moreover the multiple F-box proteins pairing with their specific substrates lead to varied assortment of biological processes such as the cell cycle control, and the inflammatory response such as $SCF^{\beta\text{-TRCP1/ I}\kappa\text{B-}\alpha}$, $SCF^{Skp2/p27}$ [60].

In some early studies, the CSN was shown to interact with the SCF E3 ligase complex via regulating cullin1 [61–63]. Both biochemical and structural reports have revealed that CRL activity is modified by reversible cycles from neddylation to deneddylation, in which neddylation is the attachment of the ubiquitin-like protein named neural precursor cell-expressed developmentally downregulated 8 (NEDD8) to cullins [64]. Similar to ubiquitination, NEDD8 is covalently bound to cullins in the conserved C-terminal region by a successive enzymatic cascade: NEDD8 activating enzyme (NAE1), conjugating enzyme (UBC12, UBE2F), and ligase (including RBX1/2, DCN1) [65–68]. Later, the CSN has been clarified to provide the catalytic function to neddylated CRLs, which is called deneddylation. Deneddylation means that CSN cleaves the NEDD8 conjugating

from CRLs, resulting in inactivated CRLs [69]. Although this metalloprotease activity is centered in CSN subunit 5, cullin deneddylation can only occur when the CSN holocomplex is fully assembled [48]. Moreover, deneddylation of cullins by the CSN is a condition of cullin-associated NEDD8-dissociated protein 1 (CAND1) binding to unneddylated state cullin which provides substrate receptors exchanging [70]. For an illustration of the CSN activity and CAND1 cycle, I am referring to figure 5.

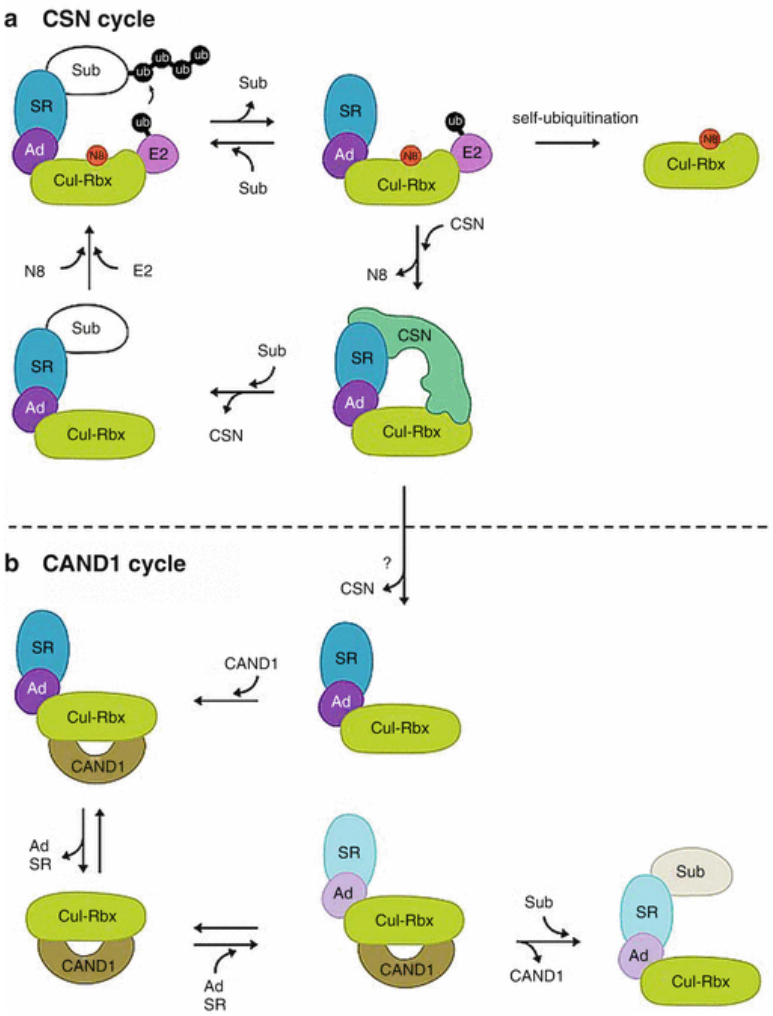

Figure 5: Schematic diagram of the CSN and CAND1 activity. (A) An assembled CRL: E2 ubiquitin (Ub)-conjugating enzyme and a substrate binding CRL (upper left). After the substrate consumption, there are two upcoming options for the CRL complex, either auto-ubiquitinate and degrade the substrate receptor (upper right) or recruit the CSN to be deneddylated (lower). (B) Following the CSN cycle, CAND1 can bind cullin to exchange the adaptor and substrate receptor resulting in the formation of a new CRL. Figure taken from [71].

1.2.2 The Crystal Structure of the Human CSN Complex

Human CSN holo-complex (350 kDa) crystal structure was resolved at 3.8 Å resolution in 2014 [72]. The CSN molecular architecture was confirmed by earlier results including biochemical studies, electron microscopy analysis and modelling assays [73, 74]. It has been revealed to have two organisational centres and described as a horseshoe-shaped ring and a large bundle. The ring is created by its PCI domains while the bundle is constructed by the carboxy-terminal-α-helices of every subunit. The MPN domain-comprising CSN5 and its dimerisation partner, CSN6, are convolutedly located at the centre of the large bundle.

To deneddylate CRL, CSN4 senses the binding and delivers the information to CSN5 under the CSN6 assistance. At the same time, the structure of CSN has also been said to resemble a wide opened hand, across which a small box is located and on the top thrones a tomato [75]. As a hand, the five fingers are digits (CSN1, 2, 4, 7, 3 and 8) and where they projecting from is the palm. On the palm where a box is sitting and at the top of this platform is the tomato composed of CSN5 and CSN6. The discovery of the structure also revealed that the CSN isopeptidase is inhibited by glutamate residue 104 and separately through the CSN4-CSN6 interface in the circumstances of non-CRL binding. This suggests that the inactive state of CSN5 is only extricated by binding to neddylated CRL, which elicits CSN4 sensing and CSN5-CSN6 dimer towards the CRL, eventually remodeling CSN5 and deneddylation. Thus, the convoluted substrate-induced CSN activity unified CSN from eIF3 and 19S lid, although they share a similar structure [72].

Later, this conformational change of the CSN complex during deneddylation was clarified by a structural and kinetic analysis [76]. For example, in the CSN binding $SCF^{kp2/Cks1}$ complex, these two parts interact with each other through a high affinity, active complex of CSN2, CSN4 and RING domain of Rbx1. This causes NEDD8 to be deconjugated and the active site of CSN5 to be rearranged, thus enabling a dynamic deneddylation-disassemble cycle [76]. Likewise, the crystal structure of CSN in complex

with neddylated CRL4A was solved at 6.4 Å resolution , and this revealed three pairs of interactions: CSN2-CUL4, CSN2-Rbx1-CSN4 and CSN1-DDB1. [77]. The latest molecular structures of CSN-CRL2∼NEDD8 complex and its deneddylated CSN-CRL2 counterpart have been described by the cryo-electron microscopy and mass spectrometry analyses [78]. For an illustration of CSN mediated deneddylation, please be referred to figure 6.

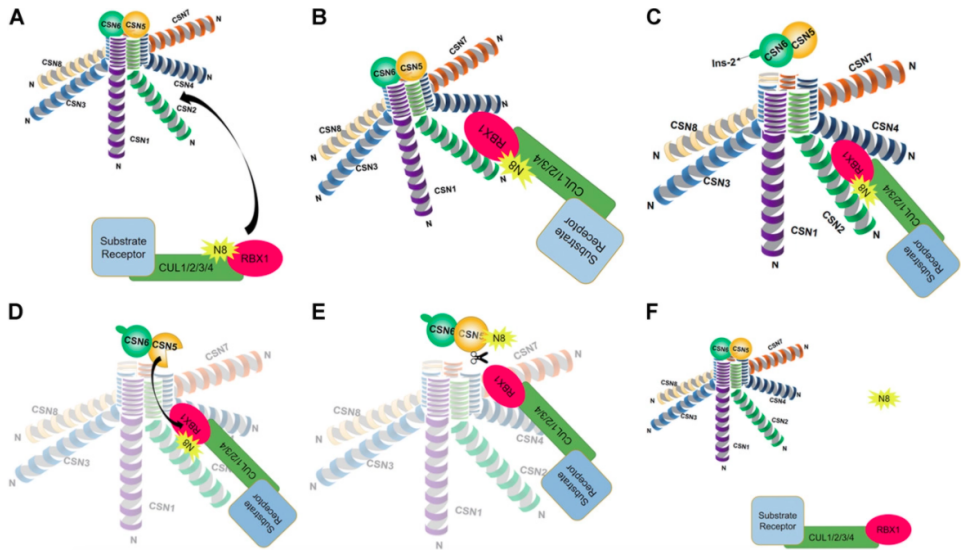

Figure 6: Shematic representation of a dynamic CSN-regulated CRL.(A) CSN is approacher a neddylated CRL. (B) Rbx1 is fastened between CSN2 and CSN4. (C) CSN5-CSN6 heterodimer was dislocated from the holo-complex and moved in the direction of CRL, because the conformational changes make CSN6 deconjugated from the CSN. (D) CSN5 active site is opened by the NEED8. (E) CSN5/CSN deneddylates the CRL. (F) NEDD8 is removed from CRL. Figure taken from [79].

1.2.3 CSN Regulates Deubiquitinylation and Protein Kinase Activity

Apart from deneddylation activity, CSN also controls CRL activity through its association deubiquitinases and protein kinases. CSN associated deubiquitinases can antagonize excessive ubiquitylation of CRLs and their substrates [80–82]. For example, the CSN modulates the nuclear factor-κB (NF-κB) signalling pathway not only through the $SCF^{\beta\text{-TRCP/I}\kappa\text{B-}\alpha}$, but CSN is also in cooperation with the ubiquitin-specific protease (USP) 15 and 48, which are mediators involved in the NF-κB signalling pathway [83]. For

an illustration of how CSN partners with USP15 and USP48 mediates NF-κB, please be referred to figure 6. USP15 protects SCFβ-TRCP1 meaning that USP15 deubiquitylates IκB-α enhancing its re-accumulation and resulting in the termination of NF-κB [83, 84]. The CSN recruits USP15 leading to the protection of IκB-α from degradation [81, 85]. In the late response of the NF-κB activation, upon TNF stimulation, CSN-associated USP48 stabilises the P65 (also known as RelA) in the nucleus by counteracting CRL2 ^{SOCS1} activity [82, 86, 87].

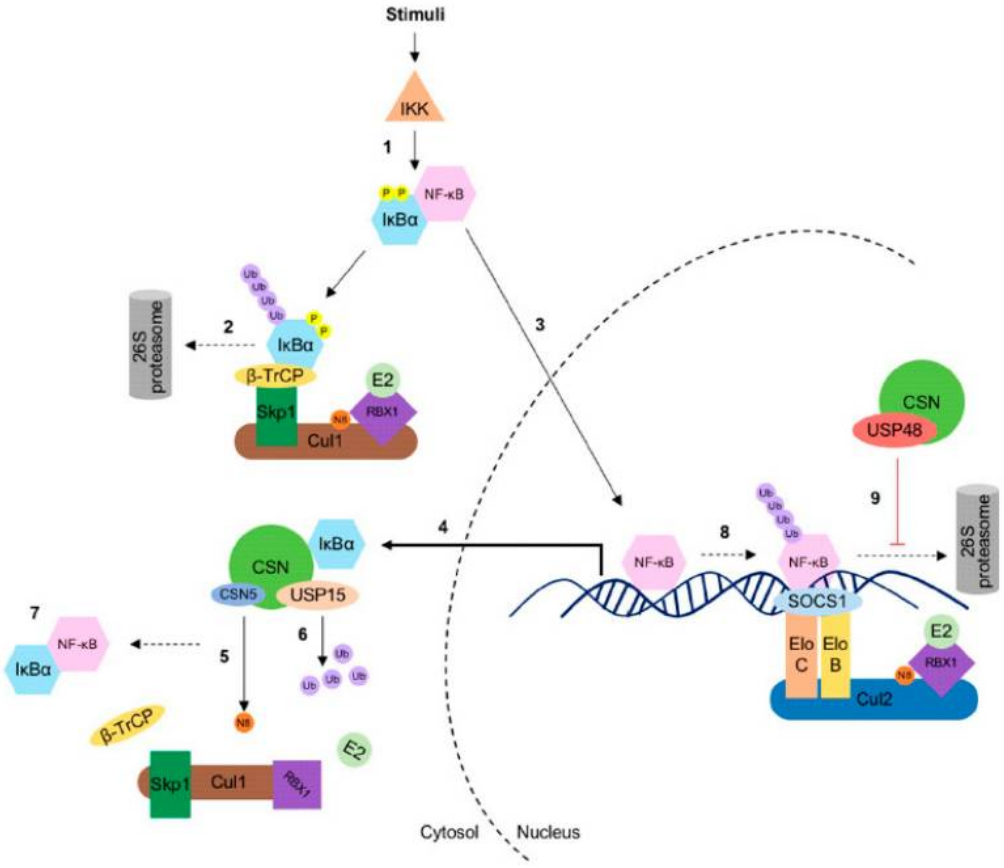

Figure 7: Schematic representation of CSN regulates NF-κB. (1, 2) In the canonical NF-κB, phosphorylation of IκBα is completed by the activated IκB kinase (IKK) complex. Phosphorylated IκBα is subsequently recognised by CRL1β and consequently degraded by the 26S proteasome. (3, 4) Once IκBα is degraded, NF-κB is then released and allowed to translocate into the nucleus. Target genes, including IκB-α, are activated, and de novo synthesised IκB-α is allowed to be phosphorylated again. (5) The CSN deneddylate CRL1β-TrCP. (6, 7) CSN-associated USP15 elevates IκBα stabilisation and re-accumulation, thus terminating NF-κB signalling. (8, 9) In a late response of NF-κB pathway, the CRL2 triggers degradation of the nuclear NF-κB (RelA) at the chromatin. Nevertheless, transcription regulation depending on NF-κB can be maintained by the activity of CSN interacting with USP48. Figure extracted from [88]

As mentioned in the last paragraph, another biochemical activity of CSN is its association with protein kinases. Already the first purification of human CSN has shown that CSN5/Jab1 has kinase activity. CSN5 phosphorylates IκB-α, c-Jun (Ser63/Ser73) and the NF-κB precursor, p105 [50]. Moreover, CSN-specific phosphorylation targeting p53 triggers p53 destabilization [89]. This phosphorylation of c-Jun and p53 by inositol 1, 3, 4-trisphosphate 5/6-kinase (ITPK1) interacting with CSN1 and CSN5 is inhibited by curcumin, a dietary pigment with various pharmacological functions, such as antioxidant, antimicrobial properties as well as anti-inflammation [62, 90, 91]. In addition to ITPK1, CSN also interacts with other protein kinases, including casein kinase II (CK-2), protein kinase ataxia-talangiectasia mutated (ATM), protein kinase D (PKD) and protein kinase B (AKT) [92–95]. Together, CSN is serving as a connecting port for kinases and some of its subunits can also be phosphorylated [50].

1.3 The CSN in Cardiovascular Diseases

Part of this chapter contains our previous paper (as a co-author), which was published in Biomolecules (DOI: 10.3390/biom9060217). All the containing subchapters are marked with '#'.

1.3.1 The CSN in Atherosclerosis#

Atherosclerosis is the crucial underlying reason of heart disease and cerebral ischemia, and it is characterized by a chronic inflammation, slowly developing lesion formation as well as luminal narrowing of arteries [96]. It is initially triggered by endothelial cell dysfunction and structural alterations such as collagen, elastin and changing proteoglycans [97]. The atherosclerotic lesion consists of cholesterol, oxidized lipids and low-density lipoproteins, and infiltration of T cells, monocyte-derived macrophage-like foam cells and smooth muscle cells [98].

For much of the last century, atherosclerosis was considered to be a cholesterol

storage disease [99]. Over the last quarter century, atherosclerosis was redefined as an inflammatory process, rather than a mere deposition of fatty material and thrombotic debris [100]. Since then, many cell types were found to drive the inflammation in atherosclerotic processes including monocyte-derived macrophages, endothelial cells, smooth muscle cells, as well as T cells, and untill now, CSN has been reported to regulate different signalling and transcriptional pathways in all of the above cell types.

The vascular endothelium reacts to the inflammation by synthesizing and metabolizing products including cytokines as well as adhesion molecules. On this point, endothelial dysfunction constitutes a risk factor of pathogens for multiple vascular diseases, including atherosclerosis [101]. Previous studies from our lab demonstrated that the expression levels of CSN5, CSN1, and CSN8 increased in specimens of human atherosclerotic plaques and the endothelial cell layer upon atheroprogression [85]. Furthermore, CSN5 knockdown led to an elevated NF-κB activity, resulting in enhanced atherogenic vascular adhesion molecules and chemokines which trigger the accumulation of monocytes onto stimulated endothelial cells. The link between CSN5 and NF-κB is not limited to CUL1 neddylation, neither is it to IkappaB kinase (IKK). The IKK's phosphorylate not only IκB, high-molecular complexes could be formed by IKK and CSN. This was shown by the co-immunoprecipitation assay, and dissociation of the complex occurs under inflammation in human umbilical vein endothelial cells (HUVECs) [85, 102]. On the contrary, mimicking hyperactivity of CSN5 by using MLN4924 completely abrogated the inflammatory response via downregulation of NF-κB activity by elevated levels of phosphor-IκB-α, and upregulation of HIF-1α in HUVECs, mouse aortic endothelial cells (MAoECs) and human aortic endothelial cells (HAoECs) [103]. Additionally, the endothelin receptor/ligand system is another important mediator controlling the endothelial permeability in atherosclerosis (Fan et al., 2000). Jab1/CSN5 was first identified to interact with endothelin type A receptor (ET(A)R) by yeast two-hybrid screening of the human heart cDNA library. Jab1/CSN5 knockdown increased levels of ET(A)R and ET-1-induced phosphorylation of ERK1/2 in HEK293T cells, whereas

Jab1/CSN5 overexpression decreased ET(A)R and ET(B)R levels through its binding to ETR promotes ET(A)R and ET(B)R ubiquitination as well as degradation [104]. However, the precise mechanism of how Jab1/CSN5 leads to the receptor degradation remains unclear.

Myeloid cells participate in all three stages of atherosclerosis from the initiation to progression of plaques and until the complications [105]. Monocytes are myeloid leukocytes which originally derive from hematopoietic stem cells and pro-genitor cells in the bone marrow. After proliferation and differentiation, they circulate into the blood and patrol the vascular endothelium [106–108]. Elevated population of BM monocytes in atherogenesis has been reported in hyper-cholesterolemic rodents [109], and monopoiesis in extramedullary organs including the spleen induced by hypercholesterolemia has also been revealed in more recent studies [108, 110]. Accumulation of monocytes from spleen and bone marrow into the growing atherosclerotic lesions depends on plenty of chemokines and their receptor interactions, such as CXCR2/CXCL1, CX3CR1/CX3CL1 (fractalkine), CCR2/CCL2 (MCP-1), and CCR5/CCL2/CCL5 interactions [111–113]. Moreover, an atypical chemokine, macrophage migration inhibitory factor (MIF) as an inflammatory cytokine has also been identified to promote recruitment of atherogenic monocyte via CXCR2 non-cognate engagement [114]. Notably, intracellular MIF directly binding to CSN5 (Jab1) mediates the JNK/AP-1 activity as well as p27 dependent cell-cycle regulation [115]. Additionally, autocrine MIF activity promoting cancer cell survival through the Akt pathway is also controlled by CSN5 [116]. Later, we have further reported that MIF secretion is enhanced significantly in the Csn5-myeloid cell deficient atherogenic mice ($Csn5^{\Delta myeloid/Apoe^{-/-}}$), which is in correlation with CSN5 controlling MIF resulting in decreased monocyte recruitment [103]. Expanding on this finding, we further investigated myeloid *Csn5* deficiency in atherosclerosis, and observed that mice lacking myeloid *Csn5* lead to exacerbated atherosclerotic lesion and higher levels of inflammatory cytokines production [103]. Similar to the endothelial cells as described in the last paragraph, MLN4924 abrogates pro-inflammatory cytokines

and chemokines expression in bone marrow-derived macrophages (BMDMs) [103]. Taken together, this suggests an athero-protective function of CSN5. In terms of the mechanism, these atherogenic cytokines and chemokines are mediated through the NF-κB signalling pathway, and we have shown that BMDM from Csn5$^{\Delta myeloid/Apoe\text{-}/\text{-}}$ mice showed lower expression levels of IκB-α under both resting state and post-stimulation by TNF-α or lipopolysaccharide (LPS) condition. In addition, *Csn5* depletion in BMDM resulted in upregulated NF-κB p65 DNA binding function and MLN4924 conversely blunted this NF-κB p65 transcriptional activity under inflammatory stimulation [103]. However, inflammation in atherosclerotic lesion is not solely controlled by the NF-κB signalling, and anti-inflammatory effects by the CSN is not only mitigated through the NF-κB pathway. The HIF-1α expression is detected in numerous different types of cells during the development of atherosclerosis, and it has also been reported to positively or negatively regulate atherosclerotic progression [117–120]. CSN5 stabilized HIF-1α levels, and Csn5 depletion attenuated HIF-1α transcriptional activity as well as HIF-1α targeting genes Edn1 and Opn1 [121–123]. Overall, these studies highlight the potential pharmacological capacity of CSN in atherosclerosis.

A prerequisite and initiating event in the atherosclerotic lesion development is the foam cells, also called cholesterol-laden macrophages, which form upon massive internalisation of modified lipoproteins by macrophages [124–126]. Scavenger receptors, including ATP-binding cassette (ABC) transporters and scavenger receptor class A (SRA) are pivotal regulators for the cholesterol homeostasis of macrophages between influx and efflux [126, 127]. For example, ABC transporters A1 (ABCA1) promotes cholesterol efflux to lipid-free apoA-1, thereby forming high-density lipoproteins (HDL), and this implies that ABCA1 acts as an athero-protective mediator by preventing foam cell formation [128]. Moreover, blocking degradation of ABCA1 protein enhances the capacity of cholesterol efflux, and thus delays atherosclerotic plaque progression [129]. Additionally, ABCA1 was reported to become susceptible to proteasomal degradation depended on ubiquitination under hypercholesterolemia [130, 131], and this leads ABCA1

turnover to the function of CSN. CSN2 and CSN5 were coprecipitated with ABCA1 when HEK293 cells were transfected with ABCA1 expression vectors, and overexpression of CSN2 decreased ubiquitinylated ABCA1 [132]. Later, CSN3 and ABCA1 were detected together in a complex and colocalised in human non-lesion coronary arteris. But once ABCA1 is phosphorylated, CSN3 and ABCA1 dissociate from each other, and this curtail cholesterol efflux as well as amplify foam cell formation [133].These studies suggest an anti-atherogenic role of CSN by controlling ubiquitinylation and deubiquitinylation of ABCA1 [132, 133].

1.3.2 The CSN in Cardiac Proteotoxicity[#]

The ubiquitin proteasome system (UPS) and autophagy are two distinct pathways, but together compose the two major proteolytic systems in eukaryotic cells. Activation or impairment of UPS has been found in numerous cardiac diseases [134–137], and the role of CSN in the heart by regulating the ubiquitination of cardiotoxic proteins as well as autophagy function in cardiotoxicity is emerging. Previous studies have demonstrated that CSN is essential for embryonic development, and the global genetic deletion of CSN subunits leads to embryonic lethality [138–141]. Therefore, cell-specific deletion of CSN with and without inducible gene targeting systems have become the approaches to study the role of CSN in mice. So far, CSN3, CSN5 and CSN8 have been investigated in cardiomyocytes [142–144]. A perinatal cardiomyocyte-restricted *Csn8* knock-out mouse model has been established by Cre-LoxP system in 2011, and *Csn8* deletion in cardiomyocytes resulted in the impairment of CSN holo-complex and UPS activity in the heart. Consequently, these mice suffered cardiac hypertrophy which swiftly resulted in heart failure and premature death. This was discovered to be because of massive cardiomyocyte necrosis and enhanced infiltration of leukocytes rather than apoptosis. This study suggested that CSN8/CSN acts an indispensable role in the heart by regulating misfolded cardiac proteins and the survival of cardiomyocytes through the UPS pathway [144]. This concept was confirmed in another study which used CSN8 hypomorphism mice, and myocardial neddylated cullins were increased while overall ubuquitination

rate was reduced by CSN8 hypomorphism [145]. When introduced to these mice, to circumvent the premature cell death caused by the 80% reduction of *Csn8*, CryAB^{R120G} cardiomyocyte-restricted transgenic mice were crossed together. CryABR^{R120G} transgenic mice were found to have a pathogenic feature of cardiac proteotoxicity in desmin-related cardiomyopathy, and this is due to the mutation of $\alpha\beta$-crystallin (CryAB^{R120G}), a bona fide misfolded cytosolic protein ,which causes the aggregation of intra-sarcoplasmic desmin-positive aberrant protein and disruption of the cytoskeletal network [146, 147]. Applying this crossed mouse model, $\alpha\beta$-crystallin is upregulated in the heart, and CSN8 hypomorphism exacerbated CryAB^{R120G}-induced cardiomyopathy as well as shortened the lifespan of CryAB^{R120G} mice. This was accompanied by increased protein aggregation, enhanced neddylated proteins, reduced levels of LC3-II and decreased ubiquitinated proteins in the heart. Collectively, this study provides evidence that CSN8 enforces the misfolded cytosolic proteins ubiquitination and degradation in cardiomyocytes, as well as protects from cardiac proteotoxicity [145].

CSN8 also plays a role in the autophagosomal function in the heart. Mice with *Csn8* depletion in the cardiomyocytes and cardiomyocyte-restricted knockout of the *Csn8* were observed with increased LC3-II and p62 protein levels [148]. Autophagosome accumulation was due to defective autophagosome removal, and this occurred before UPS impairment in *Csn8*-deficient mouse hearts. A decreased Rab7 level and cardiomyocyte necrosis accompanied with autophagosome accumulation in cardiomyocyte-restricted *Csn8* knockout hearts. Additionally, Rab7 knockdown disrupts autophagosome maturation and aggravated cell death in cultured cardiomyocytes [148]. Moreover, *Csn8* conditionally knockout in the cardiomyocytes accumulated the neddylated protein, elevated ubiquitinated protein and stabilized a proteasome surrogate substrate, and led to upregulate oxidized proteins and necrotic cardiomyocytes, as well as dilated cardiomyopathy [149]. In order to investigate the mechanism between *Csn8*-deficiency and cardiomyocyte necrosis, an analysis of the murine myocardial transcriptome was conducted, and the receptors of CRL substrates, autophagy, chromatin remodeling

genes, endocytosis, cell death, as well as vesicle trafficking were compared between homozygous myocardial-restricted *Csn8*-deficient mice, corresponding heterozygous mice and control mice [150]. Together with another study that was from the same group as well, they have revealed that CSN8 is crucial for the transcriptional regulation of CRL substrate receptors [150, 151]. The role of CSN in controlling gene-expression patterns is consistent with the study of Drosophila, which concluded that CSN4 serves as a transcriptional repressor in Drosophila development, leading to achronic gene expression in mutants of the *Csn*[152]. In addition, another study showed that CSN4 co-occupies the retinoblastoma tumor suppressor protein and its family target gene promoter with retinoblastoma binding factor (Rbf) 1 and 2, and mediates transcription via chromatin remodeling [153].

1.3.3 The CSN in Heart Failure[#]

Heart failure (HF) is caused by structural or functional cardiac abnormalities of ventricles, displaying symptomatic left ventricle dysfunction [154]. Multiple conditions can develop HF, including systemic disease, different cardiac conditions, such as myocardial infarction (MI)/ischemic heart disease (IHD), and some hereditary defects [155]. Mechanisms governing the development of HF are mainly due to the dysfunction of the UPS, the autophagic lysosomal pathway and the molecular signalling pathways to cardiomyocyte apoptosis and necrosis [156–159]. In the last subchapter, we have discussed that CSN is a key regulator in the UPS and autophagy, and mice with cardiomyocyte-restricted knockout of *Csn8* develop UPS and autophagic malfunction. A recent study also revealed an indispensable role of CSN in suppressing cardiomyocyte necroptosis [160]. In cardiomyocyte-restricted knockout of *Csn8* mice, factors of the necroptotic pathway, including receptor-interacting protein kinase (RIPK) 1 and 3, protein carbonyls, mixed lineage kinase-like (MLKL), caspase8, BCL2 and superoxide anions were increased more noticeably than in the control mice, but cleaved caspase8 was decreased. Moreover, cardiomyocyte-restricted knockout of Csn8 mice treated with a RIPK1 ki-

nase inhibitor showed less necrosis and longer median lifespan by using Evans blue dye uptake assay. Together, these results indicate that Csn8/CSN impairment causes RIPK1-RIPK3 dependent, and CSN suppresses RIPK1-RIPK3-mediated cardiomyocyte necroptosis [160].

To regulate the heart physiology response, the main role of CSN is regulating cardiotoxic proteins degradation through the CRL route as well as autophagy, but protein-protein interactions between CSN subunits and myocyte signalling pathways is also important to the heart. CSN5/Jab1 was reported to bind to the II-III linker of the α1c subunit of the L-type calcium channel by using a yeast two-hybrid system [161]. The interaction between CSN5 and the α1c subunit were proved by the co-immunoprecipitation assay in the rat heart, and colocalisation was observed at the sarcolemmal membranes and transverse tubules in cardiac myocytes. Functional assay suggested that CSN5 is involved in the mediation of cardiac L-type Ca^{2+} channels [161]. Moreover, the family of Ca^{2+} release channels is the key mediator for the calcium efflux through sarcoplasmic reticulum, and the dysregulation of these channels may result in HF and sudden cardiac death [162]. In addition to the Ca^{2+} channel, integrin signalling pathways are also necessary to the fibrotic responses in cardiac pathologies, preventing cardiac stress, hypertrophy, as well as fibrosis [163]. Notably, CSN5 was capable of binding to β2 integrin and integrin α-V to regulate c-Jun transcriptional function [164, 165]. Integrin signalling engaging CSN5 is a prerequisite for CSN5's nuclear translocation, and integrin α-V prolongs MMP1 production through CSN5 in fibroblasts [165]. Another CSN subunit has also been involved in facilitating the connection between the nucleus and the extracellular matrix. CSN3 is associated with β1D integrin, suggesting that CSN3/CSN may have a nuclear translocation function under pathological stress (e.g. ischemia, pressure or volume fluctuations) in order to assist the communication of transcriptional responses to extracellular matrix in the heart [142].

In summary, the CSN guarantees heart physiology via different signalling pathways

including transcriptional regulation, steering the ubiquitination and degradation of cardiotoxic proteins as well as protein-protein interactions. In addition, targeting CSN activity might provide future therapeutic value in cardiac remodelling for patients with HF.

1.3.4 The CSN in Cardiovascular Ischemia#

Cardiovascular diseases, including cerebral stroke and ischemic heart disease, remain the leading cause of death globally [166]. MI/IHD is an acute condition causing cardiomyocyte death as well as an inflammatory infiltration into the heart, and in the long term, MI triggers harmful conditions which could lead to HF [167]. We have discussed the links between CSN and HF in the last subchapter, and this subchapter will focus on ischemia including ischemic stroke and ischemic heart disease. Ischemic stroke makes up four out of five strokes worldwide, and it is caused by arterial occlusion in the brain, the spinal cord or the retina. In the last decade, some studies have addressed the function of CSN in chronic inflammatory disease as described above. However, to date, only very few studies included the link between CSN and ischemic heart disease or stroke.

One study observed that MIF knockout female mice triggered a larger infarct size after a tMCAo, and this was due to the upregulated CSN5 levels in mitochondrion in the MIF knockout mice [168]. MIF is a secreted chemokine-like inflammatory cytokine that supports inflammation in disease including atherosclerosis and sepsis [169, 170], and this report suggests that CSN5 could regulate the intracellular MIF which provides a neuroprotective function in female tMCAo mice [168]. It is acknowledged that after stroke, signalling pathways in the immune response vary by sex, and one explanation for the CSN5 activity in female stroke mice is that CSN5 interacts with the progesterone receptor together with the steroid receptor coactivator in order to mediate the transcription and be a cofactor for E2F1 [171–173]. Additionally, CSN5 regulating mitochondrial apoptotic through the interaction with BclGs has also been reported in

another study [174].

After ischemic stroke, the brain protects itself by several endogenous mechanisms. A main hypoxia-adaptive signalling pathway is ischemic preconditioning (IPC), and IPC has been reported to provide protective activity in different tissues, such as the heart, kidney and lung [175]). During IPC, NF-κB activity is suppressed, and extracellular accumulation of adenosine is induced. Repression of CSN5 in part reversed IPC-regulated blockade of NF-κB activity in Hela cells as well as lung tissue following the Ado A2B adenosine receptor subtype stimulation. This connection between CSN5 and anti-inflammatory adaptation to hypoxic conditions is via adenosine-regulated CUL1 deneddylation [176].

Besides the direct link between CSN and cardiovascular ischemia, several studies covered that blocking cullin neddylation by the NAE1 inhibitor, MLN4924 is of importance to both myocardial ischemia and ischemic stroke. Owing to the similar function of MLN4924 to overexpression of CSN5, these studies provide very valuable insights for research in future studies of CSN5. MLN4924 raised cell viability, reduced LDH leakage rate as well as improved cell morphology changing under H_2O_2 stimulation in cardiomyocytes [177]. Furthermore, MLN4924 reduced the cardiac infarct size in MI mice, and this function of MLN4924 was abrogated by treating it together with inhibitors of the autophagic flux. This suggested a cardioprotective action of MLN4924 in H_2O_2-induced cardiomyocytes injury and MI/R mice through restoring the impaired autophagic flux [177]. Similar protective effects of MLN4924 were also observed in cerebellar granule neurons (CGNs) against H_2O_2 stimulation [178]. H_2O_2 treatment induced CGNs damage and evaluated reactive oxygen species (ROS) production, and MLN4924 attenuated this damage through diminishing ROS production and accumulating protein levels of nuclear factor E2-related factor 2 (Nrf2) [178]. One of the most recent studies has shown that NEDD8 conjugated cullin 1 increased in MCAO mice, and inhibition of cullin neddylation by MLN4924 reduced ischemic brain infarction [179]. One of

the CRL substrate accumulated by MLN4924 treatment is neurofibromatosis 1 (NF1), and silencing this substrate abolished MLN4924-dependent inhibition of neutrophil trafficking and protection of BBB. This suggested that blocking cullin neddylation may be beneficial to ischemic stroke [179]. Additionally, MLN4924 defencing the endothelial intergrity was also observed in another paper. In the human microvascular endothelial cell line HMEC-1, MLN4924 rescued the increased endothelial permeability induced by LPS [180]. As discussed above, NF-κB activity is vital for the regulation of inflammatory processes in ischemic stroke. Akin to MLN4924, the 26S proteasome inhibitor MLN519 (also known as PS519) was found to delay NF-κB regulated neuroinflammatory response, resulting in reduced stroke outcome and improved neuro-functional recovery [181–185]. For an illustration of overall CSN function in cardiovascular diseases, please refer to figure 8.

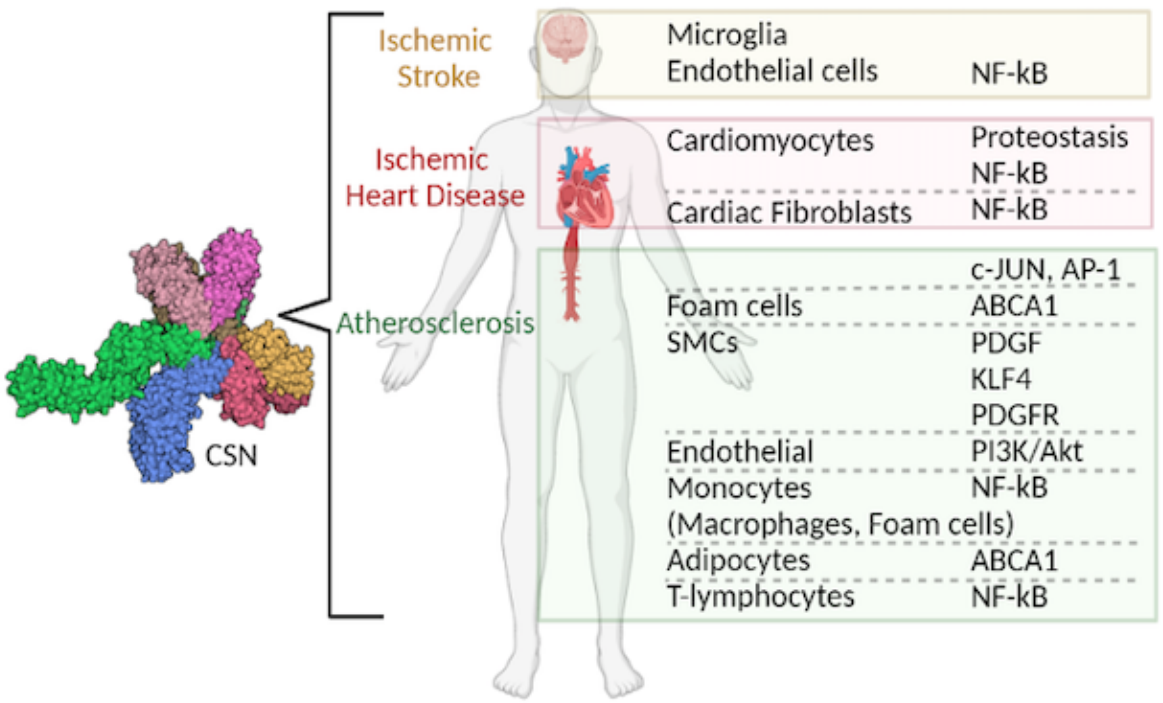

Figure 8: Scheme outlining the links between COP9 signalosome subunits (PDB ID: 4D10), signalling pathways, cell types, and organs in cardiovascular diseases. Figure modified from [186], and created with BioRender.com.

1.4 The CSN in Neurodegenerative Disorders

Apart from cardiovascular disease, the involvement of the CSN in neurodegenerative disorders, including PD and AD, has been addressed in a few papers, and the role of the CSN in the brain is emerging. Here, we will briefly introduce the backgrounds of neurodegenerative disorders as well as discuss the mechanisms contributing to disease pathogenesis which CSN may regulate .

AD is a a devastating neurodegenerative disease and mainly affects elderly individuals worldwide. Because the world's population is aging, AD is affecting more than 35 million people with a large human, social, and economic burden [187]. Pathologically, a wealth of evidence showed that AD brains show amyloidβ (Aβ)-containing neuritic plaques and tau-containing neurofibrillary tangles and marked atrophy in the brain [188]. Aβ peptide is derived from the amyloid precursor protein (APP) through a sequential proteolytic processing of β and γ secretases [189]. COPS5/CSN5 protein was found to interact with a regulator of Aβ, RanBP9 by two-hybrid analysis [190]. COPS5 and RanBP9 were colocalised in the same subcellular compartments and both increased Aβ generation and soluble APP-β, but decreased soluble-APP-α levels. Moreover, in AD brains, COPS5 levels were increased, knock-down of *Cops5* (*Cops5*, gene name of CSN5) by the siRNA reduced Aβ generation, and overexpression of COPS5 enhanced RanBP9 protein levels. These findings led to the suggestion that the increased APP processing and Aβ generation by the COPS5, is enabled through the protein-protein interaction between COPS5 and RanBP9 [190]. From the cell line study of COPS5 regulating Aβ, in vivo data from the same lab confirmed that overexpression of COPS5 also reduced spinophilin in the mouse cortex and hippocampus, resulting in deficiency of learning and memory skills [191].

Along with RanBP9, Jab1/CSN5 has other binding partners, such as IRE1α and Brain-2 (Brn-2). IRE1α is an endoplasmic reticulum (ER) stress transducer which mediates the unfolded protein response and apoptosis, and additionally, ER stress has

been reported to relate to AD and PD [192, 193]. Brn-2 is a class III POU transcription factor that has influence in the development of the cerebral cortex which is also essential for neurodegenerative diseases [194].

In conclusion, only a small number of studies have discussed the role of CSN in neurodegenerative disorders and they mainly focus on the binding partners of CSN which were found to be involved in the diseases. Although crosstalks between the ubiquitin system/the neddylation dysfunction and the toxic proteins Tau and Aβ is emerging [195, 196], it remains unclear whether and how CSN directly affects neurodegenerative diseases' progression.

1.5 Aim of the Study

While our previous studies have suggested a protective role of CSN5/CSN in all stages of atherogenesis, several other papers also indicated that the CSN exhibits anti-inflammatory activity in the heart and brain. Based on these results, the central goal of this thesis was to study the role of the CSN in neuroinflammation and ischemic stroke. Toward this aim, I first mapped the location in which brain cell types CSN subunits are enriched. Next, as the CSN is involved in the mediation of NF-κB signalling in inflammatory-elicited macrophages and endothelial cells, the similarities between macrophages and microglia were addressed to ask the first functional question: Does the CSN control microglia and microvescular endothelium in the same manner? Furthermore, specific aims were defined as follows:

1. How are the expression levels of CSN subunits in the brain?
2. Do CSN5 and the CSN exert anti-inflammatory effects in microglia cells?
3. Do CSN5 and the CSN exert anti-inflammatory effects in the blood-brain-barrier and affect its leakage?
4. Does the CSN exert protective activity in ischemic stroke?

2 Materials and Methods

2.1 Materials

2.1.1 Chemicals and Reagents

Substance & Catalog Number	Manufacturer
Tris-(hydroxymethyl)-aminomethan (Tris), 4855.2	Carl Roth, Karlsruhe
Sodium dodecyl sulfate (SDS), 201139	Serva, Heidelberg
Glycine, G8898	Sigma Aldrich, Darmstadt
Dimethylsulfoxid (DMSO), D2650	Sigma, Darmstadt
Tetramethylethylenediamine (TEMED), 1610801	BIO-RAD, USA
Recombinant murine TNF-α, 300-01A	Peprotech, USA
NUPAGE LDS sample buffer, NP0007	Thermo Fisher, Netherlands
NUPAGE transfer buffer, NP00061	Thermo Fisher, Netherlands
CozyHi prestained protein ladder, PRL0202	highQu, Kraichtal
Methanol, 0798.3	Carl Roth, Karlsruhe
Tween 20, P2287	Sigma Aldrich, Taufkirchen
Roswell Park Memorial Institute (RPMI) 1640, 61870044	Thermo Fisher, Netherlands
EndoGRO-MV complete culture media kit, SCME004	Sigma Aldrich, Darmstadt
Penicillin/Streptomycin (PS), 15070063	Thermo Fisher, Netherlands
DL-Dithiothreitol (DTT), D0632	Sigma Aldrich, Taufkirchen
Trypsin-EDTA, 25300054	Thermo Fisher, Netherlands
30% Acrylamide, 1610156	Bio-Rad, Feldkirchen

Tris-hydrochloride (Tris-HCl), 9090.4	Carl Roth, Karlsruhe
Ethanol, 20821.310	VWR, France
Ammonium persulfate (APS)	Sigma Aldrich, Taufkirchen
Dulbecco's phosphate-buffered saline (DPBS), D8537	Sigma Aldrich, Taufkirchen
SuperSignal West Dura, 34075	Thermo Fisher, Netherlands
2-Propanol, AE73.2	Carl Roth, Karlsruhe
TRIzol Reagent, 15596018	Thermo Fisher, Netherlands
Chloroform, 372978	Sigma Aldrich, Taufkirchen
Nuclease-free water, 129114	Qiagen, Hilden
First strand cDNA synthesis Kit, K1612	Thermo Fisher, Netherlands
ORA qPCR green ROXL mix, QPD0105	highQu, Kraichtal
Paraformaldehyd (PFA) 4% in PBS, 11762	Morphisto, Frankfurt am Main
Triton X-100, x100	Sigma Aldrich, Taufkirchen
Mounting medium with DAPI, H1200	Vector Laboratories, Eching
Fluorescent mounting medium, F4680	Sigma Aldrich, Taufkirchen
Ethylenediaminetetraacetic acid (EDTA), A3234	AppliChem Panreac, Darmstadt
Cell counting kit 8, 96992	Sigma Aldrich, Taufkirchen
Horse serum, 26050088	Thermo Fisher, New Zealand
Minimum essential medium, 12360038	Thermo Fisher, UK
L-Glutamin, 25030081	Thermo Fisher, Netherlands
Sodium pyruvate (SP), 11360070	Thermo Fisher, China
D-(+)-Glucose, 50997	Sigma Aldrich, Taufkirchen
4-(2-hydroxyethyl)-1-piperazineethanesulfonic acid (HEPES), HM98.3	Carl Roth, Karlsruhe
SuperBlock solution, 37515	Thermo Fisher, Netherlands
Basal medium eagle, 21010046	Thermo Fisher, Netherlands
Neurobasal medium, 21103049	Thermo Fisher, UK
B-27 supplement, 17504044	Thermo Fisher, Netherlands
Papain, LS003119	Worthington, USA

Poly-L-lysine Hydrobromide, p1399	Sigma Aldrich, Taufkirchen
CD11b microbeads, 130093634	Miltenyi Biotec, Bergisch Gladbach
Hank's balanced salt solution (HBSS), 14175095	Thermo Fisher, Netherlands
Insuline transferrin powder, I1884	Sigma Aldrich, Taufkirchen
Dulbecco's modified eagle medium (DMEM), A1443001	Thermo Fisher, Netherlands
Fetal bovine serum (FBS), 10270106	Thermo Fisher, UK
Cytosine β-D-arabinofuranoside, C1768	Sigma Aldrich, Taufkirchen
Sodium bicarbonate solution, 25080094	Sigma Aldrich, Taufkirchen
Poly-L-ornithine solution, p3655	Sigma Aldrich, Taufkirchen
Lipofectamine RNAiMAX transfection reagent, 13778030	Thermo Fisher, Netherlands
Opti-MEM reduced serum medium, 31985070	Thermo Fisher, Netherlands
Latex beads, L3030	Sigma Aldrich, Taufkirchen
Lucifer yellow (LY), L453	Thermo Fisher, Netherlands
Rat tail collagen type I, 08115	Merck Millipore, Darmstadt
Propidium iodide (PI), 81845	Sigma Aldrich, Taufkirchen
Alexa Fluor 488 phalloidin, A12379	Molecular Probes, USA
DAPI, D1306	Thermo Fisher, Netherlands
siPOOL 5 kit targeting mouse Cops5	siTools Biotech, Martinsried
MLN4924 (Pevonedistat), A-1139	Active Biochem, China
Hibernate-A medium, A1247501	Thermo Fisher, Netherlands
ROTI-Histokitt, 6638	Carl Roth, Karlsruhe
REAL-EnVision Detection System, K5007	Dako, Denmark
Mayer's hemalum solution, MHS80	Sigma Aldrich, Taufkirchen
Xylene, 28973.294	VWR, France

2.1.2 Quantitative Real-time Polymerase Chain Reaction (qPCR) Primer Pairs

Mouse

Description	**Sequence**
CCL2	5’ -CATCCACGTGTTGGCTCA-3’
	5’ -GATCATCTTGCTGGTGAATGAGT-3’
IL-12β	5’ -TTCTCACCGTGCACATCC-3’
	5’ -GACCGGCACTGAGAGGAG-3’
β-actin	5’ -GGAGGGGGTTGAGGTGTT-3’
	5’ -GTGTGCACTTTTATTGGTCTCAA-3’
TNF-α	5’ -CATCTTCTCAAAATTCGAGTGACAA-3’
	5’ -TGGGAGTAGACA AGGTACAACCC-3’
IL-6	5’ -ATGGATGCTACCAAACTGGAT-3’
	5’ -TGAAGGACTCTGGCTTTGTCT-3’
IL-1β	5’ -TGTAATGGAAGACGGCACACC-3’
	5’ -TCTTCTTTGGGTATTGCTTGG-3’

Human

Description	**Sequence**
GAPDH	5’ -AAGGTGAAGGTCGGAGTCAA-3’
	5’ -AATGAAGGGGTCATTGATGG-3’
ICAM1	5’ -CCTTCCTCACCGTGTACTGG-3’
	5’ -AGCGTAGGGTAAGGTTCTTGC-3’
VCAM1	5’ -TGCACAGTGACTTGTGGACAT-3’
	5’ -CCACTCATCTCGATTTCTGGA-3’
E-selectin	5’ -GAGTGCACATCTCAGGGACA-3’
	5’ -ACTGCCAGGCTTGAACATTT-3’
CCL2	5’ -AGTCTCTGCCGCCCTTCT-3’
	5’ -GTGACTGGGGCATTGATTG-3’

2.1.3 Antibodies

Primary antibodies

Description & Catalog Number	**Manufacturer**
Anti-NF-κ B IκB-α, 9242S	Cell Signaling, Frankfurt am Main
Anti-NF-κ B pIκB-α, 9246S	Cell Signaling, Frankfurt am Main
Anti-Cullin 1, sc-17775	Santa Cruz, Heidelberg
Anti-Cullin 3, PA517397	Thermo Fisher, Netherlands
Anti-NEDD8, 2745S	Cell Signaling, Frankfurt am Main
Anti-Occuludin, 71-1500	Thermo Fischer, Netherlands
Anti-Jab1 (CSN5), sc-13157	Santa Cruz, Heidelberg
Anti-CSN8, PW8290	Biomol, Switzerland
Anti-ERK (1/2), 9102	Cell Signaling, Frankfurt am Main
Anti-p38, 9212S	Cell Signaling, Frankfurt am Main
Anti-p-p38, 9211S	Cell Signaling, Frankfurt am Main
Anti-p-ERK, sc-7383	Santa Cruz, Heidelberg
Anti-Akt, 9272S	Cell Signaling, Frankfurt am Main
Anti-p-Akt, 9275	Cell Signaling, Frankfurt am Main
Anti-Claudin 5, 341600	Thermo Fischer, Netherlands
Anti-β-Actin, sc-47778	Santa Cruz, Heidelberg
Anti-NF-κB P65, 8242	Cell signaling, Frankfurt am Main
Anti-β-Tubulin III, T8578	Sigma Aldrich, Taufkirchen
Anti-VE-Cadherin, sc-9989	Santa Cruz, Heidelberg
Anti-NeuN, 26975-1AP	Proteintech, UK
Anti-HIF-1α, 14179	Cell Signaling, Frankfurt am Main

Secondary antibodies

Description & **Catalog Number**	**Manufacturer**
Anti-mouse HRP, ab6820	Abcam, UK
Anti-rabbit HRP, BYT-ORB43514	Biozol, Eching
Anti-rabbit Alexa Fluor 555, A-21428	Thermo Fisher, Netherlands
Anti-mouse Alexa Fluor 647, 115-605-003	Jackson ImmunoResearch, UK
Anti-rabbit Alexa Fluor 647, A32733	Thermo Fisher, Netherlands

2.1.4 Buffers and Solutions

Unless otherwise stated, the distilled water was used as a default in all the buffers .

Description	Concentration
Phosphate-buffered saline (PBS)	NaCl 137 mM
	KCl 2.7 mM
	KH_2PO_4
	Na_2HPO_4
5x Running buffer	1.514% Tris (w/v)
	Glycin (w/v) 7.205%
	2% SDS (w/v)
Resolving gel	11% acrylamide/Bis (w/v)
	375 mM Tris-HCl, pH 8.8
	0.1% (w/v) SDS
	0.1% (w/v) APS
	0.1% (w/v) TEMED
Stacking gel	5% (w/v) acrylamide/Bis
	125 mM Tris-HCl, pH 6.8
	0.1% (w/v) SDS
	0.1% (w/v) APS
	0.1% (w/v) TEMED
TBS (pH 7.2)	20 mM Tris-HCl
	150 mM NaCl
TBS-T	0.05% Tween dissolved in TBS
Blocking buffer	5% BSA or 5% non-fat milk
Dissection buffer	97.5% HBSS
	11 mg/mL sodium pyruvate
	0.1% glucose
	10 mM HEPES

2.2 Methods

2.2.1 Cell Culture and Treatment

Primary neuronal cultures

Primary neurons were derived from P0-P1 neonatal pups. Mice were decapitated by scissors, and the heads were immediately placed into ice-cold dissection buffer (97.5% HBSS Ca^{2+} and Mg^{2+} free, 110 μg/mL SP, 0.1% glucose, 10 mM HEPES PH7.3). Brain dissection was performed in the ice-cold dissection buffer on a 60 cm Petridish under Stemi 305 Zeiss microscope. Cortical tissues were separated from the brain and hippocampi were removed. The cortex was transferred by a fire-polished glass Pasteur pipette into pre-warmed 2 mg/mL papain buffer at 37 °C for 15 min. The mixed brain cell pellet was washed by the cold plating medium (86.55% MEM Eagle's with Earle's BSS, 10% FBS, 0.45% glucose, 1 mM SP, 2 mM glutamine, 1%Penicillin/Streptomycin) once and triturated in the pre-warmed plating medium with pipettes. Next, the total cell suspension was filtered with a 40 μm filter, and cells were plated on coverslips or dishes coated with poly-L-lysine 0.5 mg/mL. The plates were incubated at 37 °C, 5% CO_2 humidified incubator and medium was replaced by the growing medium (96% Neurobasal medium, 2% B-27 supplement, 2mM glutamine, 1% P/S) the next day. Half of the growing medium was then changed twice a week for 10 to 14 days before any treatment. As an illustrator, please be referred to figure 9.

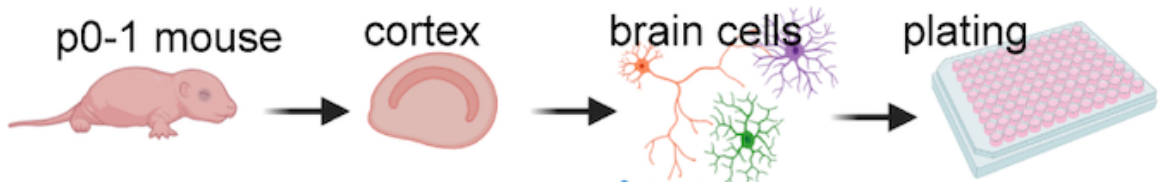

Figure 9: Cartoon of an experimental modeling of isolation primary neuronal cells. Primary neurons were derived from P0-P1 neonatal pups. Mice were decapitated by scissors. Cortical tissue was separated from the brain, and mixed cell suspension was cultured in the 96 well plates with designed neurons culture medium. Figure created with BioRender.com.

Mixed brain cell cultures
Mouse brain cortices were isolated from CX3CR1-eGFP p0-p2 pups in the Hank's balanced salt solution (HBSS) supplemented with 8% $NaHCO_3$, 1 μM HEPES. Tissues were digested in 2 mg/mL papain solution, and all the cells were plated in the common medium (MEM no phenol red, 20% glucose, 8% $NaHCO_3$, 0.1 mg/mL transferrin) added 0.5% P/S, 10% FBS, 2 mM L-glutamine, 0.025 mg/mL insulin on a 96-well cell image plate (Eppendorf). Medium were replaced the second day to common medium, and changed twice a week for two weeks.

BV2 cell culture
BV2 cell line was cultured in RPMI1640 GlutaMAX full medium supplemented with 10% FBS, 1% P/S, and maintained in a poly-L-ornithine (0.01%) coated T-75 flask in a humidified incubator containing 5% CO_2 and at 37 °C. Cells were split every 2-3 days until passage 20th.

hCMEC/D3 cell culture
The immortalized hCMEC/D3 cell line was seeded on rat tail collagen type I coated T-25 flask in EndoGRO-MV complete culture media kit, and maintained 5% CO_2 and at 37 °C exposure. Cells were split when they reached confluent monolayer (4-6 days).

Freezing and thawing of cell lines
Frozen cell stocks were stored with 1 mL complete medium containing 10% DMSO in 1.5 mL cryovials in -150 °C freezer. To freeze cell, cells were harvested, subsequently centrifuged and finally resuspended in 1 mL medium containing 2×10^6 cells. The cryovials were then kept in a cryo-container to cool down at a 1 °C/min rate, and the container was placed in a -80 °C freezer for overnight. The next day, cryovials were transfered to -140 °C for long-term storage.
Thawing frozen cell lines, the cryovials were taken out from -140°C and immersed in a 37 °C for 1 min. Cells were afterward placed into a 15 mL falcon and 9 mL growth medium was added slowly. After being centrifuged, cells were resuspended in the growth medium.

Cell treatment

All the cells were treated with 20 ng/mL murine TNF-α or 100 ng/mL human TNF-α as stated. MLN4924 and CSN5i-3 were dissolved in 100% DMSO and pre-treated on cells for 2-4 h at a concentration of 500 nM and 1 or 4 μM in all experiments.

2.2.2 Organotypic Slice Culture and Treatment

Organotypic brain slice cultures were prepared as outlined before [197] with modifications. According to German animal handling laws, brains were removed from p5-8 neonatal mice by decapitation. Hippocampi and neocortices were dissected, and hippocampal and cortical cultures are depicted in figure 10. Sagittal sections (thickness of 350 μm), were cut using a Mcllwain tissue chopper (Model TC752, Mickle Laboratory Engineering Company), and all the sections were separated by forceps in the slice dissection medium (MEM supplemented 1% P/S, 10 mM Tris, PH7.2). Intact sections were carefully chosen under a Stemi 305 Zeiss dissection microscope. Slices incubated in the cold dissection medium for 30 min before plating, and two slices were plated on each cell culture insert (0.4μm, 30 mm diameter, PICMORG50 Millipore). Slice culture medium (MEM supplemented 25% heat-inactivated horse serum, 1 mM l-glutamine and 25%HBSS) was changed one day after the seeding and subsequently twice a week.

Treatments were applied directly to the brain slice culture medium. MLN4924 and CSN5i-3 were dissolved in 100% DMSO and pre-treated on cells for 24 h at a concentration of 10 μM.

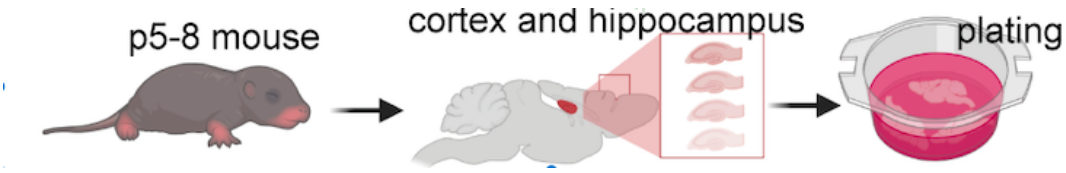

Figure 10: Cartoon of an experimental modeling of isolation organotypic slice culture. Brains were removed from p5-8 neonatal mice by decapitation. Hippocampal and cortical cultures are depicted in Sagittal sections, and maintained in the 35 mm (diameter) dishes. Figure created with BioRender.com.

2.2.3 Oxygen Glucose Deprivation (OGD)

OGD was performed on the 10-14 days primary neuronal culture, confluent monolayers of hCMEC/D3 cells and 14 days old brain slice culture. The cell culture medium was changed to the DMEM, no glucose, no glutamine, no phenol red medium instead of the glucose medium and flushed with 94% N2, 5% CO_2 for 10 min before being placed into the humidified hypoxia chamber (94% N_2, 5% CO_2, 1% O_2, 45% humidity, 37 °C) for the indicated time. OGD was terminated by returning the cells/slices into normoxic conditions with glucose-containing medium.

2.2.4 Evaluation of Cell Damage in Organotypic Slice Culture

PI was used to label injured cells in the organotypic slice culture. After the OGD/RO treatment, slices were incubated in the culture medium with 7 μM PI for 15 min at 37 °C. Afterward, images were directly acquired using Leica Dmi8 microscope with a 4X dry objective. The areas of PI-positive and total tissue have been quantified manually by ImageJ-Fiji. Quantification has been based on at least 5 independent experiments.

2.2.5 Cell Counting Kit-8 (CCK-8) Neuronal Viability Assay

Primary neuronal cells were seeded at the same density in 96-well plates with 100 μM growing medium each well, for 10-14 days. The cells were then treated with DMSO control, MLN4924 or CSN5i-3 followed by OGD as mentioned before, and cell viability was determined after 24 h re-oxygenated using CCK-8 kit. To each well of the 96 well plate, 10 μL CCK-8 compound was loaded directly into the growth medium and incubated at 37 °C for 2 h. The spectrophotometric absorbance of every sample was determined by a microplate reader (Perkin Elmer Enspire) at a wavelength of 450 nm. Each treatment was performed in triplicate, and at least in five independent experiments.

2.2.6 Microglia Morphology

In order to investigate the character of microglia phenotypes, slice cultures were isolated from CX3CR1-eGFP mice. Representative pictures from brain slices at 14 day in vitro (DIV) after different treatments as described previously have been acquired before and after fixation using 4X or 20X dry objective (Leica Dmi8) or 40X oil immersion objective (Zeiss confocal).

2.2.7 RNA Extraction and qPCR

The total RNA was isolated from cells with TRIzol reagent. To synthesize cDNA from the extracted RNA, RevertAid first strand cDNA synthesis kit was used. qPCR was performed using a RotorGene thermocycler (Qiagen Corbett), and samples contained cDNA, SYBR, as well as forward and reverse primers are prepared following the manufacturer's instructions. The cycle time (Ct) values were normalized with β-actin, and evaluated by the $\Delta\Delta$Ct method. Detailed information about the primers used for the qPCR is listed in the table in the material chapter.

2.2.8 Western Blot

To lyse the cells, NuPAGE-LDS lysis buffer containing 125 mM DTT was used. Protein fractions were separated by 11% or 15% SDS-polyacrylamide gel electrophoresis (PAGE) and blotted onto a polyvinylidene difluoride (PVDF) or nitrocellulose membrane. 3% of the BSA or 5% milk was used for blocking and applied by the following primary antibodies: anti-NF-κB IκB-α, anti-NF-κB pI-κB-α, anti-CUL1, anti-CUL3, anti-NEDD8, anti-VE-Cadherin, anti-Occuludin, anti-Jab1, anti-CSN8, anti-Akt, anti-p-Akt, anti-ERK1/2, anti-pERK1/2, anti-Claudin-5, anti-β-Actin. Primary antibodies were incubated at 4 °C overnight, and thereafter, membrane was washed three times with TBS-T. HRP-conjugated anti-rabbit or anti-mouse antibodies were used as secondary antibodies.

The membrane was incubated with secondary antibodies at room temperature for 1 h in 1%BSA. Blots were washed three times with TBS-T before being developed by SuperSignal West Dura Extended Duration Substrate (34076 Thermo Fisher), visualized using Li-COR and quantified by ImageJ-FIJI.

2.2.9 Immunofluorescent Microscopic Analysis

BV2, hCEMC/D3 cells and primary neuronal cells were cultured on the coverslips in the 24 well plate. To stain BV2 cells and primary neuronal cells, after treatments, cells were washed once with PBS and fixed with 4% PFA for 15 min in the dark. Followed by the permeabilisation, 0.2% Triton X-100 was incubated with cells for 10 min. Subsequently, cells were blocked with SuperBlock solution for 1 h and incubated with primary antibody as follows: anti-NF-κB P65, anti-β-tubulin III overnight at 4 °C. Three washes with PBS (10 min each) were performed on the cells before the incubation with secondary antibody. Coverslips were then mounted with mounting medium containing DAPI and sealed on the slides. For hCMEC/D3 cells, after treatment, cells were fixed with 37 °C pre-warmed PFA for 15 min, permeabilized for 5 min, and blocked with SuperBlock solution for 1 h. After incubation with anti-VE-Cadherin primary antibody overnight at 4 °C, cells were washed twice with PBS-T (containing Mg^{2+}, and Ca^{2+}) and once with PBS. Following incubation with secondary antibody which contain DAPI and Alexa Fluor 488 phalloidin (Molecular Probes) for 1h at room temperature, coverslips were washed twice with PBS-T (containing Mg^{2+}, and Ca^{2+}) and once with PBS, and finally affixed and sealed on the slides. All the fluorescent microscopic image acquisition was performed using a Leica Dmi8 fluorescence microscope or a Zeiss confocal microscope.

2.2.10 Immunohistochemical Staining

Frozen brain section slices were thawed on the hot plate for 1 min at 37 °C and dried by air for 30 min before fixation by 4 °C acetone. After fixing in acetone for 6 min,

the slices were dried by air for 30 min and encircled with a Super PAP pen. In order to quench endogenous peroxidase function, the slices were blocked with 3% H_2O_2 for 15 min, followed by three 3 min wash with PBS. Next, 60 μL of PBS blocking buffer containing 1% BSA and 5% goat serum was added to each section to reduce non-specific hydrophobic interactions. After 1 h of blocking, slices were then incubated with anti-CSN5 antibody in the humid chamber at 4 °C overnight, and washed three times with PBS. HRP secondary antibody was diluted in the blocking buffer and added onto the slice. After 1 h of incubation, slices were rinsed five times with PBS. One drop 3,3'-diaminobenzidine (DAB) chromogen was mixed with 1.5 mL DAB substrate and heated for 30 min at 37 °C in advance, and 100 μL of the mixed DAB solution was incubated with the slices for 1-10 min (Monitor the staining intensity under a microscope). Once the intensity of the tissue staining is highly observed, the samples were washed with PBS five times for 3 min each. Slices were counterstained with Mayer's hemalum solution for 20 seconds, then immediately rinsed with tap water and applied to series of ethanol, 70% ethanol for 3 min, 96% ethanol for 3 min, and 100% ethanol for 3 min. At the end, slices were incubated with xylene for 3 min, and covered up with mounting medium. THe visualizing of the tissue was performed under with a microscope (Leica Dmi8) using bright-field illumination.

2.2.11 Transfections of BV2 Cells With siPool

Knockdown experiments were performed by transfection of siPools. BV2 cells were cultivated in the RPMI medium as described above. Specific siPools of the *Cops5* (CSN5 gene name) gene were designed by the siTOOL Biotech and used at a concentration of 5 nM. Transfection of BV2 cells was accomplished using Lipofectamine RNAiMax diluted in Opti-MEM medium following the manufacturer's protocol. Cells were treated after 48 h of the transfection, and harvested after the treatments.

2.2.12 Phagocytosis Assay

BV2 cells and primary microglia were cultured into 24-well plates on the coverslips at densities of 5×10^4 and 1×10^5 cells per well, respectively. Cells were pre-treated with MLN4924 or DMSO control for 2 h in serum-free medium and incubated with or without TNF-α containing 0.05% Latex beads for 24 h or 6 h. After treatment, cells were washed by ice cold PBS for 5 times, followed by fixation using 4% PFA for 15 min in the dark. In order to visualise nuclear staining, cells were subsequently permeabilised using 0.2% Triton X-100 for 10 min. Before sealing, coverslips were finally introduced to the aqueous anti-fade mounting medium containing DAPI. Slices were observed by fluorescence microscope (Leica Dmi8). Phagocytic cells (%) = Number of cells that phagocytosed/number of total cells (DAPI).

2.2.13 Transwell Permeability Assay

To test microvascular permeability, transwell system was established. hCMEC/D3 cells were seeded at a density of 2×10^5 cells in 300 μL endothelial medium on the membrane of each transwell insert (6.5 mm Transwell-COL Collagen-Coated 0.4 μm Pore PTFE Membrane Insert 3495 Corning). After the treatments mentioned before, 5 μM LY was loaded to the upper chamber of the insert and incubated (5% CO_2, 37 °C) for 60 min. For quantification, 100 μL of medium from the lower chamber were transferred to a 96-well black polystyrene plate and measured at 530 nm (excitation at 485 nm) with a fluorescence microplate reader (Perkin Elmer Enspire). Apparent permeability (Papp) was expressed as cm/s and calculated according to the following equation: Papp = (dQ / dt) / (A x C). where dQ / dt ((μg/s)) is the quantity of the LY transportation within a given period; A (cm^2) indicates the surface area of the insert; and C (μm/mL) is the original concentration of the LY in the administered side.

2.2.14 Microglia Random Migration Assay

Mixed brain cells were placed on a 96-well cell image plate (0030741030 Eppendorf) in Hibernate-A medium, pre-treated with DMSO control or MLN4924 and stimulated with or without CXCL12 100 ng/mL. Cells were monitored under FITC-channel of fluorescence microscope (Leica Dmi8) every 5 min for 14 h by live-imaging. Tracking of individual microglia migration analysis was carried out with "Manual Tracking" ImageJ plugin (National Institutes of Health, NIH, Bethesda, USA). The quantification was further analysed with the Chemotaxis and the Migration Tool software to evaluate the accumulated distance.

2.2.15 Statistical Analysis

The data were showed as mean or mean $\pm$ standard deviation (SD) as stated from at least three independent experiments. Statistical significance (P-value) was tested by one-way or two-way ANOVA with Bonferroni or Dunnett post-test using GraphPad Prism software (version 8).

3 Results

3.1 CSN5 Is Highly Expressed in Human Brain

To begin the investigation of the role of CSN, and especially CSN5, the only subunit with catalytic function, in neuroinflammation and stroke, we first observed the gene expression profiles of CSN5 in normal human tissues from the GTEx Analysis Release V8 Data, and found that CSN5 mRNA is highly expressed in the brain, arteries, colon, esophagus and other organs. So, CSN5 displays low tissue- and region-specificity in human tissues (figure 11).

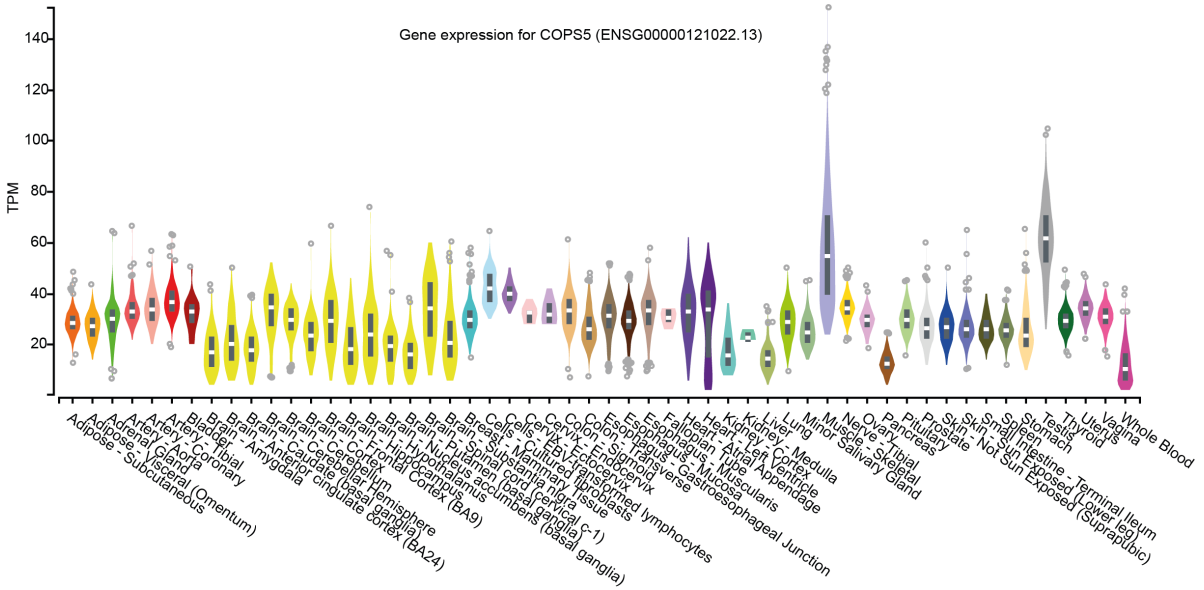

Figure 11: CSN5 is highly expressed in human tissue at transcription level. Violin plots show bulk gene expression profiles of CSN5 in normal human tissue. Each color represents a type of tissue; TPM: transcripts per million. (Figure taken from GTEx Analysis Release V8, https://www.gtexportal.org/home/gene/COPS5#geneExpression).

Next, we obtained the protein expression levels of CSN5 from the Human Protein Atlas, which showed a consistent finding that aligns with the mRNA levels. The expression levels of CSN5 according to the staining intensity and percentage of stained cells were reported as high, high, medium in neuronal cells, glial cells and endothelial cells with the antibody CAB004242 in this section (figure 12). Another tested antibody showed a high expression level in all three cell types provided by the Human Protein Atlas (not shown here). Conjointly, these data demonstrate that CSN5 is highly expressed and low cell specific in the human cerebral cortex.

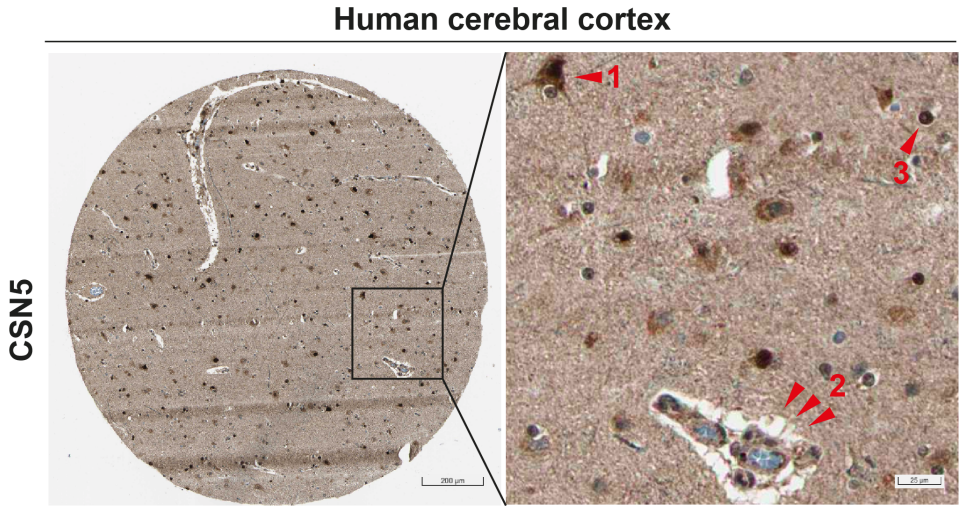

Figure 12: CSN5 is highly expressed in human brain. The human cerebral cortex was stained for CSN5. The neuronal cell (red arrow 1) and glia cell (red arrow 3) and the area with typical histological features of blood vessels (red arrow 2) show positive staining of CSN5. Antibody CAB004242 against CSN5/COPS5 was used in this section; Scale bar: 200 μm, 25 μm. (Data credit: Human Protein Atlas. Images were obtained from https://www.proteinatlas.org/ENSG00000121022-COPS5/tissue, and modified.)

3.2 CSN Subunits Are Highly Expressed in Mouse Brain

To verify whether the high expression level of CSN5 is also found in mouse, the protein level of CSN5 in normal mouse brain sections was detected by IHC (figure 13A). We found a strong expression of CSN5 staining in the mouse brain section, except for the corpus callosum (CC) area. The CC forms the largest white matter (WM) in mammals, and the reason of weak staining might be the unique structure of the CC, lipid-rich myelin coated axons representing around 40% of the dry weight of WM [198]. However,

to conclude the expression level in WM, a further study is needed. This thesis mainly focuses on the cortex (CTX) (figure 13A, right) and hippocampus region of the brain due to the fact that CTX is the most affected area under the most common stroke, middle cerebral artery stroke. Subsequently, we re-analyzed a recent single cell (sc) RNA-seq dataset (GSE123335) comparing *Cops5* gene expression on individual brain cells. Following unsupervised clustering of all the cells into 24 groups by t-distributed stochastic neighbor-embedding (t-SNE) dimensionality reduction analysis, we detected the CSN5 gene to be expressed within all the clusters (figure 13B, C).

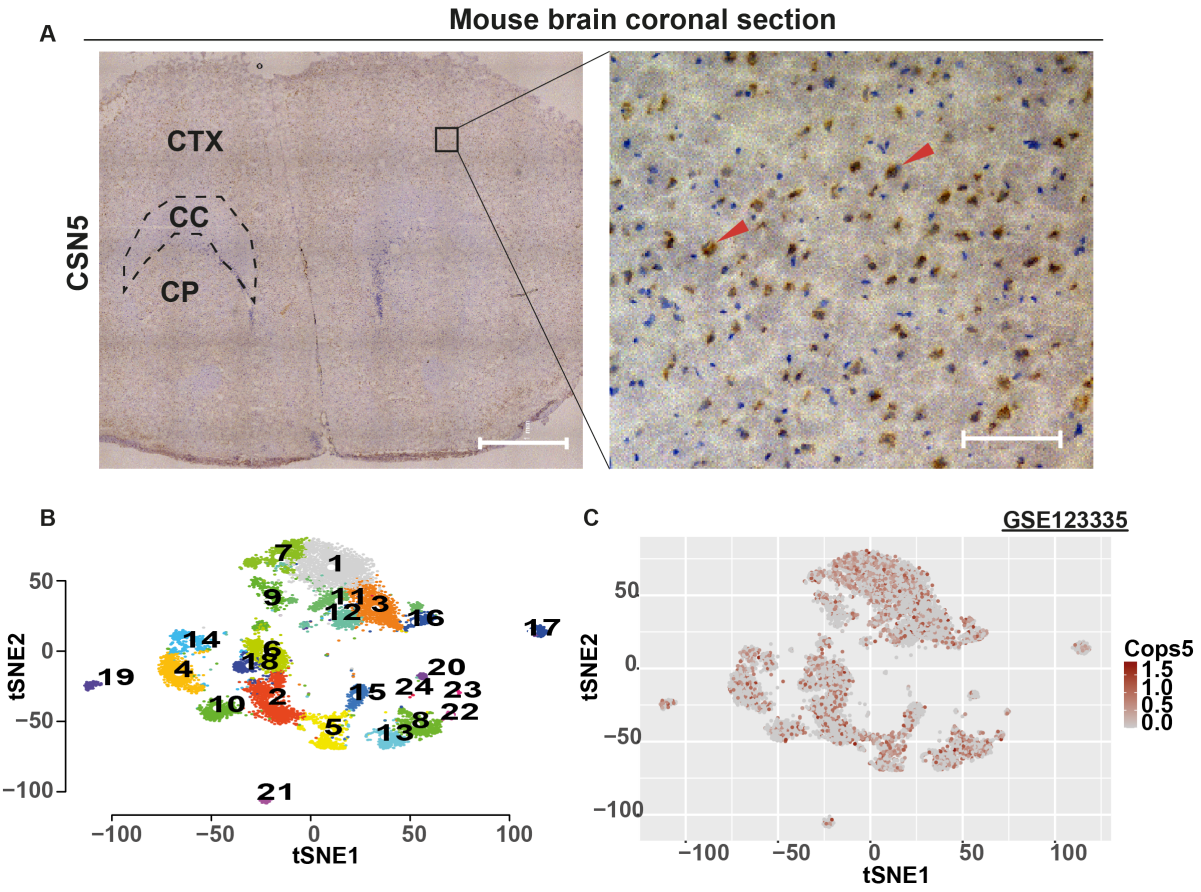

Figure 13: CSN subunits are highly expressed in the mouse brain. (A) Brains from C57BL/6J mice were prepared for the frozen section, and CSN5 was detected by anti-CSN5 antibody and visualized by DAB IHC staining. Nuclei were visualized by hematoxylin. Arrows point to CSN5 positive stained cells. Scale bar: 1 mm, 200 μm. CP, caudoputamen. (B) Re-analysis of scRNA data from [199]. tSNE plot showing cluster assignments of cells (RNA-seq dataset :GSE123335). Each number shows one cluster. (C) Feature plot visualizing expression level of *Cops5* from the clusters in (B).

However, we found only a small population of microglia (cluster 21) in all of the brain cells. Therefore, to evaluate CSN5 and other CSN subunit levels in inflamed mice, an scRNA-seq dataset on sorted microglia and $CD45^+$ non-microglia cells was analysed (GSE157480). Unsupervised clustering by the Seurat package in R/Rstudio was performed on 14310 cells from control and lipopolysaccharide (LPS)-injected mice. A total of 24 clusters was visualized by tSNE project (figure 14A), and all the genes for cluster identification were according to [200]. Two microglia clusters (cluster 5 and 6) were identified based on the expression of *Sparc* (a known microglia marker). Interestingly, all of the CSN subunits were at similar levels in the LPS-challenged microglia (cluster 5) compared to the microglia from the control mouse (cluster 6), although the microglia profile had completely shifted according to the very small overlap clusters between control and LPS groups (figure 14B). Similar observations could also be made in T cells (cluster 1, 2 and 14). A slight upregulated levels of *Cops5* and *Gps1* (*Gps1*, gene name of CSN1) was observed in LPS-injected macrophages (cluster 13 comparing to cluster 4), and different expression levels of the CSN subunit were detected in different subtypes of monocytes (cluster 0 and 3 cells are *Ly6c2*$^+$ monocytes, cluster 8 cells are *Ly6c2*$^-$ monocytes), neutrophils (cluster 10, 17), B cells (cluster 11, 15, 16), as well as in different subtypes of dendritic cells (DCs) (cluster 9, 12, 19).

Moreover, in agreement with the whole brain scRNA-seq data (figure 13C), *Cops5* was highly expressed in microglia and immune cells which infiltrated the brain under inflammation, except cluster 10, one subtype of neutrophils (figure 14C). Due to the small population of neutrophils in the control brain and the short lifespan of neutrophil, further investigation of those subtypes of neutrophils is needed. Taken together, these data prove that CSN5 is highly expressed in the mouse brain and immune cells, also pointing to an essential role of CSN in the brain.

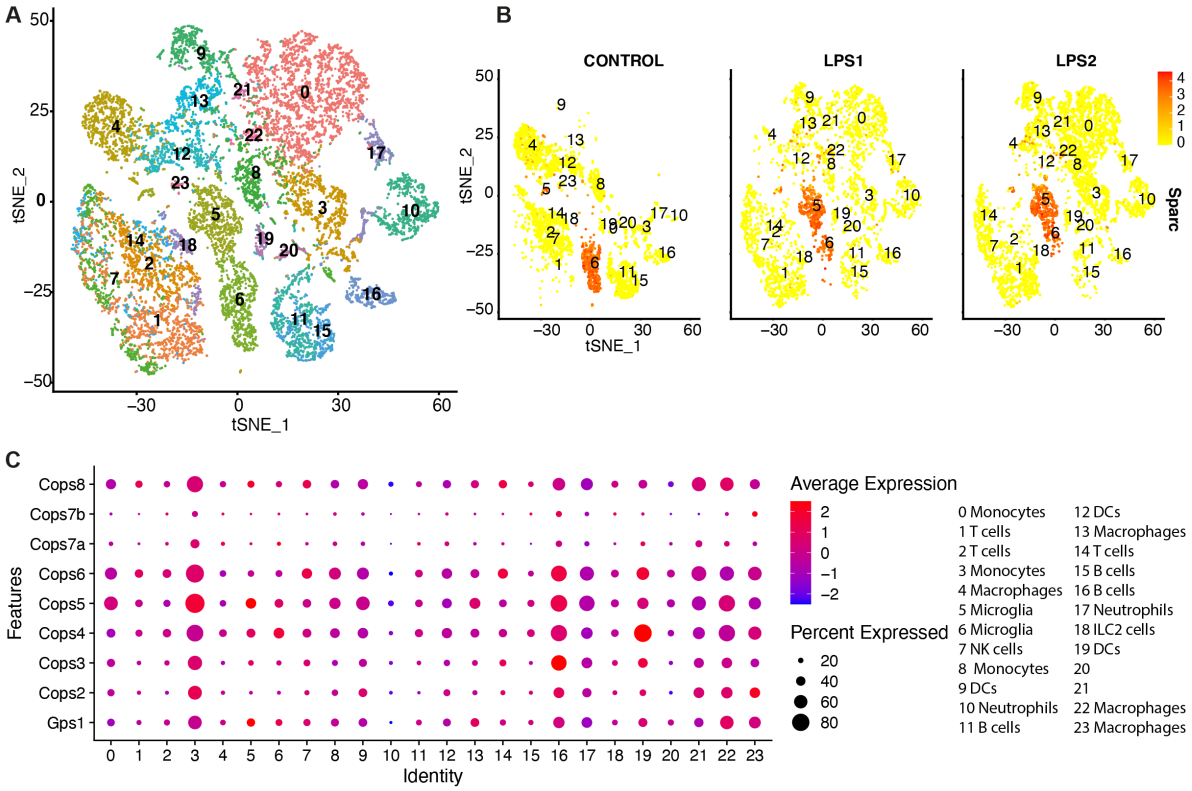

Figure 14: Re-analysis of scRNA data (from [201]) shows that CSN subunits levels are not changing in LPS-treated mouse microglia. (A) tSNE plot identified immune cell populations via clustering on scRNA-seq data (GSE157480). (B) Feature plot visualizing expression levels of *Sparc* from the clusters in A with the separated groups showing the cells from control or LPS challenged brains, and red color intensity indicating the expression level of *Sparc* in each cell. (C) Dot plot visualizing *Cops1-8* expression level and the percentage of cells within each cell cluster (average expression). ILC2, type 2 innate lymphoid.

3.3 Inhibition of Neddylation by MLN4924 Reduces Microglia Phagocytic Activity

As shown in figure 14B, microglia profiles have a striking change under LPS injection. Unlike other immune cells that only infiltrate the brain under certain conditions, it is known that microglia are considered brain resident macrophages. Microglia are the first defense during brain stimulation, and CSN is found to play an essential role in controlling the inflammatory response in macrophages. Thus, we assumed that CSN

could also regulate microglial inflammation. Moreover, microglia survey the brain to detect any alterations in the micro-environment. When there are damage-associated ligands and pathogens, phagocytosis, one of the microglia main functions, is crucial for controlling inflammation in the brain [202]. Previous studies have shown that both pro-inflammatory and anti-inflammatory microglia are associated with phagocytic activity. For example, TNF-α activates microglia through TNF receptors which triggers pathogen removal and pro-inflammatory responses [203]. On the other hand, receptors recognizing apoptotic cells, including triggering receptor expressed on myeloid cell-2 (TREM2), are usually related to an anti-inflammatory response which also leads to phagocytic activity [204].

Because of the catalytic function to deneddylate CRLs via cleaving the NEDD8 from CRL by CSN5 [205], the pharmacological inhibitor of NEDD-activating enzyme (NAE) 1, MLN4924, is partially mimicking the hyperactivity of CSN5 [206]. Additionally, MLN4924 has been safely used in several clinical trials in patients with both haematological and non-haematological malignancies [206–208]. To assess whether CSN plays a role in this phagocytic activity of microglia, the effect of MLN4924 on cullin neddylation was examined at first. As shown in figure 15, MLN4924 led to a complete blockage of CUL1 neddylation.

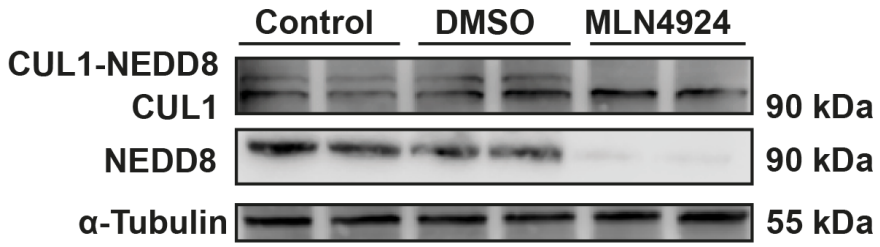

Figure 15: Inhibition of CUL1 neddylation by MLN4924 in BV2 microglial cells. Analysis of the inhibition of MLN4924 on CUL1 neddylation. BV2 cells were untreated or treated with a DMSO control or MLN4924 (500 nM) for 4h before lysed for Western blot analysis. Corresponding antibodies were used in immunodetection of CUL1, NEDD8 and α-tubulin. The Western blot shown is representative of 3 independent experiments.

Next, 0.1% DMSO control (described as DMSO control below) or MLN4924 pre-treated BV2 were cultured with or without TNF-α and incubated with latex beads. As shown in figure 16A, fluorescent labeled latex beads were phagocyted by BV2 microglia. While TNF-α enhanced microglia capacity to phagocytose latex beads, MLN4924 produced a significant reduction in phagocytosing microglia (figure 16B-C).

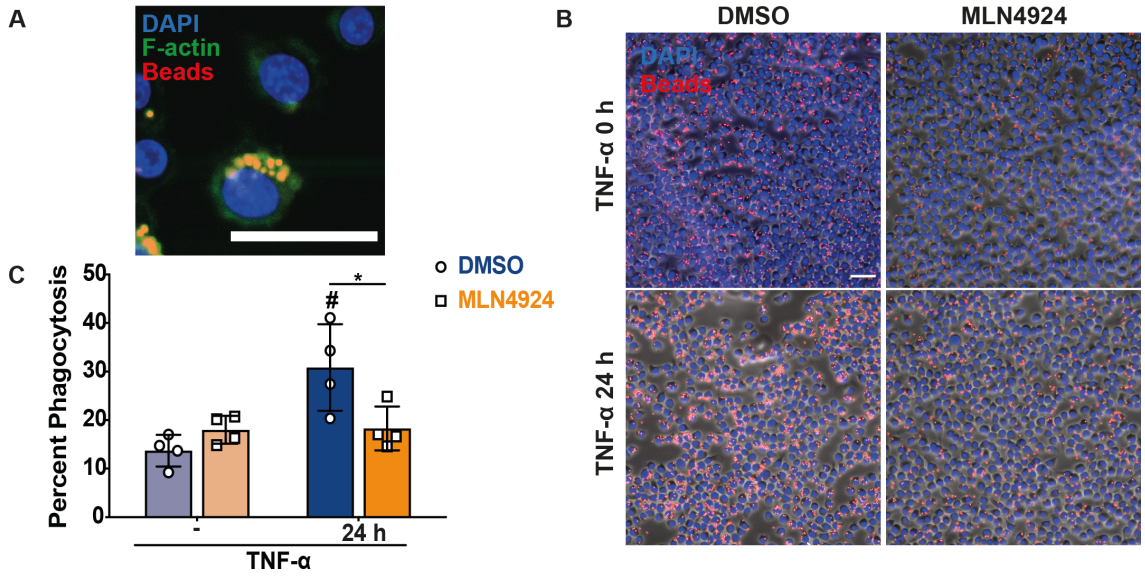

Figure 16: Inhibition of neddylation by MLN4924 reduces BV2 microglia phagocytic activity. (A) Microglia phagocytosis of latex beads: BV2 cells were stained with F-Actin (green), up-taken latex beads (red) and DAPI (blue). Scale bar: 50 μm. (B) Representative images of BV2 cells pre-treated with DMSO control or MLN4924 followed by latex beads with or without TNF-α (20 ng/mL) stimulation for 24 h. Blue, DAPI-stained nuclei; red, latex beads. Scale bar: 50 μm. (C) Percentage of the phagocytosis cells was quantified from B. Bars represent mean $\pm$ SD, n = 4; $^{*}P<0.05$, two-way ANOVA with Bonferroni post-test was checked for comparison with DMSO control; $^{\#}P<0.05$, two-way ANOVA with Dunnett post-test was performed for comparison with non-TNF-α treated control in DMSO or MLN4924 pre-treated group.

Although the BV2 cell line is the most frequently used substitute cell model for primary microglial cells due to an enormous number of similarities, there are some phagocytic receptor expression differences upon LPS treatment between BV2 cells and primary microglia as shown in previous studies [209]. Thus, the effect of MLN4924 on BV2 cells was then tested in primary microglia (figure 17A), and the similar results were observed in primary microglia (figure 17B, C). Hence, these data unambiguously proved that mimicking upregulated CSN5 by MLN4924 impairs TNF-α triggered activated microglia phagocytic activity.

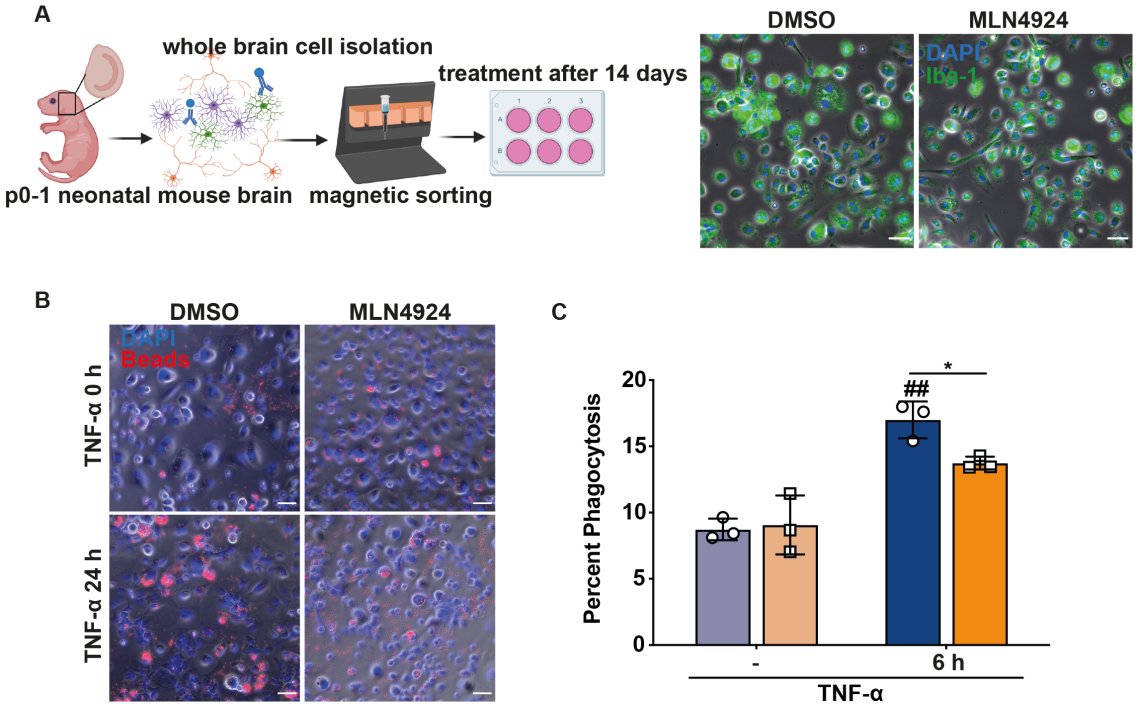

Figure 17: Inhibition of neddylation by MLN4924 reduces primary microglia phagocytic activity. (A) Schematic representation of microglia isolation from C57BL/6J p0-1 pups by the CD11b microbeads and immunofluorescence staining of Iba-1 (green) in microglia pre-treated with DMSO control or MLN4924. Scale bar: 50 μm. (B) Representative images of primary microglia pretreated with DMSO control or MLN4924 followed by latex beads with or without TNF-α stimulation for 6h. Blue, DAPI-stained nuclei; red, latex beads. Scale bar: 50 μm. (C) Quantification of the percent phagocytosis from G. Bars represent mean $\pm$ SD, n = 3; $^{*}P<0.05$, two-way ANOVA with Bonferroni post-test was checked for comparison with DMSO control; $^{\#\#}P<0.01$, two-way ANOVA with Dunnett post-test was performed for comparison with non-TNF-α treated control in DMSO or MLN4924 pre-treated group.

3.4 MLN4924 Attenuates Microglia Inflammatory Responses via the NF-κB pathway

As discussed in detail in the introduction (neuroinflammation and inflammation after stroke), microglia make up the innate immune system of the CNS and the activation of microglia is critical for neuroinflammatory processes. Additionally, our prior work has shown that MLN4924 reduces atherosclerosis lesions and inhibits inflammation in both macrophages and endothelial cells [103]. Thus, we determined the effect of MLN4924

on inflamed microglia. While 6 h TNF-α stimulation significantly enhanced the gene expression of IL-6, TNF-α, blockade of CUL neddylation by MLN4924 suppresses the proinflammatory cytokine milieu of microglia (figure 18).

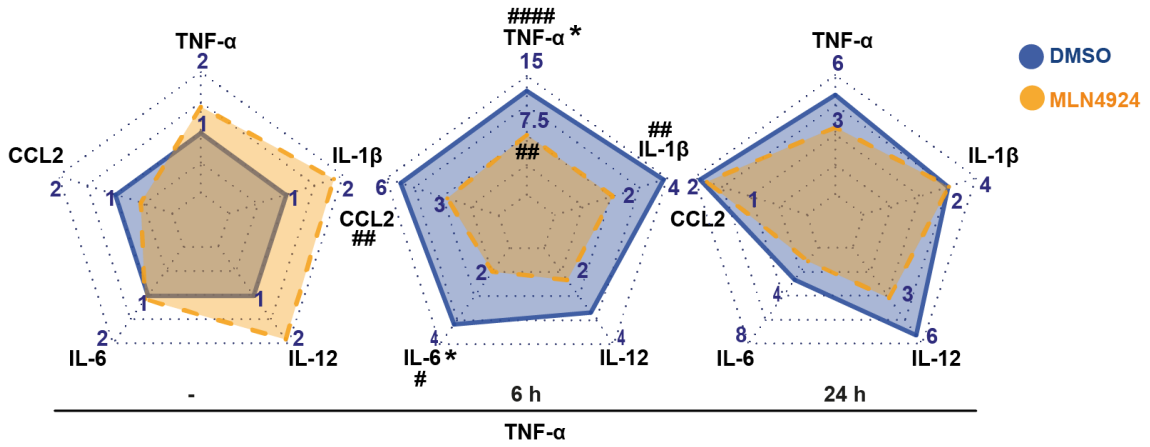

Figure 18: Inhibition of neddylation by MLN4924 attenuates microglia inflammatory responses. Radar plot representation of proinflammatory gene expression at baseline (left) and 6 h (middle) or 24 h (right) of TNF-α stimulation, quantified by qRT-PCR. plots represent mean, n = 3-4; $^{*}P<0.05$, two-way ANOVA with Bonferroni post-test was checked for comparison with DMSO control; $^{\#}P<0.05$, $^{\#\#}P<0.01$, two-way ANOVA with Dunnett post-test was performed for comparison with non-TNF-α treated control in DMSO or MLN4924 pre-treated group.

Next, we investigated the underlying mechanisms by which blocking CUL1 neddylation decreases the production of pro-inflammatory cytokines and chemokines in microglia. As a central mediator of pro-inflammatory gene induction, NF-κB pathway is activated by TNF-α triggering phosphorylation of IκB-α via the IKK complex, which is controlled by the CRL [210–212]. Therefore, we inferred that MLN4924 would decrease NF-κB signalling upon inflammation in microglia. Our data showed that MLN4924 delayed the p65 nuclear translocation induced by TNF-α to 30 min, while the translocation was increased at 10 min of activation in the DMSO control group (figure 19A). The reason for the postponed p65 translocation is that MLN4924 markedly triggered the accumulation of phosphorylated IκB-α at 10 min TNF-α treatment (figure 19B, C). Together, these results suggest that cullin-1 deneddylation impairs the NF-κB signalling via the activity of CRL-driven ubiquitination processes, resulting in the modulation of inflammation in microglia cells.

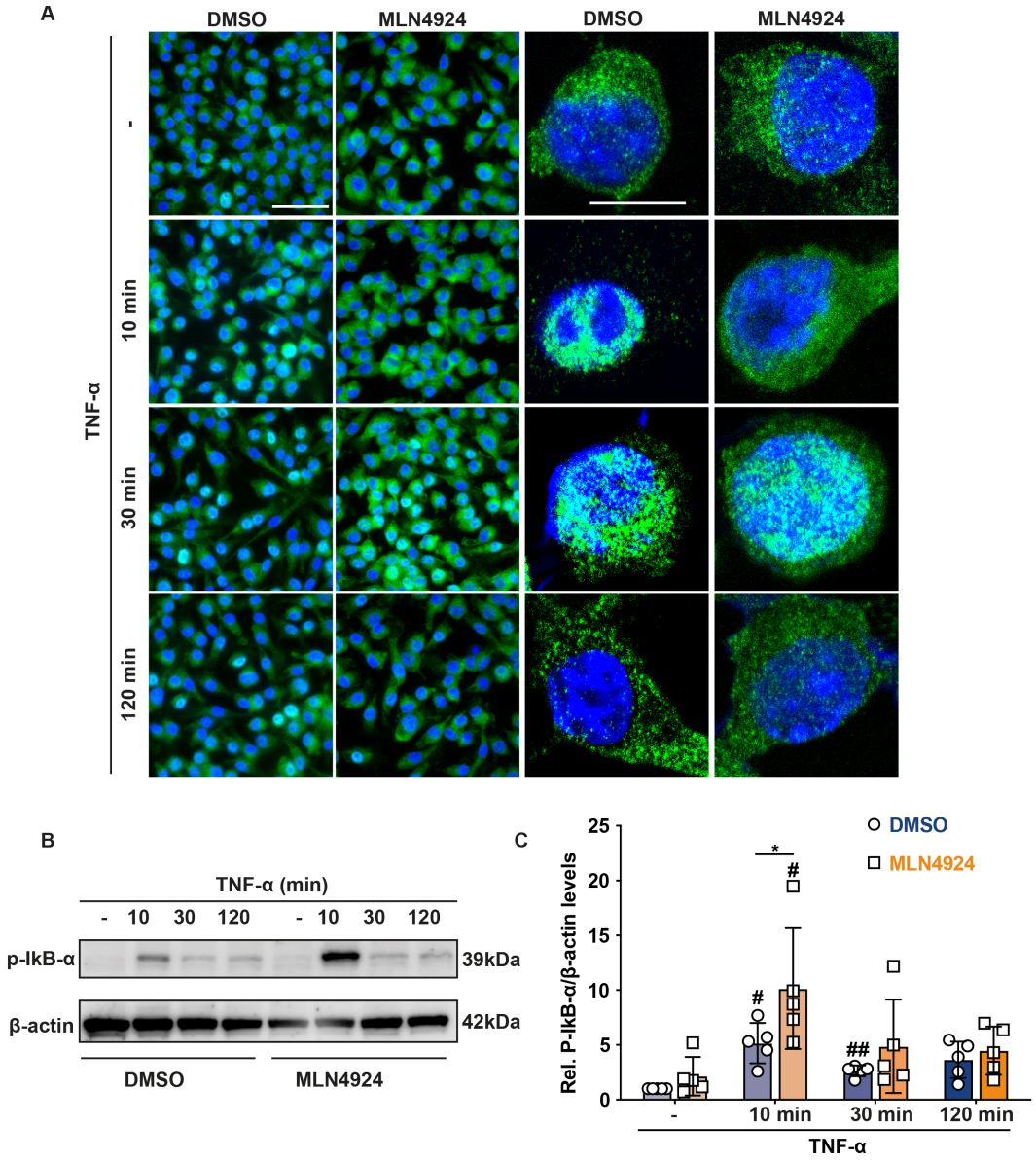

Figure 19: MLN4924 attenuates NF-κB activation. BV2 cells pretreated with DMSO control or MLN4924 were then challenged with TNF-α for 0, 10, 30, 120min. (A) MLN4924 blocks for 10min TNF-α induced p65 nuclear translocation. Translocation of p65 was visualized by using Alexa Fluor 647 antibody (green), and nuclei were counterstained by DAPI (blue). Scale bar: 50 and 20 μm. (B) Representative Western blot images of p-IκB-α and β-actin in cell lysates from BV2 cells treated as stated. (C) Quantification of (B); β-Actin was used as loading control. Bars represent mean $\pm$ SD, n = 5; $^{*}P<0.05$, two-way ANOVA with Bonferroni post-test was checked for comparison with DMSO control; $^{\#}P<0.05$, $^{\#\#}P<0.01$, two-way ANOVA with Dunnett post-test was performed for comparison with non-TNF-α treated control in DMSO or MLN4924 pre-treated group.

3.5 MLN4924 Inhibits MAPK and Reduces Microglia Motility via AKT Pathway

Along with NF-κB signalling, it has been reported that mitogen-activated protein kinase (MAPK) and phosphoinositide 3-kinases (PI3Ks)/Akt pathways also contribute to up-regulate cytokine production in CNS inflammation [213–216]. For example, the p38 MAPK is a crucial enzyme in regulating the production of IL-1β and TNF-α, and it is a drug development target for peripheral inflammatory disorders [217]. Here, we found that MLN4924 decreased phosphorylation of ERK1/2, p38 and Akt in microglia stimulated with TNF-α or CXCL12 (figure 20). These results imply that MLN4924 exerts a broad suppressive effect on MAPK and AKT pathways.

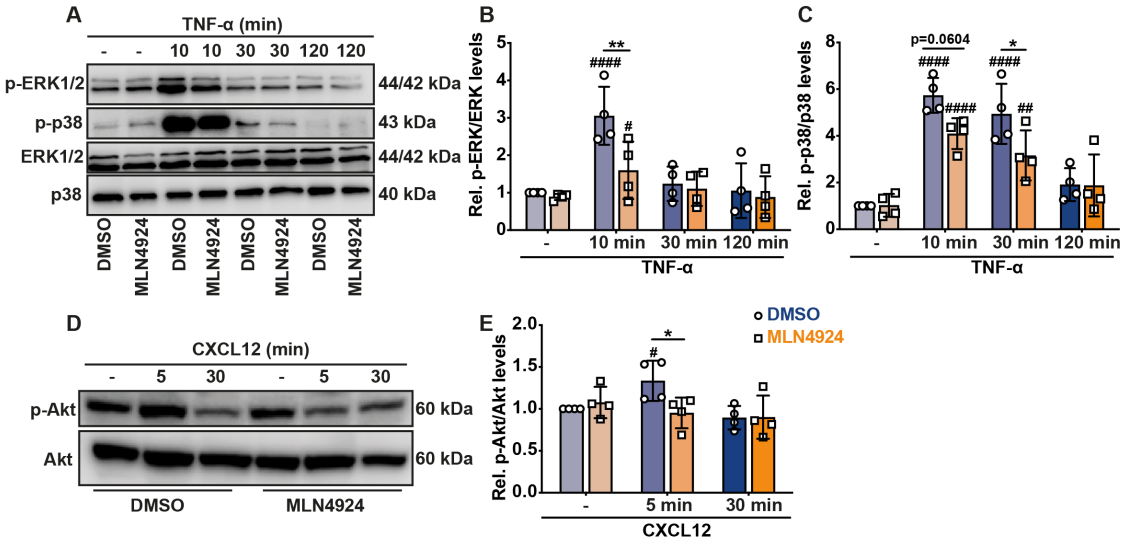

Figure 20: MLN4924 treatment inhibits MAPK and AKT signalling. (A-C) Inhibition of TNF-α-triggered ERK1/2 and P38 MAPK phosphorylation by MLN4924 in BV2 cells. (A) representative immunoblots. (B) quantification of p-ERK. (C) quantification of p-P38. Total ERK1/2 and P38 were used as loading control (mean $\pm$ SD, n=4; two-way ANOVA with Bonferroni's multiple comparison were performed for the statistical significance. (D, E) Immunodetection of CXCL12 induced Akt phosphorylation in cell lysates from BV2 cells pre-treated with DMSO control or MLN4924. (D) representative Western blot. (E) quantification of p-Akt. Total Akt was used as loading control. (B, C, E) Bars represent mean $\pm$ SD, n = 3-4; $^{*}P<0.05$, two-way ANOVA with Bonferroni post-test was checked for comparison with DMSO control; $^{\#}P<0.05$, $^{\#\#}P<0.01$, $^{\#\#\#\#}P<0.0001$, two-way ANOVA with Dunnett post-test was performed for comparison with non-TNF-α/ CXCL12 treated control in DMSO or MLN4924 pre-treated group.

Interestingly, Akt signalling is associated with cell motility, and microglia are highly

motile [218, 219]. We then decided to study the outcome of MLN4924 treatment on microglia random migration using whole brain mixed cells from CX3CR1-eGFP+ mice (figure 21A). We observed that the CXCL12-induced total random migrated distance of microglia was inhibited by MLN4924 (figure 21B, C). Taken together with (figure 20), the diminution of microglia motility by MLN4924 is through AKT pathway.

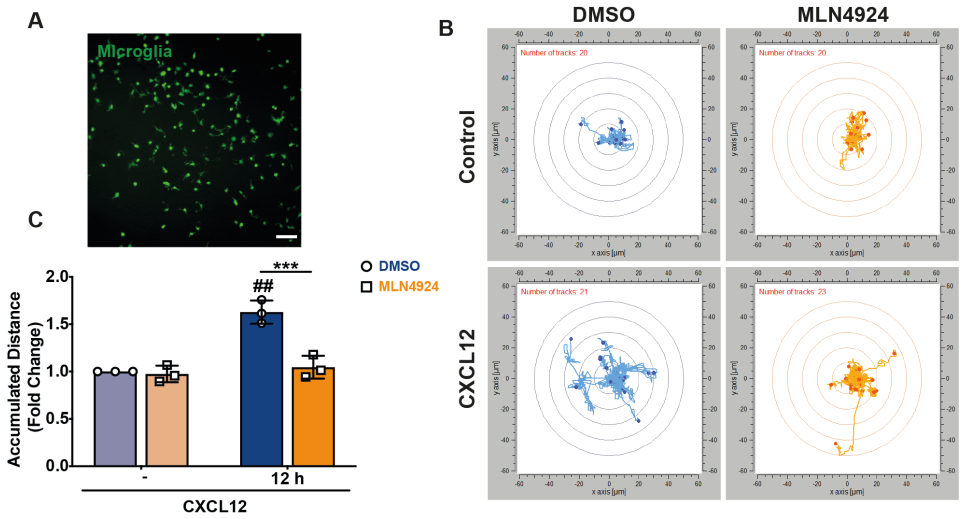

Figure 21: MLN4924 treatment inhibits reduces microglia motility. (A) Live fluorescence microscopic image of Cx3cr1-EGFP+ microglia in the brain mixed cells culture after 14 days. (B) Representative experiment demonstrating microglia random motility assessed by live-image of single-cell tracks. Microglia pre-treated with DMSO (blue) or MLN4924 (orange) followed by stimulation with (upper) or without (lower) CXCL12. (C) Quantification of B; the accumulated distance of track of 20-23 randomly selected cells per view, 4-5 views per treatment, three independent experiments were recorded. Bars represent mean $\pm$ SD, n = 3; $^{***}P<0.001$, two-way ANOVA with Bonferroni post-test was checked for comparison with DMSO control; $^{\#\#}P<0.01$, two-way ANOVA with Dunnett post-test was performed for comparison with non-CXCL12 treated control in DMSO or MLN4924 pre-treated group.

3.6 siRNA-based Sliencing or Inhibition of CSN5 Increases CUL1 Neddylation in Microglial Cells and Targets the NF-κB Pathway

To obtain initial insight into the effect of CSN5 on the response to neuroinflammation, including the transcription factor NF-κB, we performed a *Csn5* knock-down by the siPOOL

approach and achieved a CSN5 reduction on transcription and translation levels (figure 22A-C). Notably, other CSN subunits showed little or no change on mRNA levels while CSN5 silencing, and no change on CSN8 protein levels while displaying a significant reduction of CSN5 protein level (figure 22A-C).

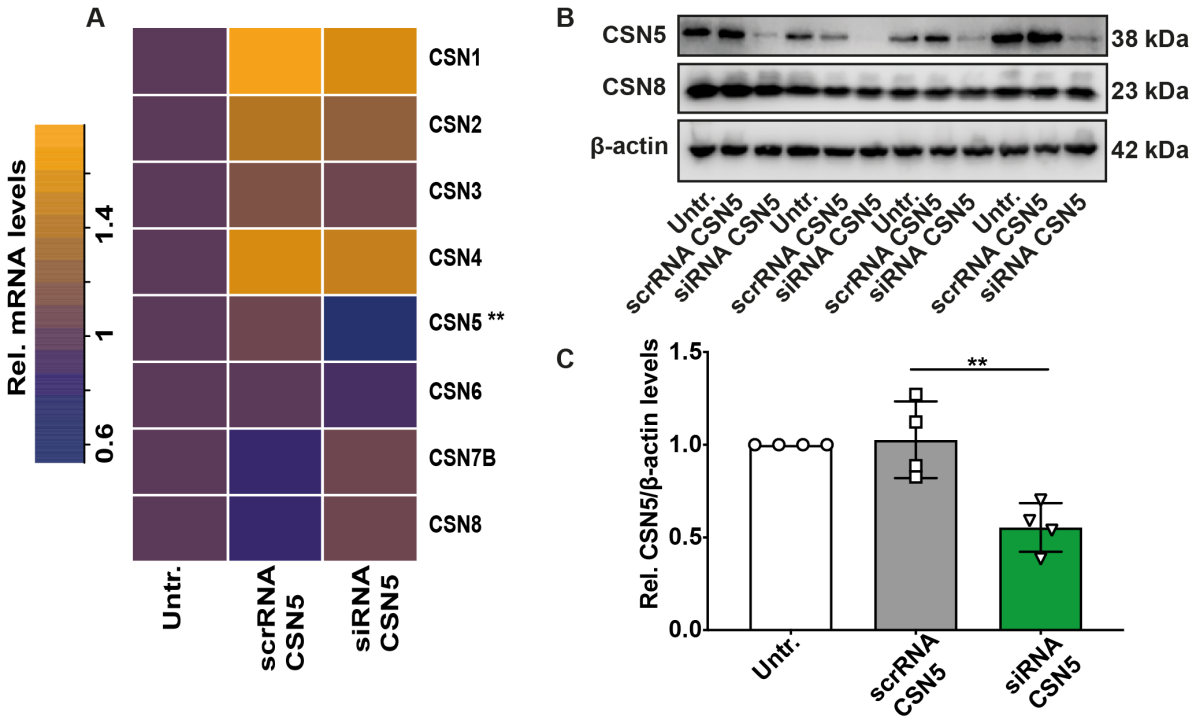

Figure 22: CSN5 expression was silenced using siPOOL technology. BV2 cells were transfected either with siPOOL which targets CSN5 (siRNA CSN5) or scrambled control (scrRNA CSN5) for 72 hours. (A) Relative mRNA levels of CSN subunits in BV2 cells with or without transfected (mean ± SD, n=4, one-way ANOVA with Dunnett's multiple comparison were performed for the statistical significance). (B) Western blot profiles of CSN5, CSN8 using corresponding antibodies. β-actin was used as loading control. (C) Densitometric quantification of C relative to untreated control. Bars represent mean ± SD, n = 4; $^{**}P<0.01$, one-way ANOVA with Dunnett's multiple comparison were performed for comparison with scRNA CSN5 control.

However, the increased CUL1 neddylation implies that the depletion of CSN5 was sufficient to disrupt the function of the CSN holo-complex figure (23A, B). Furthermore, a NF-κB p65 translocation from cytoplasm into nucleus was observed due to the absence of CSN5 figure (23C). To address the possibility of nuclear translocation of P65, we detected a significant downregulation for basal IκB-α meaning that silencing CSN5

induced the degradation of IκB-α. This is supported by the re-accumulated IκB-α levels in the controls over time whereas they are delayed upon CSN5 knock-down figure (23D, E). These results align with our understanding of the CSN5 function in the CUL1 neddylation state and the mediating function of NF-κB via IκB-α degradation and match the previous results with mimicking overexpression of CSN5 by MLN4924.

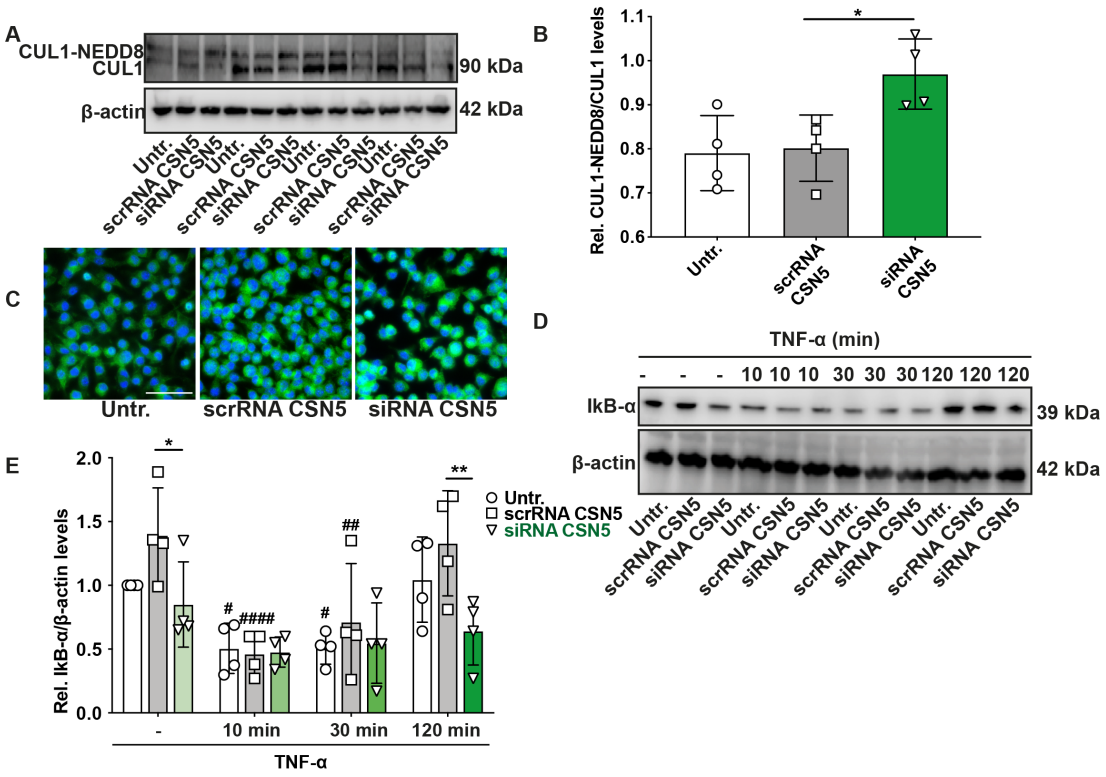

Figure 23: CSN5 silencing increases cullin1 neddylation and targets the NF-κB pathway. BV2 cells were transfected with either siPOOL which targets CSN5 or scrambled control for 72 hours. (A) Increased CUL1 neddylation by siPOOL-based knockdown CSN5 in BV2 cells. (B) A bar graph showing quantification of D from four independent experiments (mean $\pm$ SD, n=4; $^{**}P<0.01$, one-way ANOVA with Dunnett's multiple comparison were performed for comparison with scRNA CSN5 control.). (C) P65 nuclear translocation was detected in untreated or transfected with scrambled control or siPOOL CSN5 BV2 cells. Blue, DAPI-stained nuclei; green, P65. Scale bar: 50 μm. (D-E) Representative Western blot images of IκB-α and β-Actin in cell lysates of BV2 cells treated with TNF-α for the stated time points, and quantification of IκB-α normalized to β-Actin. Bars represent mean $\pm$ SD, n = 4; $^{*}P<0.05$, $^{**}P<0.01$, two-way ANOVA with Dunnett post-test was checked for comparison with scRNA CSN5 control; $^{\#}P<0.05$, $^{\#\#}P<0.01$, $^{\#\#\#\#}P<0.0001$, two-way ANOVA with Dunnett post-test was performed for comparison with non-TNF-α stimulated control in untreated (described as untr. in the figure) or scRNA/siRNA CSN5 treated group.

In addition to the last figure, using the CSN5i-3 to inhibit CSN activity led to enhanced

CUL1 neddylation and reduced re-accumulated IκB-α levels upon TNF-α stimulation (figure 24B). These results are in support of figure 21, sliencing or inhibition of CSN5 increases CUL1 neddylation in microglial cells and targets the NF-κB pathway.

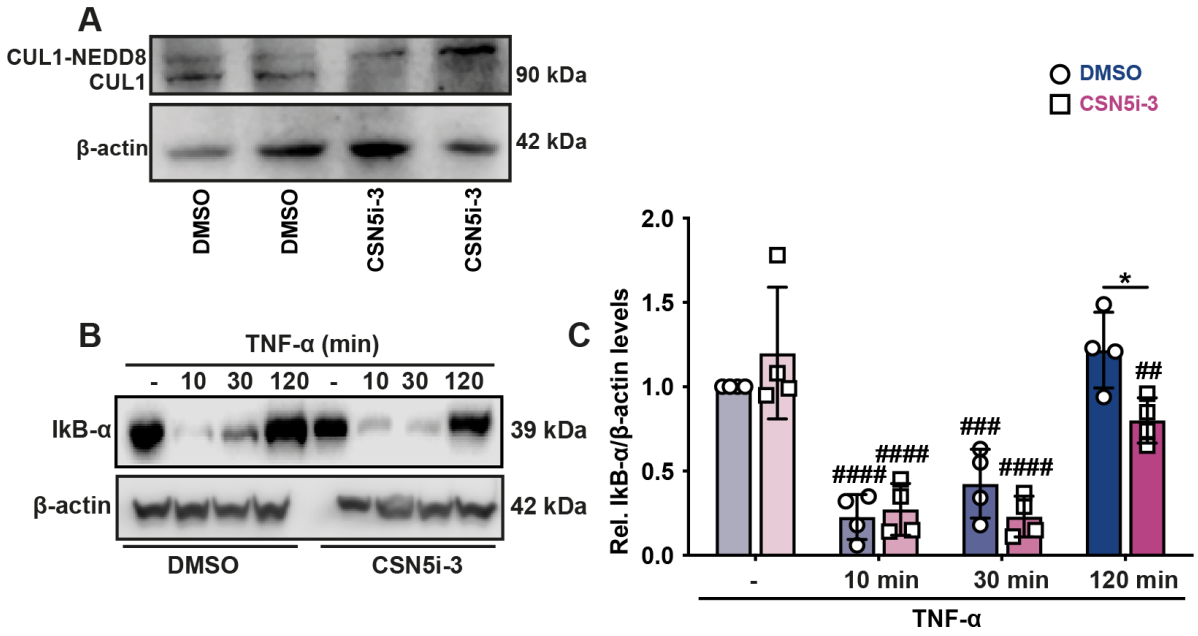

Figure 24: Inhibition of CSN5 enhances cullin1 neddylation and targets the NF-κB pathway. (A) Western blot analysis of Cullin1 after treatment with DMSO control or CSN5i-3 (4 µM) in BV2 cells. (B) Representative immunodetection of IκB-α and β-Actin in cell lysates from BV2 cells treated as indicated. (C) Quantification of B from four independent experiments. Bars represent mean $\pm$ SD, n = 4; $^{*}P<0.05$, two-way ANOVA with Bonferroni post-test was checked for comparison with DMSO control; $^{\#\#}P<0.01$, $^{\#\#\#}P<0.001$, $^{\#\#\#\#}P<0.0001$, two-way ANOVA with Dunnett post-test was performed for comparison with non-TNF-α stimulated control in DMSO or CSN5i-3 pre-treated group.

3.7 MLN4924 Suppresses NF-κB and MAPK Signalling Pathways in Inflammatory-Elicited Microvascular Endothelial Cells

To determine how CSN5 affects neuroinflammation and stroke, we then tested a key component of the blood-brain barrier (BBB), endothelium, using human microvascular endothelial cells (hCMEC/D3), whose disruption is mediated by many factors including TNF-α-secreted by microglia. TNF-α markedly triggered gene expression of adhesion

molecules *VCAM-1* and *ICAM-1* in hCMEC/D3 cells, and blocking the CUL1 neddylation by MLN4924 completely lowered the *VCAM-1* and *ICAM-1* expression at 4h TNF-α (figure 25A, B).

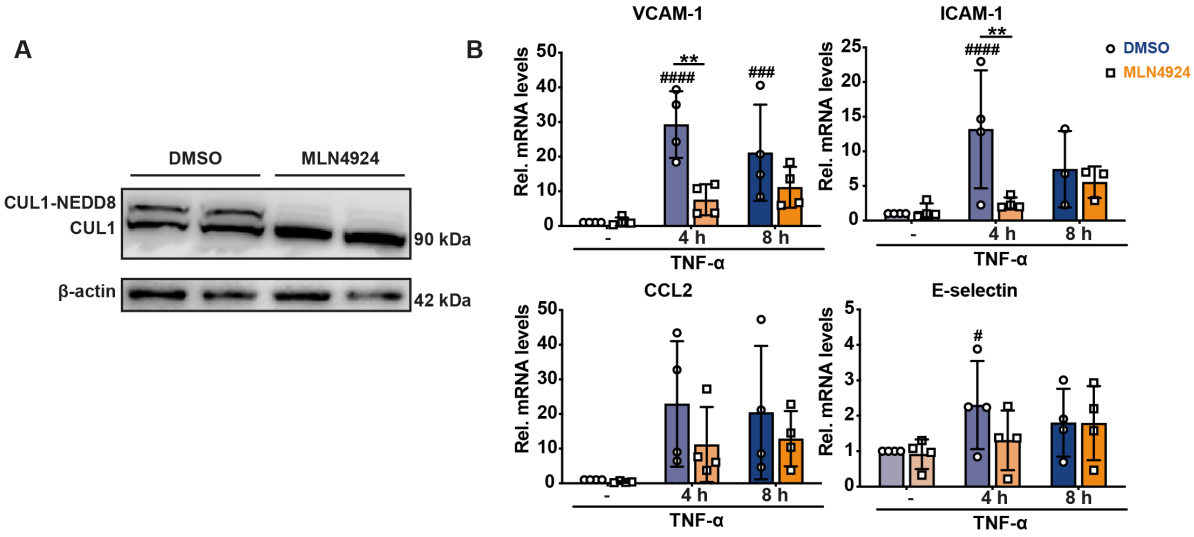

Figure 25: MLN4924 suppresses inflammatory responses in endothelial cells. hCMEC/D3 cells pretreated with DMSO control or MLN4924 were stimulated with or without TNF-α for the indicated time points. (A) Inhibition of CUL1-NEDD8 by MLN4924 in hCMNEC/D3 cells. (B) Relative *VCAM-1*, *ICAM-1*, *CCL2* and *E-selectin* mRNA expression levels were measured by qRT-PCR in TNF-α challenged hCMEC/D3 cells. mRNA levels were normalized to GAPDH and expressed relative to DMSO control without TNF-α treatment. Bars represent mean $\pm$ SD, n = 3-4; $^{**}P<0.01$, two-way ANOVA with Bonferroni post-test was checked for comparison with DMSO control; $^{\#\#\#\#}P<0.0001$, two-way ANOVA with Dunnett post-test was performed for comparison with non-TNF-α treated control in DMSO or MLN4924 pre-treated group.

To further confirm whether the suppressive effect of MLN4924 on the inflammation is associated with NF-κB signalling, we observed an accumulation of phosphor-IκB-α and a concomitant delayed P65 nuclear translocation, implying the effect of MLN4924 on CRL substrates degradation (figure 26). Consisting with BV2 cells (figure 20A, B), MLN4924 also blocks the MAPK pathway by reducing phosphor-ERK1/2 and P38 (figure 26C, D). Collectively, these results suggest that MLN4924 inhibits CUL1 neddylation and inflammation of microvascular endothelial cells correlated with NF-κB and MAPK signalling.

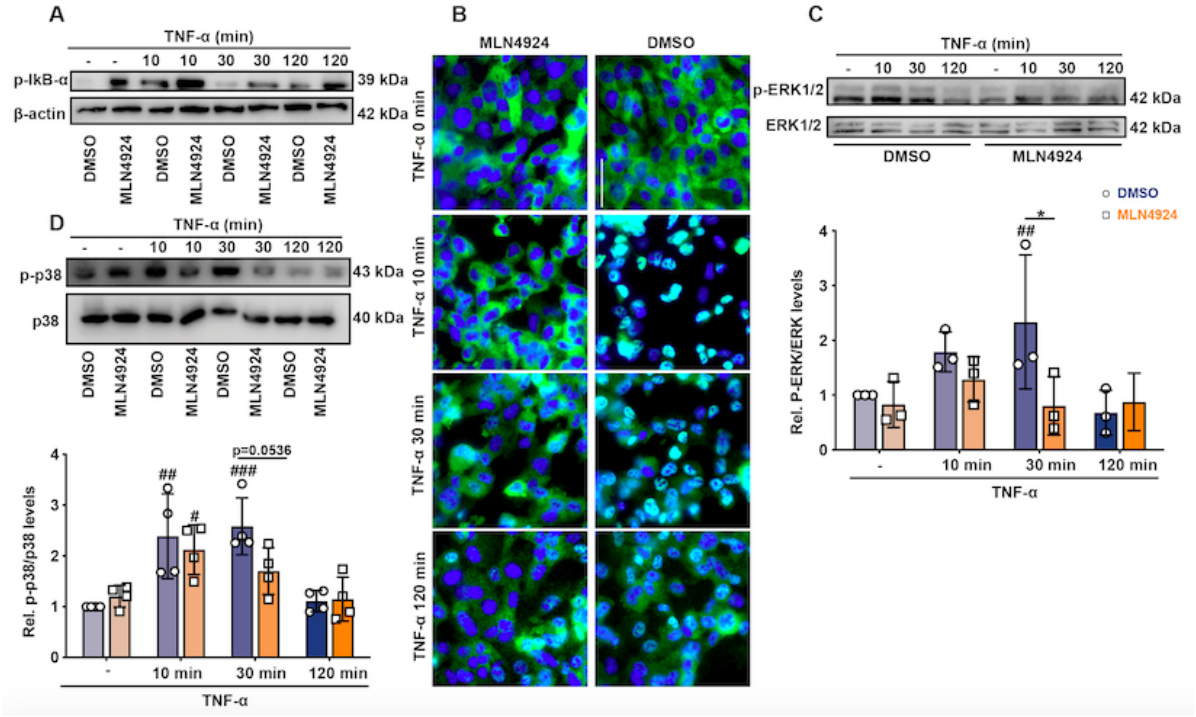

Figure 26: MLN4924 suppresses NF-κB and MAPK activation in inflammatory-elicited microvascular endothelial cells. hCMEC/D3 cells pretreated with DMSO control or MLN4924 were stimulated with or without TNF-α for the indicated time points. (A-B) MLN4924 reduces NF-κB activity in microvascular endothelial cells. (A) Representative Western blot images of three independent experiments for p-IκB-α and β-Actin in cell lysates of hCMEC/D3 cells under TNF-α. (B) The locations of P65 were determined by fluorescence microscopy. Blue, DAPI-stained nuclei; green, P65. Scale bar: 50 μm. (C-D) MLN4924 attenuates MAPK pathway signalling in microvascular endothelial cells. The expression levels and activation status (phosphorylation) of ERK1/2 (C) and p38 (D) were analyzed by Western blotting. Protein levels were quantified by densitometry and normalized to total ERK1/2 and p38. Bars represent mean $\pm$ SD, n = 3-4; $^{*}P<0.05$, two-way ANOVA with Bonferroni post-test was checked for comparison with DMSO control; $^{\#\#}P<0.01$, $^{\#\#\#}P<0.001$, two-way ANOVA with Dunnett post-test was performed for comparison with non-TNF-α treated control in DMSO or MLN4924 pre-treated group.

3.8 CSN5i-3 Exacerbates and MLN4924 Protects the BBB Integrity Loss Induced by the OGD/RO

One of the hallmarks of stroke is the BBB dysfunction, allowing the infiltration of peripheral immune cells to exaggerate the inflammation [220]. Given our observation that mimicking CSN5 hyperactivity exerts anti-inflammatory processes, we examined the influence of neddylation/deneddylation on the BBB function in the presence of

mimicking stroke by the OGD (figure 27A). OGD significantly increased HIF-1α levels in hCMEC/D3 cells (figure 27B). MLN4924 was shown to stabilize HIF-1α, which is controlled by the CUL2-RING ligase. Thus, this aligns with the reduction of ubiquitin ligase activity due to deneddylated cullin (figure 27B).

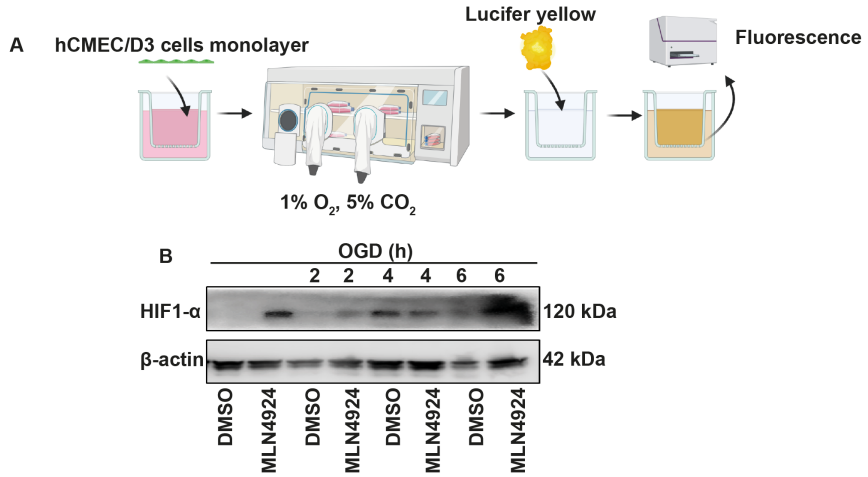

Figure 27: OGD increases HIF-1α expression levels and MLN4924 stabilizes HIF-1α in endothelium. (A) Schematic representation of hCMEC/D3 cell culture, OGD/RO conditions and lucifer yellow assay for determination of the endothelial barrier function. (B) Representative immunodetection of three independent experiments for HIF-1α expression in hCMEC/D3 cells. HIF-1α induced by OGD and MLN4924 stabilizes HIF-1α in endothelium.

In contrast to the prevention of deneddylation of CUL1 by MLN4924, we observed increased neddylated CUL1 upon CSN5i-3 incubation (figure 28A). Furthermore, to detect the effects of CSN5 on BBB permeability, we undertook a transwell assay using hCMEC/D3 cells (figure 27A). While OGD/RO dramatically enhanced microvascular permeability, MLN4924 protected this integrity loss and CSN5i-3 exacerbated it (figure 28B). Consistent with the above observations, OGD/RO weakened the staining for vascular endothelial cadherin (VE-cadherin) at extracellular cell-cell contact sites and CSN5i-3 enhanced these effects, whereas MLN4924 abolished them (figure 28C). Moreover, immunoblotting revealed that adhesion junction protein VE-cadherin and tight junction proteins occluding and claudin-5 were partially degraded after OGD/RO in the control and CSN5i-3 but not MLN4924 (figure 28D). These results support the view that CSN5 activity mediates the BBB integrity under OGD/RO.

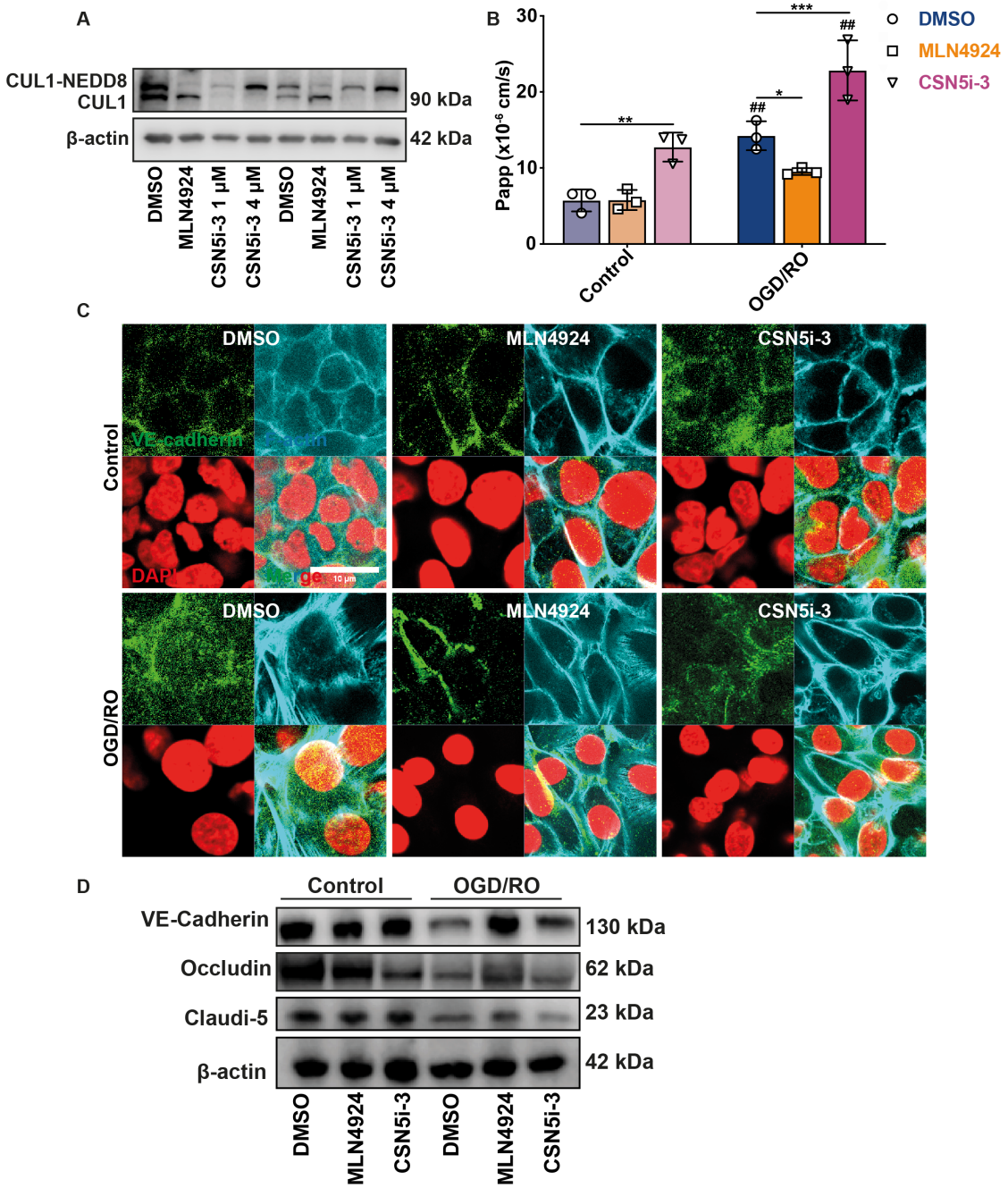

Figure 28: CSN5i-3 exacerbates MLN4924 protects the BBB integrity loss induced by the OGD/RO. (A) Western blot analysis of CUL1 neddylation after treatment with DMSO control, MLN4924 (500 nM) or CSN5i-3 (1 μM or 4 μM). (B) Evaluation of BBB permeability determined by lucifer yellow assay. Bars represent mean ± SD, n = 3; $^{*}P<0.05$, $^{**}P<0.01$, $^{***}P<0.001$, two-way ANOVA with Dunnett post-test was checked for comparison with DMSO control; $^{\#\#}P<0.01$, two-way ANOVA with Bonferroni post-test was performed for comparison with non-OGD/RO control in DMSO, MLN4924 or CSN5i-3 pre-treated group. (C) Assessment of F-actin (cyan) and VE-cadherin (green) in DMSO control versus MLN4924 or CSN5i-3 treated hCMEC/D3 cells upon non-OGD/RO or OGD/RO counterstained with DAPI (blue). Scale bar represents 20 μm. (D) Representative immunodetection of three independent experiments for VE-cadherin, occluding and claudin-5 in cell lysates of pre-treated with DMSO, MLN4924 or CSN5i-3 hCMEC/D3 cells control versus OGD/RO.

3.9 CSN5i-3 Aggravates and MLN4924 Attenuates Neuronal Damage Produced by OGD/RO

Having established the mediating efficacy of CSN5 by using MLN4924 and CSN5i-3 in multiple classical assays in vitro, we developed two new culture systems in our lab, the primary neuronal cell cultue and organotypic brain slice cultures (OBSCs). Mixed brain cells were isolated from cortexes of p0-1 neonatal pups and maintained in the medium which is designed for neurons only (figure 29A). To identify the neuronal cells in the culture, β-tubulin III was used as a neuron-specific marker (figure 29B). Moreover, we established OBSCs, in order to further study the effect of CSN5 in a physiologically relevant brain model which offers all the resident cell types (figure 29A). OBSCs were harvested from p5-8 mouse and maintained for two weeks. To characterise the newly introduced model, images from day 2 after in vitro and day 5 have been acquired, and the structure of the slice became more clear (figure 29C).

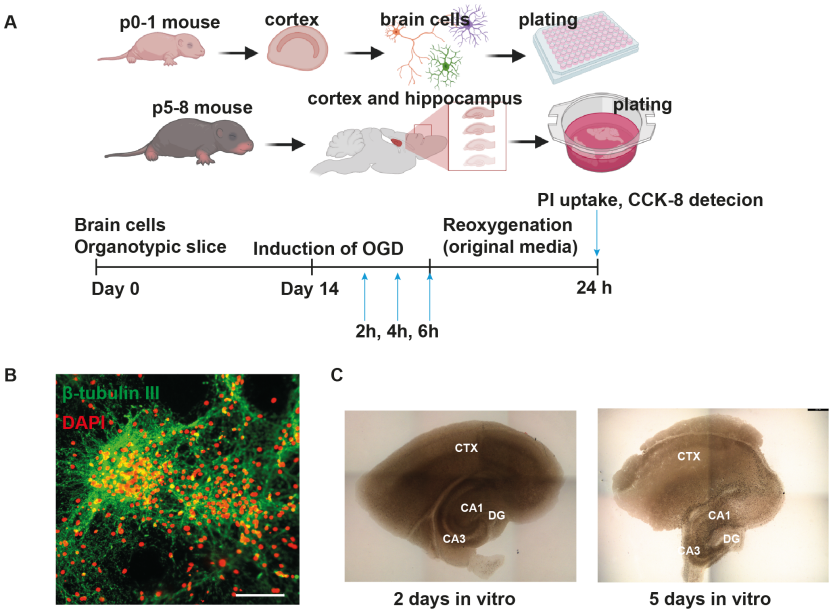

Figure 29: Establishment of primary neuronal cell culture and organotypic brain slice cultures. (A) Cartoon of an experimental modeling of isolated primary neuronal cells, as well as organotypic hippocampal and cortical slice culture in OGD/RO conditions. (B) Control primary neurons stained for β-III tubulin (green), a well-known neuronal marker and DAPI (blue). Scale bar: 100 μm. (C) Phase-contrast image of a control organotypic hippocampal and cortical slice 2 and 5 days after in vitro maintenance. Scale bar: 500 μm.

Neuronal death was finally investigated in primary neurons with or without OGD/RO (figure 29A, 30). OGD/RO significantly decreased neuronal viability in a time-dependent manner, and MLN4924 was able to attenuate neuronal death induced by 2 h and 4 h OGD/RO (figure 30).

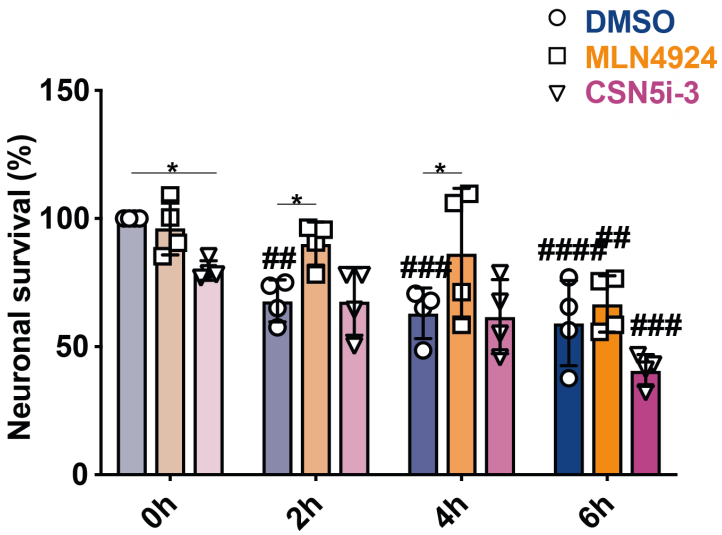

Figure 30: CSN5i-3 aggravates and MLN4924 attenuates neuronal damage produced by OGD. CCK8 showing neuronal cell viability of DMSO control, MLN4924 or CSN5i-3 pre-treated neuronal cells with or without OGD/RO. Bars represent mean ± SD, n = 4; $^{*}P<0.05$, two-way ANOVA with Dunnett post-test was checked for comparison with DMSO control; $^{\#\#}P<0.01$, $^{\#\#\#}P<0.001$, $^{\#\#\#\#}P<0.0001$, two-way ANOVA with Dunnett post-test was performed for comparison with non-OGD/RO control in DMSO, MLN4924 or CSN5i-3 pre-treated group.

To further examine the link between CSN5 and OGD/RO-induced neuronal cell death, we extended the cell viability assay to ex vivo (figure 31A). OGD/RO markedly increased propidium iodide (PI) uptake in the mouse hippocampal and cortical cultures, and the MLN4924 group has shown less propidium iodide (PI) uptake and CSN5i-3 enhanced the OGD/RO caused cell death comparing to the DMSO control, which is corresponding to the primary neuronal cells (figure 31B). Notably, there is a co-localization between the CX3CR1-eGFP microglia and the PI positive cells suggesting that the scavenger role of activated microglia was triggered by the dead cells (figure 31C). In addition, this co-localization was only present in the DMSO control and CSN5i-3 treated slices, and this is analogous to the microglia chemokinesis assay in vitro (figure 21B, C).

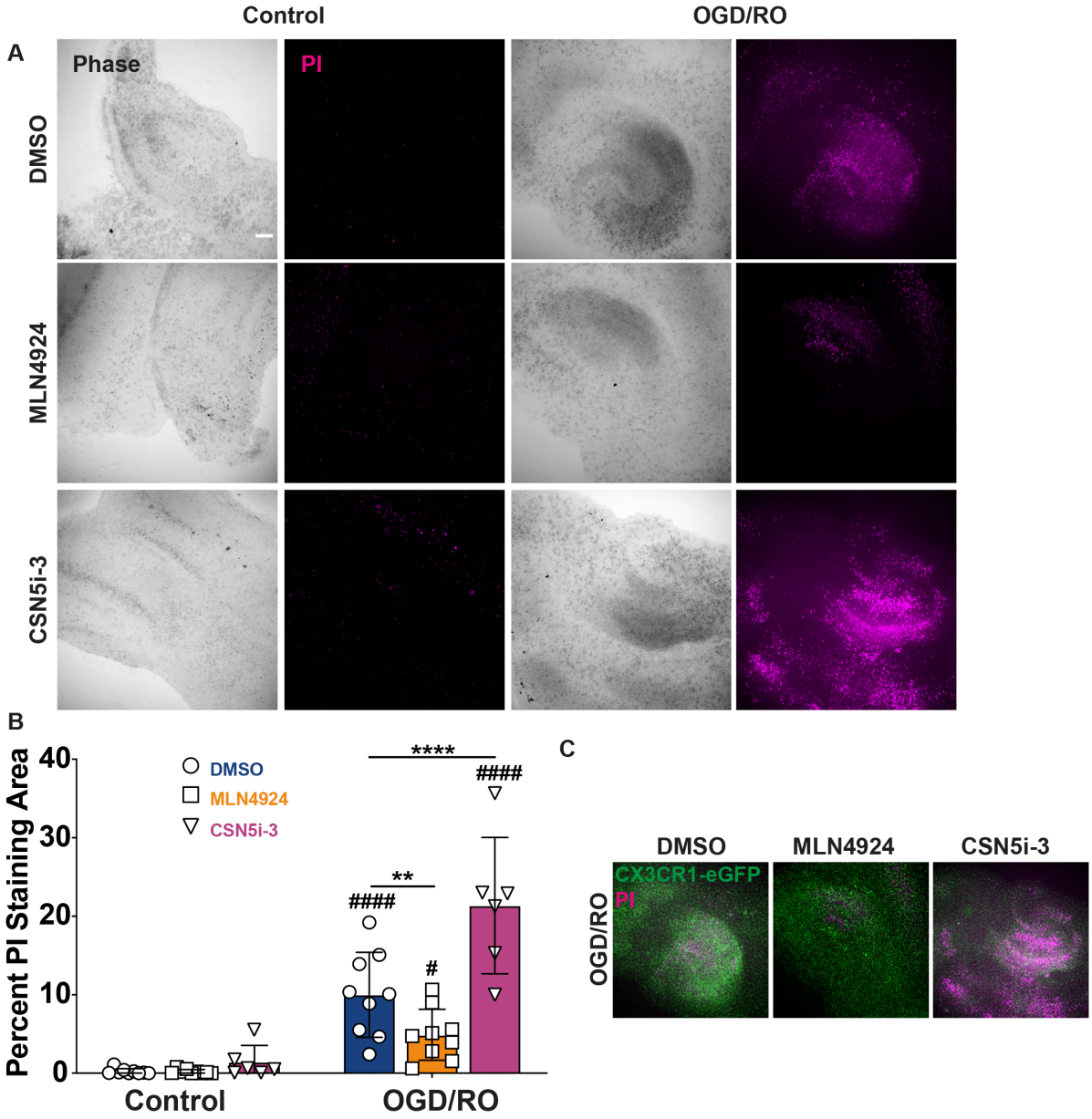

Figure 31: CSN5i-3 aggravates and MLN4924 attenuates neuronal damage produced by OGD. (A) Images of PI uptake in slices treated with DMSO, MLN4924 or CSN5i-3 exposed to non-OGD/RO or OGD/RO. Scale bar: 200μm. (B) The area of PI-positive (magenta) is normalized to the total area. Bars represent mean $\pm$ SD, n = 6-9; $^{****}P<0.0001$, two-way ANOVA with Dunnett post-test was checked for comparison with DMSO control; $^{\#}P<0.05$, $^{\#\#\#\#}P<0.0001$, two-way ANOVA with Dunnett post-test was performed for comparison with non-OGD/RO control in DMSO, MLN4924 or CSN5i-3 pre-treated group. (C) Locations of Cx3cr1-EGFP+ microglia (green) and PI positive cells (magenta) in the slices exposed to OGD/RO conditions. Scale bar: 200μm.

Moreover, to support the result that OGD/RO triggered increased PI positive areas, neuronal cells were stained by a neuronal marker, NeuN, and the NeuN areas were significant larger in the MLN4924 group under OGD/RO stress comparing to DMSO control (figure 32A, B). CSN5i-3 treatment showed a trend towards smaller NeuN expression area comparing to it in DMSO control. In summary, these results demonstrate that MLN4924 protects stroke outcome ex vivo and CSN5i-3 aggravates it.

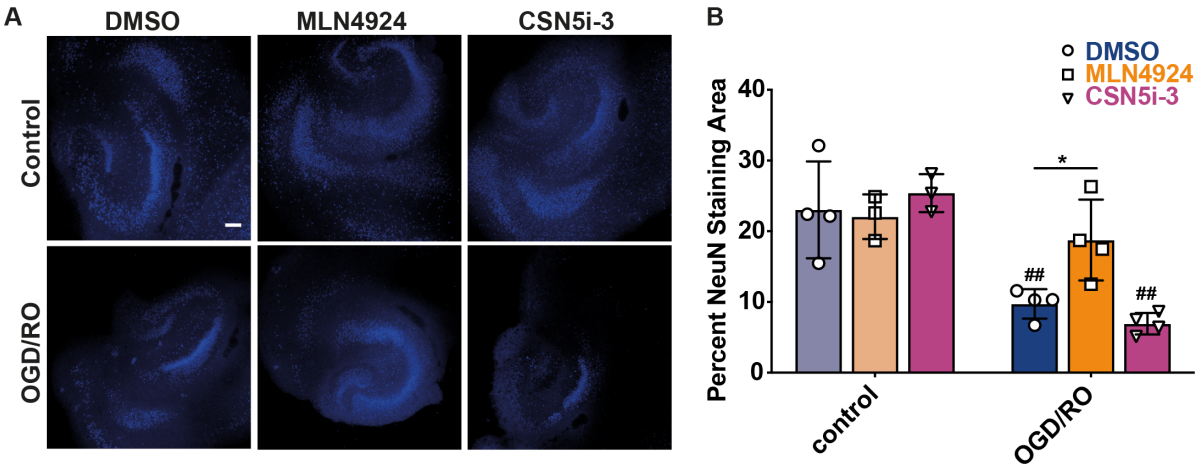

Figure 32: MLN4924 protects neuronal damage induced by OGD. (A) NeuN (blue) staining of brain slices treated with DMSO, MLN4924 or CSN5i-3 exposed to non-OGD/RO or OGD/RO. (B) The area of NeuN-positive (blue) is normalized to the total area. Bars represent mean ± SD, n = 3-4; $^{*}P<0.05$, two-way ANOVA with Dunnett post-test was checked for comparison with DMSO control; $^{\#\#}P<0.01$, two-way ANOVA with Dunnett post-test was performed for comparison with non-OGD/RO control in DMSO, MLN4924 or CSN5i-3 pre-treated group.

3.10 MLN4924 Changes Microglia Morphology and This Is a Reversible Process

Strikingly, the microglia morphology change that has been observed are the ones under MLN4924 and CSN5i-3 treatment. MLN4924 treated CX3CR1-eGFP microglia showed ameboid-like microglia and CSN5i-3 changed microglia to an activated shape (figure 33A) [221]. To address if the alteration of microglia morphology by the Cullin-neddylation states change is reversible, we have washed off the reagent after 48 hours, and microglia appear ramified within 72 hours (figure 33B). However, the link between

this morphology change and neuronal death requires a further study.

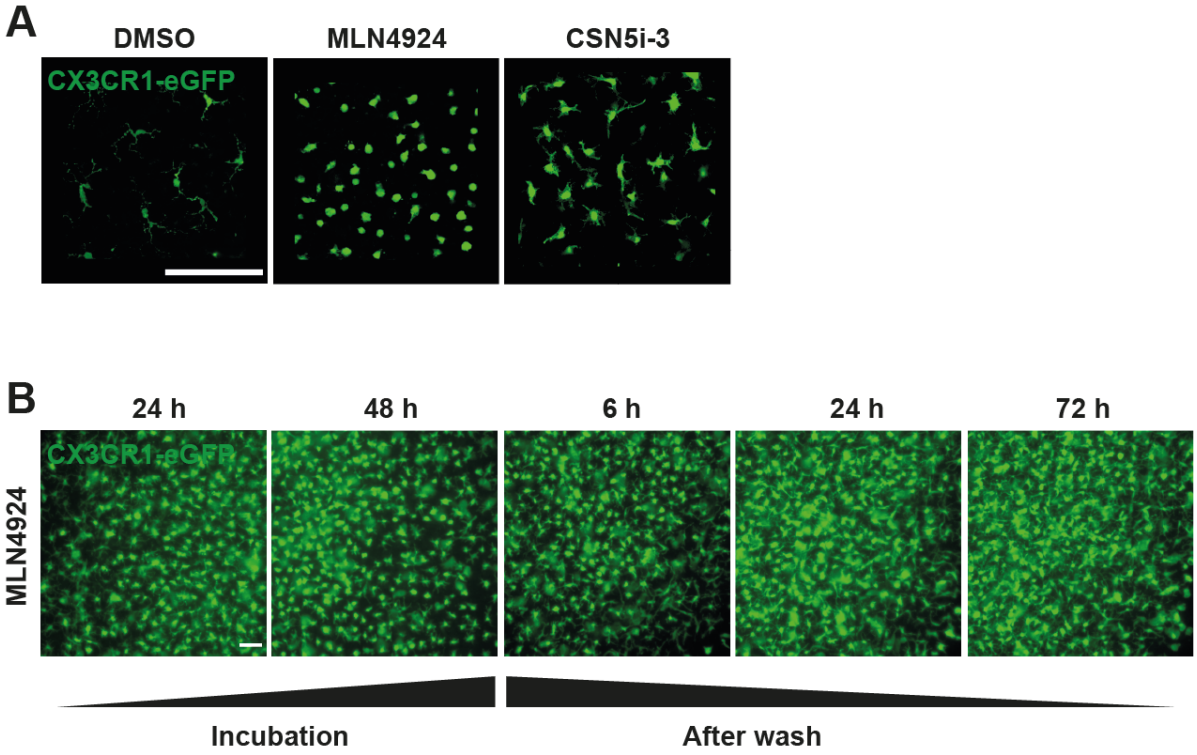

Figure 33: MLN4924 and CSN5i-3 change microglia morphology and it is reversible. (A) Representative images of nine independent experiments for Cx3cr1-EGFP+ microglia (green) different morphologies upon DMSO control, MLN4924 and CSN5i-3 exposure for 48 hours. (B) Representative images of four independent experiments for Cx3cr1-EGFP+ microglia morphology changing in the time course of MLN4924 treatment. Scale bar: 50 μm.

3.11 TNF-α Neutralization Protects Brain Damage Induced by OGD/RO

Collectively, we have observed that MLN4924 reduced the inflammatory response by inhibiting the proinflammatory cytokines and chemokines (including TNF-α) in activated microglia cells (figure 18), and attenuates neuronal damage produced by OGD. We then hypothesized that TNF-α neutralization by an antibody could also reduce the brain damage during OGD/RO. Indeed, PI staining indicated that neutralizing TNF-α by Infliximab decreased OGD/RO induced neuronal death ex vivo (figure 34).

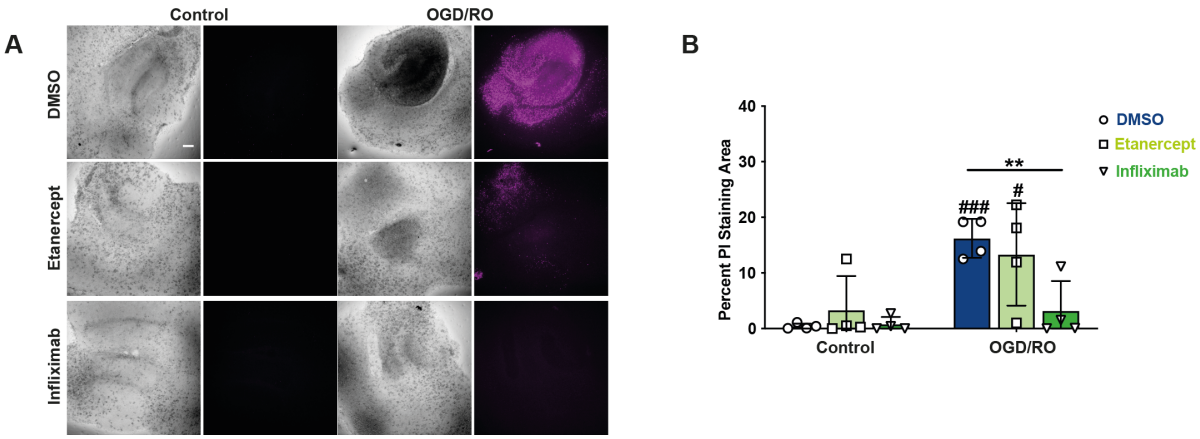

Figure 34: TNF-α neutralization protects brain damage induced by OGD/RO. (A) Images of propidium iodide (PI) uptake in slices treated with DMSO, Etanercept or Infliximab exposed to non-OGD/RO or OGD/RO. Scale bar: 200μm. (B) The area of PI-positive (magenta) is normalized to the total area. Bars represent mean $\pm$ SD, n = 4; $^{**}P<0.01$, two-way ANOVA with Dunnett post-test was checked for comparison with DMSO control; $^{\#}P<0.05$, $^{\#\#\#}P<0.001$, two-way ANOVA with Bonferroni post-test was performed for comparison with non-OGD/RO control in DMSO, Etanercept or Infliximab pre-treated group.

3.12 DCN1 Inhibitors Have No Effect on Microglia Phagocytic Activity

To further determine the activity of CSN on the NEDD8 pathway in the brain. MLN4924 is potent in achieving broad blockade of all CRLs, thus it is merely partially mimicking the CSN5 hyperactivity. To this end, it is also necessary to see the effect on blocking individual CRL members, and we have subsequently tested inhibitors of the defective in cullin neddlylation protein 1 (DCN1)-ubiquitin conjugating enzyme E2 M (UBE2M) interaction on the microglia phagocytic acticity. TNF-α increased the percentage of phagocytosis microglia, but DCN1 inhibition did not have any significant effect on the capacity of microglia phagocytose (figure 35A, B). The cullin 1 and 3 NEDDylation tests did not exhibit significant differences with DCN1 inhibitors in BV2 cells either (figure 35C, D). However, NAcM-COV reduced cullin 3 neddylation in hCMEC/D3 cells (figure 35E, F), and this suggested to check the expression levels of DCN1. Indeed, DCN1 (also known as DCUN1D1) expression levels in hCMEC/D3 is higher than in BV2 cells (figure

35G). According to the previous study that DCN1 expression levels partially correlates to the sensitivity of DCN1 inhibitors [222], we assume that DCN1 inhibitors have no effect on microglia phagocytic activity may due to the potential low expression of DCUN1D1 in BV2 cells. These results suggest further investigation of hCMEC/D3 cells with the DCN1 inhibitors, as well as other CUL family members in both cell lines.

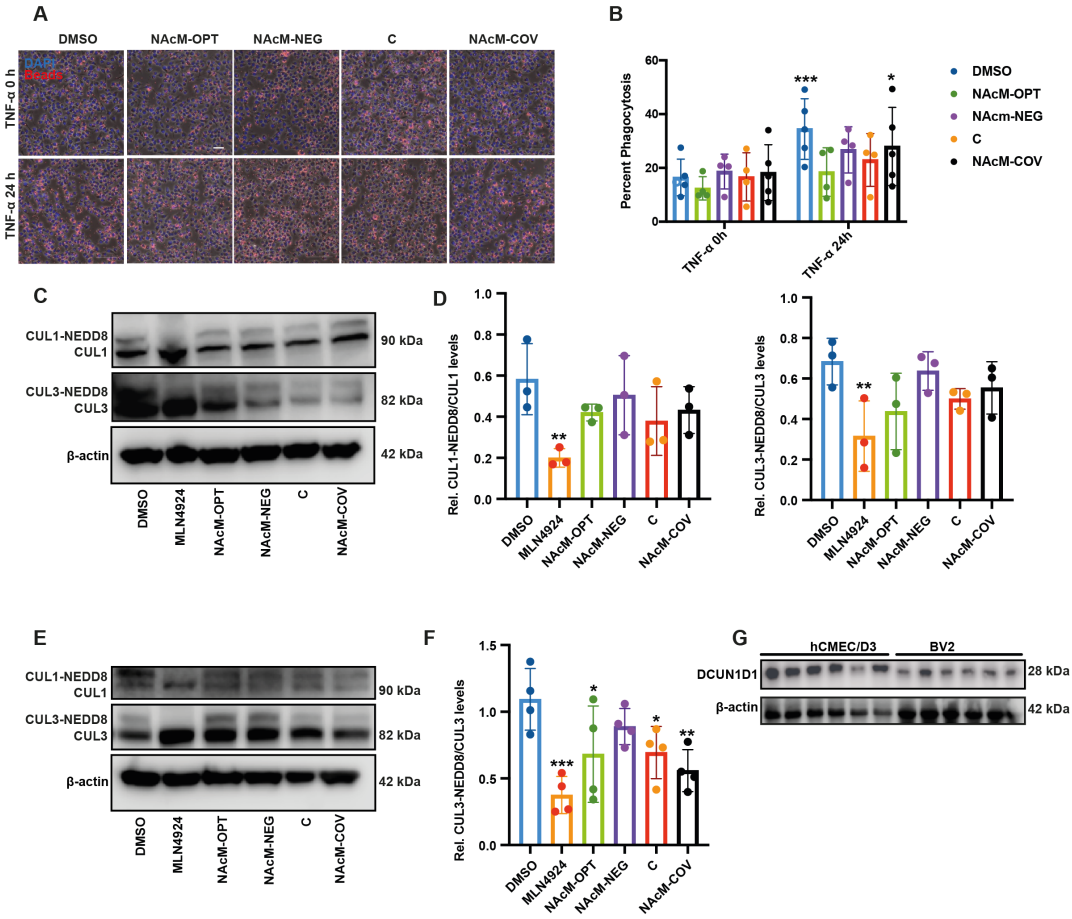

Figure 35: DCN1 inhibitors have no effect on microglia phagocytic activity. (A) Representative images of BV2 cells pre-treated with a DMSO control or NAcM-OPT, NAcM-NEG, C (detail unknown DCN-1 inhibitor compound), NAcM-COV and incubated with latex beads under treatment of TNF-α or non-TNF-α for 24h. Blue, DAPI-stained nuclei; red, latex beads. (B) Quantification of percent phagocytosis cells from A. Bars represent mean $\pm$ SD, n = 5; *P<0.05, ***P<0.001, two-way ANOVA with Dunnett post-test was performed for comparison with non-TNF-α control in pre-treated group. (C, D) Immunodetection of cullin 1 neddylation in BV2 cells and quantification. (E) Decreased cullin 3 neddylation by NAcM-COV in hCMEC/D3 cells. (F) A bar graph showing quantification of (E) from four independent experiments (mean $\pm$ SD, n = 4, *P<0.05, **P<0.01, ***P<0.001, one-way ANOVA with Dunnett's multiple comparison were performed for the statistical significance). (G)Representative immunodetection of two independent experiments for DCUN1D1 in BV2 and hCMEC/D3 cells.

4 Discussion and Outlook

In the current study, we provide evidence for the role of the COP9 signalosome subunit in attenuating neuroinflammation and stroke in vitro and ex vivo. We observe that MLN4924, a pharmacological inhibitor of NEDD8-activating enzyme (NAE), at least partially mimicking the hyperactivity of CSN5, reduces microglia and microvascular endothelial inflammation, protects BBB integrity under hypoxia conditions, and prevents oxygen glucose deprivation/reoxygenation-induced neuronal damage. In support of this finding, inhibiting CSN5 by a recently available small molecule inhibitor of the CSN5 deneddylase activity results in a disruption of BBB integrity and exacerbates ischemic outcome. With regards to the mechanism, our findings suggest these effects are mediated by the deneddylation of cullins, at least in part, owing to the negative regulation of inflammatory factor expression via the NF-κB pathway.

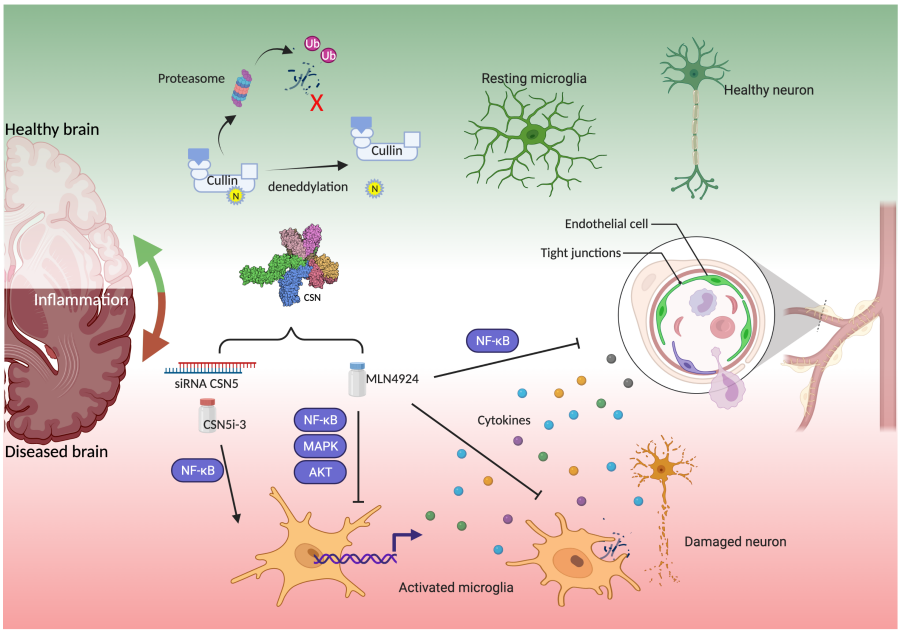

Figure 36: Graphical summary of the CSN5 in the neuroinflammation. Induction of brain inflammation initiates microglia activation, BBB disruption, neuronal damage, and also leads to cytokine secretion and leukocyte infiltration. Based on the deneddylation function of CSN, mimicking hyperactivity of CSN5 by MLN4924 can reduce microglial and endothelial inflammatory signaling, BBB permeability and neuronal death. On the contrary, inhibition of CSN5 activity accelerates inflammatory processes. The scheme was generated with BioRender.

4.1 Expression Levels of CSN Subunits

Previous studies demonstrated that the CSN is essential for mouse embryonic development. Using knockout technology, targeted disruption of CSN subunits led to embryonic lethality [223–226]. CSN8 is the only subunit that has been looked at in embryo development, and it is expressed throughout the whole early mouse embryo development, starting from zygote, preimplantation embryos, continuing to post-implantation embryos, predominantly located in the inner cell mass of E3.5 blastocyst and highly expressed in E9.5 embryos [227]. In humans, CSN5 and CSN6 are observed in a variety of human cancers including breast cancer [228], glioblastoma [229], hepatocellular carcinoma [230], ovarian cancer [231] and pancreatic carcinoma [232]. However, the expression levels of CSN subunits in normal tissues of mice and humans have so far not yet been systematically studied and documented.

In this thesis, we have collected the gene expression profiles of CSN5 from GTEx Analysis Release V8 and staining data of CSN5 in human brain from the Human Protein Atlas (figure 11). In agreement with human results, two sets of scRNA data of mouse pups at p0 and adults from Gene Expression Omnibus (figure 13) were analyzed and revealed that the CSN subunits in both mouse and human brain are highly expressed and display little cell specificity. This is an agreement with our hypothesis and previous research by many other laboratories that the COP9 signalosome is found in all eukaryotes and is essential for mammalian development [51]. Subsequently, the scRNA analyses also suggested that CSN subunit levels remain comparable upon LPS challenge (figure 13D, E). This is, however, distinct from upregulated translation levels of CSN5 in atherosclerotic endothelium [85] and cancer tissues (described in the last paragraph) suggesting further studies on the protein level in inflamed brain tissue. Also, recent studies into mRNA-protein relationship have shown a poor correlation between mRNA and proteins with merely hovering around 40% explanatory power [233, 234], and this would argue for an exploration of the correlation between mRNA and proteins of CSN subunits in future research.

4.2 MLN4924 and CSN5i-3 in Microglia

Over the last decade, CSN has been suggested to play a significant role in the modulation of multiple cancers by regulating cell cycle control, signal transduction as well as apoptosis [235, 236]. This has led to the potential use of CSN as a biomarker and therapeutic target for cancer patients [237]. Thereby, MLN4924, a neddylation inhibitor, as mentioned in the result chapter, has been discovered and tested to exert excellent anti-tumor effects by initiating apoptosis induction, senescence as well as autophagy via antagonizing NEDD8-related protein degradation [238]. Similarly, but differently in relevant respects, CSN5i-3, a CSN5 inhibitor has been later found to suppress tumour cells and growth of human xenografts in mice [239]. Furthermore, the role of the CSN as a control hub for CRLs has been studied in inflammation and cardiovascular diseases such as atherosclerosis and cardiomyopathy [103, 186, 240]. Some recent studies linked CSN with some mediators, leading to regulate stroke outcome. For example, CSN3 stabilising suppressor of cytokine signaling 3 (SOCS3) could restrict neuroinflammatory responses during ischemia [179], and MLN4924 may be beneficial in stroke [241]. However, the role of CSN in microglia-associated neuroinflammation and stroke including the involved mechanisms remain mostly unknown.

In this regard, our study fills an important research gap as to how, mechanistically, the CSN mediates neuroinflammation and stroke. In line with our previous study on macrophages in the context of atherosclerotic inflammation [103], *Tnf-*α, *Il-6*, and *Ccl2* mRNA expression levels were potently suppressed by MLN4924 in microglia (figure 18), indicating that MLN4924 treated microglia produce lower levels of pro-inflammatory cytokines. Additionally, these pro-inflammatory cytokine expression is elevated in cerebral ischemia and they usually represent M1 type microglia, which would contribute to neuronal apoptosis [242, 243]. Therefore, our results suggest neuroprotective effects of CSN5 by reducing microglial inflammation.

Another important characteristic similarity shared between microglia and macrophages

is their ability to phagocyte. Upon central nervous system injury, such as stroke, phagocytosis is initially performed by microglia and then followed by the recruited macrophages. Phagocytosis of apoptotic cells with an “eat-me” signal and the removal of damaged myelin may be beneficial, as it prevents release of cytotoxic and promotes axon regeneration and remyelination [202, 241]. However, live neurons may be phagocytosed by microglia. For example, in peri-infarct ischemia area, inflammation induces the reversible exposure of the neuronal “eat-me” signal phosphatidylserine, leading to the phagocytosis of stress-related but still living neuronal cells and resulting in brain atrophy and motor dysfunction [29]. A similar phenomenon has also been shown in other studies. Bal-Price’s group noticed that rapid phagocytosis of dead or dying cells leads to disappearance of neurons without any increase in apoptotic or necrotic cells, and with a mere blockade of this phagocytic activity despite the ongoing inflammatory condition, more neurons survive rather than die [244, 245]. Therefore, preventing loss of viable brain tissue in the peri-infarct areas and reducing neuronal death in the inflammatory process by blocking microglia phagocytosis is beneficial. Our observation that MLN4924 reduces TNF-α induced microglia phagocytic activity (figure 16), and particularly, that SCF-dependent ubiquitylation and proteasomal degradation mediate phagocytosis has been shown before [246]. As a consequence of MLN4924 reducing and CSN5i-3 increasing neuronal death upon OGD/RO (figure 29), CSN5 controlling microglial phagocytosis activity might be a potential therapeutic target for stroke.

Considering the cell culture system, microglia cultures, including primary microglia, human immortalized microglia (e.g. HMO6), retroviral immortalized microglia (e.g. BV2) and spontaneously immortalized rodent microglia (e.g. HAPI cells), are very commonly used to examine neuroinflammatory phenomena [247]. In this thesis, we have used BV2 cells and primary microglial cells. Primary microglia were extracted directly from p0-p1 mouse pups, having similar functional characteristics comparable to the endogenous cells, including secretory products and cell surface markers [247, 248]. Especially in AD studies, it has been shown that *in vitro* primary microglia contribute to

the same amyloid-β clearance by its phagocytic ability, and this is due to the amoeboid state of microglia which is the only type from the isolation procedure[249]. The amoeboid microglia are usually the M2 state microglia acting as an anti-inflammatory type, with the function of ingesting cell debris, promoting tissue repair, as well as releasing neurotrophic factors. Additionally, amoeboid state *in vitro* can be changed only by stimulation with agents, such as retinoic acid [250]. Considering this limitation and the time consuming preparation (14 days) in primary microglia, we have only used pure primary microglia for the phagocytosis assay, but an immortalized cell line, BV2 and mixed brain cells for the other experiments. BV2 cells have been originally generated from primary microglia cells by infecting a v-raf/v-myc carrying retrovirus (J2) [251]. An assessment of BV2 cells for microglial markers showed a 90% positivity rate for non-specific esterase activity, all lacked peroxidase activity, as well as similar phagocytic ability [251], and BV2 cells have been positively used in a lot of studies related to brain disorders. However, in some stimulatory respons, BV2 cell line shows similar activities to primary microglia, yet not to the same extent [252]. In our study, the percent phagocytosis of BV2 cells is 20%, which is similar to others' [253]. The isolated primary microglia were observed with higher phagocytic capacity in this study within the same incubation time (all cells had uptaken beads, result not shown here), so we have shortened the experiment time. This higher phagocytic capacity of primary microglia has also been shown before [254]. So the phagocytosis experiment was shortened in primary microglia, and the results are similar to some studies as well [255]. Moreover, the BV2 cell line is only for the *in vitro* murine model. Together, it would be important to extend the experiments of MLN4924 and CSN5i-3 to human immortalized microglia and mouse *in vivo* in the future.

4.3 The CSN and NF-κB Signaling Pathway

NF-κB encompasses a group of five structurally related inducible transcription factors: NF-κB1 (also known as p50), NF-κB2 (also known as p52), RelA (also known as p65),

RelB, and c-Rel [256]. These family members form as hetero- or homo- dimers that transactivate a large array of genes by interacting with a κB enhancer. Given normal condition, NF-κB is sequestered in the cytoplasm under the control of a family of inhibitory proteins, including IκBs [257]. When cells are exposed to a multitude inflammatory stimuli, NF-κB can be activated through two distinct pathways: the canonical (also known as classical) and noncanonical (also known as alternative) [257]. The canonical NF-κB pathway can be activated by diverse stimuli, including TNF-α and IL-1. When canonical NF-κB is activated, IKK rapidly phosphorylates IκB leading to an IκB ubiquitination and proteasomal degradation, which releases the NF-κB dimer into the nucleus for gene transcription. Importantly, IκB-α ubiquitination is done through the SCF$^{\beta\text{TrCP}}$-CRL. Thus, IκBα is a CRL substrate [210], and this links the CSN to the NF-κB pathway. Additionally, past studies outlined the involvement of CSN in NF-kB activation in endothelial cells, myeloid cells, T cells, Hela cells, cardiomyocytes, cardiac fibroblasts, and MLN4924 reduced NF-kB signaling in B-cells, cervical cancer cells, myeloid leukemia cells, and macrophages [83, 103, 176, 186, 258].

Moreover, since it was first observed that the expression of RelA/p65 and NF-κB1/p50 was enhanced in human cerebral infarction [259], NF-κB has always been considered a central modulator of neuroinflammation and stroke. For example, IKK/NF-κB dependent microglia activation elevates kainic acid-induced neuronal death through the induction of inflammatory mediators [260]. Hence, we assumed that MLN4924 treated microglia and endothelial cells express lower levels of pro-inflammatory cytokines and adhesion molecules, respectively, are partially due to the NF-κB pathway. MLN4924 rapidly accumulates phosphorylation of IκB-α and blunts RelA/p65 nuclear translocation, and thus indeed blocked NF-κB activation. Additionally, MLN4924 had no effect on the basal NF-κB levels (figure 19A).

On the other hand, the role of CSN in the fine-tuning of NF-κB is also checked by silencing and inhibiting CSN5. Although whether steady levels of IκB-α interfered with the CSN is controversial, CSN2 and CSN5 knockdown increased basal IκB-α in HeLa cells, but decreased in thymocytes and HUVECs [85, 258, 261]. Our data show that

silencing CSN5 resulted in a reduced IκB-α and increased p65 activation, suggesting a cell-specific reason. However, knockdown and inhibition of CSN5 both reduced the re-accumulation of the CRL substrate IkB-α after its TNF-α-induced degradation, and this is comparable to the results that were obtained in HeLa cells during CSN2 and CSN5 knockdown and CSN5 silencing in HUVECs [85, 261].

4.4 Neddylation Independent Activities of MLN4924

We observed that MLN4924 blocked TNF-α-induced activation of the MAPK pathway in microglia and microvescular endothelial cells, and this contributes to the inhibition of inflammatory cytokines expression along with the NF-κB pathway. Similar phenomena were observed in a pulmonary fibrosis study, where MLN4924 was confirmed to act against bleomycin-induced pulmonary fibrosis by abrogating NF-κB responses, MAPK activity and the secretion of TNF-α-induced proinflammatory cytokines and MCP1-elicited chemokines [262]. In terms of the mechanism, this might be due to the recently discovered activities of MLN4924 which are independent of the well-characterized blockade of neddylation activity. These activities are listed as follows:

MLN4924 triggers epidermal growth factor receptor (EGFR) activation through EGFR dimerisation and furthermore targets its downstream signalling pathways including RAS/RAF/MEK/ERK and PI3K/AKT1/mTOR pathways, resulting in raised tumor sphere formation, accelerated EGF-regulated wound healing, as well as inhibited ciliogenesis [263–265].

Extracellular acidification rate (ECAR) is an indicator for measuring glycolytic activity. MLN4924 was found to increase ECAR, cellular utilization of glucose, production of glycolysis and its products (pyruvate and lactate), as well as to affect energy metabolism. Concerning the mechanism, this is via MLN4924 function in enhancing pyruvate kinase M2 (PKM2) tetramerisation [266].

MLN4924 reduces IL-17A-regulated activation of NF-κB signalling pathway to attenuate pulmonary inflammation through two possibilities. One is that MLN4924 stabilizes IκB-α (a CRL1 substrate mentioned in the last section). The other one is that MLN4924 blocks the binding between NF-κB activator (ACT) 1 and tumor necrosis factor receptor-associated factor (TRAF) 6, yet how MLN4924 targets this protein-protein interaction remains unclear [267].

Using a luciferase-based reporter analysis and a ChIP-based DNA binding analysis, MLN4924 was found to inhibit interferon regulatory transcription factor (IRF) 3 interaction with the interferon-β (IFN-β) promoter to reduce the production of IFN-β in mouse peritoneal macrophages and *in vivo* [268].

MLN4924 itself or together with TNF-related apoptosis-inducing ligand (TRAIL), initiates apoptosis to decrease cell survival. MLN4924 induces the activation of the c-Jun N-terminal kinase (JNK) pathway, and JNK activation downregulates cellular FLICE-inhibitory protein (c-FLIP) which suppresses apoptosis. Therefore, MLN4924 promotes TRAIL-triggered apoptosis. [269].

4.5 CSN in the BBB Integrity

Fundamentally, the microvascular endothelial cell is a key component of the BBB which controls CNS homeostasis, and the dysfunction of the BBB is strictly associated with pathophysiology disorders including stroke [270]. In order to study the BBB *in vitro*, we have chosen the brain microvascular endothelial cell line hCMEC/D3 which is grown relatively easily, reproducible, and more importantly, it is closely mimicking the *in vivo* phenotype. This cell line was developed in 2005. The cerebral microvessel endothelial cells were derived from human temporal lobe microvessels and the microvessels were originally collected from tissue excised in the surgery for epilepsy control, and

transduced by lentiviral vectors incorporating human telomerase or SV40 T antigen. According to which stable immortalized clones were selectively isolated by limited dilution cloning, one was selected for expression of brain endothelial markers [271]. Since then, hCMEC/D3 has been studied on different aspects of brain microvascular endothelial biology and pharmacology [272]. In the later studies, monolayers of hCMEC/D3 are detected positive for adhesion and tight junction proteins including VE-cadherin, and if grown as confluent monolayers show restricted permeability to different hydrophobic and hydrophilic low molecular weight compounds such as lucifer yellow [271, 273]. Together, this makes hCMEC/D3 a suitable tool for our study. There are, however, shortcomings, and one is that monolayers of hCMEC/D3 develop a mere low to medium value of transendothelial electrical resistance (TEER), around 30-50 Ωcm^2 in multiple reports [272], also in this study (around 30 Ωcm^2), but the TEER levels of BBB *in vivo* are above 1000 Ωcm^2 [274]. Therefore, a future direction to increase the TEER levels and to get closer to an *in vivo* environment is to co-culture hCMEC/D3 with other cells, such as astrocytes.

Our data revealed that OGD/RO elicites a BBB hyperpermeability, and neddylated cullins by CSN5-i3 renders the weakened barrier more vulnerable. Conversely, blockade neddylation cullins by MLN4924 protects the BBB integrity upon OGD/RO. By contrast, a previous study demonstrated that MLN4924 increases HUVECs permeability in a time dependent manner via the cullin-3-Rbx1-KCTD10 complex regulating K63 ubiquitination of RhoB [275]. Knock-down of Cullin-3 by siRNA and long treatment (72 h) with MLN4924 would deplete VE-cadherin protein localized at the cell membrane. Short term treatment with MLN4924 combined with drug increased RhoB also leads to a higher permeability of the cultured HUVECs [275, 276]. Additionally, disrupted cullin neddylation in the opposite way by CSN5-i3 induced expression of RhoB as well [276]. Hence, they concluded that Cullin-3 is the key regulator of RhoB degradation and HUVECs integrity. Another study identified that Cullin-2-Rbx1-SRS is the key regulator of RhoB degradation in liver cancer cell line [277]. Together, these studies indicate a

tissue-specific activity of cullin isoforms as well as substrate receptors. In particular, these light up our future approach to the time course of the MLN4924/CSN5-i3 treatment and microvascular endothelial cells specific CRL-substrate related to the permeability. Nevertheless, our finding is more alike to a HMEC-1 cell study in which MLN4924 ameliorated barrier dysfunction induced by LPS [180] and MLN4924 prevented oxidized low-density lipoprotein (OxLDL)-induced HAEC dysfunction [278]. On one hand, this is in agreement with the previous studies, suggesting a cell specificity or a different CRL substrate manner. On the other hand, our study is focusing on the OGD/RO later time point (6h), and the delayed BBB leakage is mainly contributed to the gelatinase B/MMP-9 activity [279, 280]. MLN4924 was shown to repress MMP9 and inhibitors of MMP9 reduced barrier leakage 4-6 post OGD, indicating that regulating MMP9 through NEDDylation may be a target for the BBB integrity loss in stroke [280]. However, there are some limitations to the current study: An early leakage time study is needed, and in the chronic stage of ischemia, MMPs participating in tissue repair ought to be considered in the future research.

4.6 CSN in Stroke

4.6.1 CSN in Primary Neuronal Cells

To shed some light on the initial effect of CSN in stroke, we first investigated whether CSN has impacts on neuronal cell death triggered by OGD/RO. Although neuronal cell lines are commonly applied to investigate neurobiology and neurotoxicity, and much easier to handle compared to the primary neuronal cells, there remain some differences to neurons *in vivo* and disadvantages of the immortalized neuronal cells lines. For example, such cell lines are easily induced to display physiological differences comparing to the original cell which they were derived from [281, 282]. Therefore, we decided to use more genetically stable neurons, the primary neuronal cells for our model, and using a classic lineage-specific marker for neuronal cells, β-tubulin-III, to check the purity of the culture [282].

Oxidative injury, which indicates to an excessive generation of ROS, is the fundamental pathogenesis of ischemic stroke [283], and this can be mimicked in cultured neuronal cells by an OGD/RO procedure [284, 285]. In this thesis, OGD/RO enhanced neuronal death, and MLN4924 markedly attenuated neuronal death upon OGD/RO. This protective function of MLN4924 has been shown before in a previous study where MLN4924 significantly reduced H_2O_2-induced cerebellar granule neurons damage. This cytoprotective effect of MLN4924 functions through diminishing the ROS production by the accumulation of nuclear factor E2-related factor 2 (Nrf2) protein [178]. Nrf2 was shown to be one of the master mediators of endogenous antioxidant defense. Under normal circumstances, Nrf2 is restricted by the Cullin-3-Rbx-1-Keap-1 with a short half-life of less than half an hour [286]. But in response to oxidative stress, Nrf2 then become dislocated from Keap1, and enters the nucleus, heterodimerises with small musculo-aponeurotic fibrosarcoma (Maf) proteins, interacts with ARE and triggers the transcription of a battery of antioxidative genes [287]. In addition to the study which Cullin-3-Rbx-1-Keap-1 regulates Nrf2, recent studies revealed a novel pathway for Nrf degradation which function under some circumstances such as oxidant or electrophilic injury, and are controlled by Cullin-1-β-TrCP ligase [288]. Notably, these "dual degradation" pathways are both controlled by the CRLs and thus by the CSN. The role of Nrf2 pathway in stroke as well as the potential clinical interventions of ischemic stroke by targeting Nrf2 have been studied over the past years, and the controlling role of CSN in this pathway has been clarified too [289]. However, the connection between CSN and stroke has not been revealed, and this thesis shows great promise for the future studies.

4.6.2 CSN in Organotypic Slice

Following up on our the observation of CSN in microglia, microvascular endothelial cells and primary neurons, we used brain slices as an *ex vivo* model for stroke. The organotypic slices provide unique advantages comparing to other *in vitro* and *in vivo* platforms in that

they maintain many characteristics of *in vivo* biology, including the tissue architecture of the brain and neuronal activities, and simultaneously, they are easy to access and control precisely, compared to *in vivo* [290]. Additionally, many pharmacological manipulations in the studies of neurochemical behaviors *in vivo* have been shown to be reproducible in organotypic slice culture [291, 292]. Another consideration is that only two papers have demonstrated that MLN4924 could pass across the blood-brain barrier by the effect on glioblastoma or stroke [179, 293], and no evidence yet for whether CSN5-i3 crossing the blood-brain barrier. Generally, only compounds with a low molecular weight ($\leq$400Da) and lipid soluble molecules may cross the BBB [294]. Even though MLN4924 and CSN5-i3 are both lipid soluble, but at respective molecular weights of 443.2 g/mol and 505.57 g/mol, the efficiency is unclear of them delivering into the brain by subcutaneous injection. Overall, the organotypic slice is most suitable for this study here, *in vivo* studies are nevertheless required in the next step.

Consistent with the protective role of CSN in vitro and other studies that both neddylation inhibition and CSN3 showed protective function against ischemic stroke [179, 295], we speculate that CSN5 exerts a protective role in the ischemic condition. Our data demonstrated that the anti-inflammatory and protective BBB effects of MLN4924 were accompanied by reduced neuronal death in the organotypic brain slice culture, and converse results were observed by CSN5i-3.

Furthermore, we examined the most suppressed pro-inflammatory cytokines upon MLN4924 in microglia (figure 18), TNF-α. We showed that inhibition of TNF-α by Infliximab, but not Etanercept, also leads to the reduction of neuronal death, indicating that MLN4924 offered protection against OGD/RO which partially depends on the blocking TNF-α level. Anti-TNF-α therapy has been identified clinically for the treatment of rheumatoid arthritis (RA) [296]. The modulating immune process activity of TNF-α requires the interaction with its two receptors, TNF receptor 1 (TNFR1) and TNF receptor 2 (TNFR2) [297]. Currently, there are three anti-TNF-α drugs: infliximab,

etanercept and adalimumab which haven been proven to suppress RA. The two main strategies of TNF-α neutralization are monoclonal IgG antibody (e.g. Infliximab, a mouse-human chimeara monoclonal antibody) and soluble TNF-α receptor (e.g. Etanercept, a soluble TNFR2-Fc recombinant) [298]. Due to the different structures, the main functional differences between infliximab and etanercept can be listed as follows: a. Infliximab binds both active and inactive forms of soluble TNF, whereas etanercept only binds to the active form [299, 300]. b. Infliximab and TNF-α form stable complexes, whilst etanercept forms unstable complexes which allow dissociation of TNF-α [299]. c. Etanercept is capable to bind TNF-β [301]. d. Infliximab can lyse cells that express TNF-α on their surface, but not etanercept [302]. Because of the variation between those two inhibitors, we have observed only infliximab reduced brain damage during OGD/RO. This function of infliximab has been shown in a tMCAO mouse model with RA, where infliximab reduced the stroke infarct volume, increased neurological performance, and protected BBB disruption [303]. However, there is no comparison between WT tMCAO mice with and without infliximab in this study. Additionally, two studies have demonstrated that etanercept showed no effect on the infarct volume of pMCAO mice, but improved functional outcomes [255, 304]. This is similar to our study, and we may come to the functional outcomes in the mouse model in the future. One limitation of this study is the use of DMSO as a control to Infliximab and Etanercept. IgG antibodies are able to regulate immune responses through interacting with Fc receptors alone [305], therefore, an isotype IgG control is more reasonable in this study.

In addition, microglia morphological transformation also plays a role in neuroinflammation and pathological progression [306]. When the inflammation starts after stroke, the activation states change of a microglia will reflect in its morphology change. Resting/surveilling microglia are highly ramified with long processes and a small soma [307]. A rapid morphological transformation happens once damage associated molecular patterns are in the microenvironment. Ramified microglia transform to an amoeboid cell type in a short time, and the new morphology allows them to migrate to the injury,

as well as to phagocytose [308]. However, the two classes of microglial shape cannot present the whole range of microglial morphological changes. Therefore, some tools for microglial morphological quantification have been created. For example, Liesz's lab has developed an automated image analysis tool, which can analyze microglia from Z-stack 3 dimensions images based on a novel algorithm [309]. This new method and our microglia phenotypes upon the neddylation states change, suggest future studies to quantify, identify and elucidate the different roles of microglia.

5 Summary

Ischemic stroke constitutes one of the main reasons for death and disability globally. The only pharmacological therapy of acute ischemic stroke is rtPA, and it has a short administration time window as a limitation. Thus, a minority of stroke patients is able to benefit from these options, and the majority of stroke patients obtain a poor outcome. Although a thousand of translational stroke studies have been conducted in the past, essentially all failed in clinical trials. Therefore, novel strategies for the treatment of post-stroke pathophysiology are urgently needed.
Microglia-associated neuroinflammation is a crucial pathological event of ischemic stroke, which causes a secondary damage of the brain and leads to a poor recovery outcome. Microglia can rapidly undergo different functional and morphological changes due to the subtle changes in the brain. M1 type microglia are associated with a pro-inflammatory response, which damages neurons and BBB. In contrast, M2 type microglia produce anti-inflammatory factors and promote neuronal repair. Thus, modulation microglial polarization in different stages of ischemic stroke would be a good therapeutic strategy. Moreover, our previous study showed an anti-inflammatory function of CSN in both macrophages and endothelial cells. We have also revealed an athero-protective role of CSN in vivo.

Therefore, the goal of my thesis was to investigate (1) how the expression levels of CSN subunits in the brain are and (2) whether CSN5 and the CSN exert anti-inflammatory effects in microglia cells and how they affect the blood-brain-barrier. Moreover, we were interested to explore (3) if CSN affects BBB leakage and (4) if it exerts protective activity in ischemic stroke.

We were able to show that MLN4924, partially mimicking the hyperactivity of CSN5, reduced microglial and microvascular endothelial inflammation, and this is at least partially related to its modulation of the NF-κB signaling pathway. Functional assays showed that MLN4924 also modulated the microglia phagocytic activity and motility, which are both highly associated with the clearance of neuronal debris and the second wave of inflammatory response after ischemia. In addition, MLN4924 protected BBB permeability under hypoxia condition in a hCMEC/D3 model. Correspondingly, inhibiting CSN5 by CSN5i-3 resulted in a disruption of BBB integrity.
After the characterization of the role of the CSN in activated microglia and microvascular endothelial cells, we focused on the investigation on the ischemic outcome. We detected that MLN4924 prevented and CSN5i-3 exacerbated OGD/RO-induced neuronal damage, as determined both in a cell cultue model of mixed neuronal cultures and in an ex vivo brain organoid model. With regards to the mechanism, our findings suggested that these effects by deneddylation of cullins, at least in part, is owing to the negative regulation of inflammatory factor expressioin. Hence, we hypothesized that neutralization of TNF-α (the most downregulated gene upon MLN4924) by antibodies would also reduce the neuronal death. We indeed found that one of the two TNF-α antibodies, Infliximab, significantly improved OGD/RO-induced brain slice damage.

Taken together, our study was able to confirm that mediating microglia-associated neuroinflammation by the CSN is a potential therapeutic approaches for ischemic stroke. Nevertheless, future investigations are needed to understand all the mechanisms of the interaction between CSN and neuroinflammation as well as other post-ischemic events.

6 Zusammenfassung

Der ischämische Schlaganfall zählt global zu den Hauptursachen für Todesfälle und Behinderungen. Die einzige pharmakologische Therapie akuter ischämischer Schlaganfälle ist rtPA - limitiert durch ein nur kurzes Zeitfenster der Anwendung. Diese Option steht daher nur einem Bruchteil der Schlaganfallpatienten zur Verfügung und die meisten Patienten haben daher nur begrenzte Aussichten auf Genesung. Obschon in der Vergangenheit tausende translationale Forschungsvorhaben hierzu durchgeführt wurden, scheiterten alle in klinischen Studien. Daher sind neue Strategien zur Behandlung pathophysiologischer Veränderungen nach einem Schlaganfall dringend notwendig.

Mikroglia-assoziierte Neuroinflammation ist ein kritisches pathologisches Ereignis des ischämischen Schlaganfalls, welches sekundäre Schäden des Gehirns hervorruft und zu einer nur ungenügenden Genesung führt. Mikroglia können, ausgelöst von subtilen Veränderungen des Gehirns, rasche funktionale und morphologische Veränderungen zeigen. Typ M1 Mikroglia sind mit einer pro-inflammatorischen Reaktion assoziiert, welche Neurone und die Blut-Hirn-Schranke schädigt. M2 Mikroglia hingegen produzieren anti-inflammatorische Mediatoren und unterstützen neuronale Reparaturmechanismen. Daher bietet die Modulierung der Polarisierung von MIkroglia eine gute therapeutische Option zu verschiedenen Stadien des ischämischen Schlaganfalls. Weiterhin zeigen unsere bisherigen Arbeiten eine anti-inflammatorische Wirkung von CSN sowohl in Makrophagen als auch Endothelzellen. Wir konnten auch eine athero-protektive Rolle von CSN in vivo zeigen. Die Zielsetzung meiner Arbeit war daher (1) die Expression von CSN Untereinheiten im Hirn zu untersuchen und (2) herauszufinden ob CSN5 und CSN einen anti-inflammatorischen Effekt in Mikroglia und auf die Blut-Hirn-Schranke haben. Zudem sind wir daran interessiert herauszufinden ob (3) CSN die Durchlässigkeit der Blut-Hirn-Schranke beeinflusst und protektive Aktivitäten im ischämischen Schlaganfall

zeigt.

Wir konnten zeigen dass MLN4924, welches teilweise die Hyperaktivierung von CSN5 imitiert, die Inflammation von Mikroglia und des mikrovaskulären Endothels reduziert und der NF-κB Signalweg dazu beiträgt. Funktionale Assays zeigten dass MLN4924 auch die Phagozytose-Aktivität und Motilität von Mikrogliazellen beeinflusst - zwei Mechanismen die stark mit der Beseitigung von neuronalen Zelltrümmern in der zweiten inflammatorischen Welle nach einer Ischämie verknüpft sind. Zusätzlich bewahrte MLN4924 die permeabilität der Blut-Hirn-Schranke unter hypoxischen Bedingungen. Dementsprchend führte eine Inhibierung von CSN5 durch CSN5i-3 zu einer Schädigung der Integrität der Blut-Hirn-Schranke.

Nach der Charakterisierung von CSN in aktivierten Mikroglia und mikrovaskulären Endothelzellen konzentrierten wir uns auf die Untersuchung von Folgeerscheinungen der Ischämie. Wir fanden dass OGD/RO-induzierte neuronale Schäden durch MLN4924 verhindert und durch CSN5i-3 verstärkt wurden. Bezüglich eines zugrundeliegenden Mechanismus deuten unsere Studien darauf hin, dass diese Effekte zuindest teilweise auf die Deneddylierung von Cullinen beruhen, aufgrund von negativer Regulierung der Expression inflammatorischer Faktoren. Wir stellten daher die Hypothese auf, dass die Neutralisierung von TNF-α (das durch MLN4924 am stärksten herunterregulierte Gen) durch Antikörper neuronalen Zelltod ebenfalls reduziert. Tatsächlich konnten wir zeigen dass einer von zwei TNF-α Antikörpern, Infliximab, die durch OGD/RO induzierten schäden in Kulturen von Gehirn-Schnitten mildert.

Zusammenfassend konnten wir in dieser Studie bestätigen dass eine Modulierung der Mikroglia-vermittelten Neuroinflammation durch CSN einen potenziellen therapeutscher Ansatz des ischämischen Schlaganfalls darstellt. Dennoch ist weitere Forschung notwendung um die Gesamtheit der zusammenhänge zwischen CSN und der Neuroinflammation sowie anderen post-ischämischen Prozessen zu Verstehen.

References

1. Campbell, B. C. V. & Khatri, P. Stroke. *Lancet* **396,** 129–142 (2020).
2. Who.Int. *Cardiovascular Diseases* `http://www.who.int/health-topics/cardiovascular-diseases#tab=tab_2`.
3. Dichgans, M., Pulit, S. L. & Rosand, J. Stroke genetics: discovery, biology, and clinical applications. *Lancet Neurol* **18,** 587–599 (2019).
4. Feigin, V. L., Stark, B. A., Johnson, C. O., Roth, G. A., Bisignano, C., Abady, G. G., Abbasifard, M., Abbasi-Kangevari, M., Abd-Allah, F., Abedi, V., *et al.* Global, regional, and national burden of stroke and its risk factors, 1990–2019: a systematic analysis for the Global Burden of Disease Study 2019. *Lancet Neurol* **20,** 795–820 (2021).
5. Luengo-Fernandez, R., Violato, M., Candio, P. & Leal, J. Economic burden of stroke across Europe: a population-based cost analysis. *Eur Stroke J* **5,** 17–25 (2020).
6. Murray, C. J., Aravkin, A. Y., Zheng, P., Abbafati, C., Abbas, K. M., Abbasi-Kangevari, M., Abd-Allah, F., Abdelalim, A., Abdollahi, M., Abdollahpour, I., *et al.* Global burden of 87 risk factors in 204 countries and territories, 1990–2019: a systematic analysis for the Global Burden of Disease Study 2019. *Lancet* **396,** 1223–1249 (2020).
7. Campbell, B. C., De Silva, D. A., Macleod, M. R., Coutts, S. B., Schwamm, L. H., Davis, S. M. & Donnan, G. A. Ischaemic stroke. *Nat Rev Dis Primers* **5,** 1–22 (2019).
8. O'Collins, V. E., Macleod, M. R., Donnan, G. A., Horky, L. L., van der Worp, B. H. & Howells, D. W. 1,026 experimental treatments in acute stroke. *Ann Neurol* **59,** 467–477 (2006).
9. DiSabato, D. J., Quan, N. & Godbout, J. P. Neuroinflammation: the devil is in the details. *J Neurochem* **139,** 136–153 (2016).
10. Iadecola, C. & Anrather, J. The immunology of stroke: from mechanisms to translation. *Nat Med* **17,** 796–808 (2011).
11. Lipton, P. Ischemic cell death in brain neurons. *Physiol Rev* **79,** 1431–1568 (1999).
12. Amantea, D., Nappi, G., Bernardi, G., Bagetta, G. & Corasaniti, M. T. Post-ischemic brain damage: pathophysiology and role of inflammatory mediators. *FEBS J* **276,** 13–26 (2009).
13. Dirnagl, U. & Endres, M. Found in translation: preclinical stroke research predicts human pathophysiology, clinical phenotypes, and therapeutic outcomes. *Stroke* **45,** 1510–1518 (2014).

14. Davis, B. M., Salinas-Navarro, M., Cordeiro, M. F., Moons, L. & De Groef, L. Characterizing microglia activation: a spatial statistics approach to maximize information extraction. *Sci Rep* **7,** 1–12 (2017).

15. Bachiller, S., Jiménez-Ferrer, I., Paulus, A., Yang, Y., Swanberg, M., Deierborg, T. & Boza-Serrano, A. Microglia in neurological diseases: a road map to brain-disease dependent-inflammatory response. *Front Cell Neurosci* **12,** 488 (2018).

16. Alliot, F., Godin, I. & Pessac, B. Microglia derive from progenitors, originating from the yolk sac, and which proliferate in the brain. *Brain Res Dev Brain Res* **117,** 145–152 (1999).

17. Graeber, M. B. Changing face of microglia. *Science* **330,** 783–788 (2010).

18. Norden, D. M., Trojanowski, P. J., Villanueva, E., Navarro, E. & Godbout, J. P. Sequential activation of microglia and astrocyte cytokine expression precedes increased iba - 1 or GFAP immunoreactivity following systemic immune challenge. *Glia* **64,** 300–316 (2016).

19. Zhou, H., Lapointe, B. M., Clark, S. R., Zbytnuik, L. & Kubes, P. A requirement for microglial TLR4 in leukocyte recruitment into brain in response to lipopolysaccharide. *J Immunol* **177,** 8103–8110 (2006).

20. Davalos, D., Grutzendler, J., Yang, G., Kim, J. V., Zuo, Y., Jung, S., Littman, D. R., Dustin, M. L. & Gan, W.-B. ATP mediates rapid microglial response to local brain injury in vivo. *Nat Neurosci* **8,** 752–758 (2005).

21. Nguyen, K. D., Qiu, Y., Cui, X., Goh, Y. S., Mwangi, J., David, T., Mukundan, L., Brombacher, F., Locksley, R. M. & Chawla, A. Alternatively activated macrophages produce catecholamines to sustain adaptive thermogenesis. *Nature* **480,** 104–108 (2011).

22. Yenari, M. A., Kauppinen, T. M. & Swanson, R. A. Microglial activation in stroke: therapeutic targets. *Neurotherapeutics* **7,** 378–391 (2010).

23. Patel, A. R., Ritzel, R., McCullough, L. D. & Liu, F. Microglia and ischemic stroke: a double-edged sword. *Int J Physiol Pathophysiol Pharmacol* **5,** 73 (2013).

24. Perego, C., Fumagalli, S. & De Simoni, M.-G. Temporal pattern of expression and colocalization of microglia/macrophage phenotype markers following brain ischemic injury in mice. *J Neuroinflammation* **8,** 1–20 (2011).

25. Hu, X., Li, P., Guo, Y., Wang, H., Leak, R. K., Chen, S., Gao, Y. & Chen, J. Microglia/macrophage polarization dynamics reveal novel mechanism of injury expansion after focal cerebral ischemia. *Stroke* **43,** 3063–3070 (2012).

26. Lambertsen, K. L., Meldgaard, M., Ladeby, R. & Finsen, B. A quantitative study of microglial-macrophage synthesis of tumor necrosis factor during acute and late focal cerebral ischemia in mice. *J Cereb Blood Flow Metab* **25,** 119–35 (Jan. 2005).

27. Zhang, W., Zhao, J., Wang, R., Jiang, M., Ye, Q., Smith, A. D., Chen, J. & Shi, Y. Macrophages reprogram after ischemic stroke and promote efferocytosis and inflammation resolution in the mouse brain. *CNS Neurosci Ther* **25,** 1329–1342 (2019).

28. Neumann, H., Kotter, M. R. & Franklin, R. J. M. Debris clearance by microglia: an essential link between degeneration and regeneration. *Brain* **132,** 288–295 (2009).

29. Neher, J. J., Emmrich, J. V., Fricker, M., Mander, P. K., Théry, C. & Brown, G. C. Phagocytosis executes delayed neuronal death after focal brain ischemia. *Proc Natl Acad Sci U S A* **110,** E4098–E4107 (2013).

30. Abbott, N. J. Blood – brain barrier structure and function and the challenges for CNS drug delivery. *J Inherit Metab Dis* **36,** 437–449 (2013).

31. Rosenberg, G. A., Estrada, E. Y. & Dencoff, J. E. Matrix metalloproteinases and TIMPs are associated with blood-brain barrier opening after reperfusion in rat brain. *Stroke* **29,** 2189–2194 (1998).

32. Kuroiwa, T., Cahn, R., Juhler, M., Goping, G., Campbell, G. & Klatzo, I. Role of extracellular proteins in the dynamics of vasogenic brain edema. *Acta Neuropathol* **66,** 3–11 (1985).

33. Yang, C., Hawkins, K. E., Doré, S. & Candelario-Jalil, E. Neuroinflammatory mechanisms of blood-brain barrier damage in ischemic stroke. *Am J Physiol Cell Physiol* **316,** C135–C153 (2019).

34. Rosenberg, G. A. Matrix metalloproteinases in neuroinflammation. *Glia* **39,** 279–291 (2002).

35. Rosell, A., Cuadrado, E., Ortega-Aznar, A., Hernández-Guillamon, M., Lo, E. H. & Montaner, J. MMP-9 – positive neutrophil infiltration is associated to blood – brain barrier breakdown and basal lamina type iv collagen degradation during hemorrhagic transformation after human ischemic stroke. *Stroke* **39,** 1121–1126 (2008).

36. Wan, R., Mo, Y., Chien, S., Li, Y., Li, Y., Tollerud, D. J. & Zhang, Q. The role of hypoxia inducible factor-1 α in the increased MMP-2 and MMP-9 production by human monocytes exposed to nickel nanoparticles. *Nanotoxicology* **5,** 568–582 (2011).

37. Yang, Y. & Rosenberg, G. A. Blood – brain barrier breakdown in acute and chronic cerebrovascular disease. *Stroke* **42,** 3323–3328 (2011).

38. Cui, J., Chen, S., Zhang, C., Meng, F., Wu, W., Hu, R., Hadass, O., Lehmidi, T., Blair, G. J. & Lee, M. Inhibition of MMP-9 by a selective gelatinase inhibitor protects neurovasculature from embolic focal cerebral ischemia. *Mol Neurodegener* **7,** 1–15 (2012).

39. Yang, Y., Thompson, J. F., Taheri, S., Salayandia, V. M., McAvoy, T. A., Hill, J. W., Yang, Y., Estrada, E. Y. & Rosenberg, G. A. Early inhibition of MMP activity in ischemic rat brain promotes expression of tight junction proteins and angiogenesis during recovery. *J Cereb Blood Flow Metab* **33,** 1104–1114 (2013).

40. Liu, J., Jin, X., Liu, K. J. & Liu, W. Matrix metalloproteinase-2-mediated occludin degradation and caveolin-1-mediated claudin-5 redistribution contribute to blood – brain barrier damage in early ischemic stroke stage. *J Neurosci* **32,** 3044–3057 (2012).

41. Song, L., Ge, S. & Pachter, J. S. Caveolin-1 regulates expression of junction-associated proteins in brain microvascular endothelial cells. *Blood* **109,** 1515–1523 (2007).

42. Li, H., Gao, A., Feng, D., Wang, Y., Zhang, L., Cui, Y., Li, B., Wang, Z. & Chen, G. Evaluation of the protective potential of brain microvascular endothelial cell autophagy on blood – brain barrier integrity during experimental cerebral ischemia – reperfusion injury. *Transl Stroke Res* **5,** 618–626 (2014).

43. Zhang, S., An, Q., Wang, T., Gao, S. & Zhou, G. Autophagy-and MMP-2/9-mediated reduction and redistribution of ZO-1 contribute to hyperglycemia-increased blood – brain barrier permeability during early reperfusion in stroke. *Neuroscience* **377,** 126–137 (2018).

44. Redzic, Z. Molecular biology of the blood-brain and the blood-cerebrospinal fluid barriers: similarities and differences. *Fluids Barriers CNS* **8,** 1–25 (2011).

45. Tunggal, J. A., Helfrich, I., Schmitz, A., Schwarz, H., Günzel, D., Fromm, M., Kemler, R., Krieg, T. & Niessen, C. M. E- cadherin is essential for in vivo epidermal barrier function by regulating tight junctions. *EMBO J* **24,** 1146–1156 (2005).

46. Wei, N. & Deng, X.-W. COP9: a new genetic locus involved in light-regulated development and gene expression in arabidopsis. *Plant Cell* **4,** 1507–1518 (1992).

47. Chamovitz, D. A., Wei, N., Osterlund, M. T., von Arnim, A. G., Staub, J. M., Matsui, M. & Deng, X.-W. The COP9 complex, a novel multisubunit nuclear regulator involved in light control of a plant developmental switch. *Cell* **86,** 115–121 (1996).

48. Wei, N. & Deng, X. W. The COP9 signalosome. *Annu Rev Cell Dev Biol* **19,** 261–286 (2003).

49. Wei, N. & Deng, X.-W. Characterization and purification of the mammalian COP9 complex, a conserved nuclear regulator initially identified as a repressor of photomorphogenesis in higher plants. *Photochem Photobiol* **68,** 237–241 (1998).

50. Seeger, M., Kraft, R., Ferrell, K., Bech-Otschir, D., Dumdey, R., Schade, R., Gordon, C., Naumann, M. & Dubiel, W. A novel protein complex involved in signal transduction possessing similarities to 26S proteasome subunits. *FASEB J* **12,** 469–478 (1998).

51. Deng, X.-W., Dubiel, W., Wei, N., Hofmann, K. & Mundt, K. Unified nomenclature for the COP9 signalosome and its subunits: an essential regulator of development. *Trends Genet* **16,** 289 (2000).

52. Hofmann, K. & Bucher, P. The PCI domain: a common theme in three multiprotein complexes. *Trends Biochem Sci* **23,** 204–205 (1998).

53. Wei, N., Serino, G. & Deng, X.-W. The COP9 signalosome: more than a protease. *Trends Biochem Sci* **33,** 592–600 (2008).

54. Chamovitz, D. A. & Segal, D. JAB1/CSN5 and the COP9 signalosome: A complex situation. *EMBO Rep* **2,** 96–101 (2001).

55. Soucy, T. A., Smith, P. G., Milhollen, M. A., Berger, A. J., Gavin, J. M., Adhikari, S., Brownell, J. E., Burke, K. E., Cardin, D. P. & Critchley, S. An inhibitor of NEDD8-activating enzyme as a new approach to treat cancer. *Nature* **458,** 732–736 (2009).

56. Petroski, M. D. & Deshaies, R. J. Function and regulation of cullin – RING ubiquitin ligases. *Nat Rev Mol Cell Biol* **6,** 9–20 (2005).

57. Brown, N. G., Watson, E. R., Weissmann, F., Jarvis, M. A., VanderLinden, R., Grace, C. R., Frye, J. J., Qiao, R., Dube, P. & Petzold, G. Mechanism of polyubiquitination by human anaphase-promoting complex: RING repurposing for ubiquitin chain assembly. *Mol Cell* **56,** 246–260 (2014).

58. Sarikas, A., Hartmann, T. & Pan, Z.-Q. The cullin protein family. *Genome Biol* **12,** 1–12 (2011).

59. Skaar, J. R., Pagan, J. K. & Pagano, M. Mechanisms and function of substrate recruitment by F-box proteins. *Nat Rev Mol Cell Biol* **14,** 369–381 (2013).

60. Nguyen, H. C., Wang, W. & Xiong, Y. Cullin-RING E3 ubiquitin ligases: bridges to destruction. *Subcell Biochem,* 323–347 (2017).

61. Lyapina, S., Cope, G., Shevchenko, A., Serino, G., Tsuge, T., Zhou, C., Wolf, D. A., Wei, N., Shevchenko, A. & Deshaies, R. J. Promotion of NEDD8-CUL1 conjugate cleavage by COP9 signalosome. *Science* **292,** 1382–1385 (2001).

62. Schwechheimer, C. The COP9 signalosome (CSN): an evolutionary conserved proteolysis regulator in eukaryotic development. *Biochim Biophys Acta* **1695,** 45–54 (2004).

63. Cope, G. A., Suh, G. S., Aravind, L., Schwarz, S. E., Zipursky, S. L., Koonin, E. V. & Deshaies, R. J. Role of predicted metalloprotease motif of Jab1/Csn5 in cleavage of Nedd8 from Cul1. *Science* **298,** 608–611 (2002).

64. Podust, V. N., Brownell, J. E., Gladysheva, T. B., Luo, R.-S., Wang, C., Coggins, M. B., Pierce, J. W., Lightcap, E. S. & Chau, V. A Nedd8 conjugation pathway is essential for proteolytic targeting of p27Kip1 by ubiquitination. *Proc Natl Acad Sci U S A* **97,** 4579–4584 (2000).

65. Pan, Z.-Q., Kentsis, A., Dias, D. C., Yamoah, K. & Wu, K. Nedd8 on cullin: building an expressway to protein destruction. *Oncogene* **23,** 1985–1997 (2004).

66. Huang, D. T., Ayrault, O., Hunt, H. W., Taherbhoy, A. M., Duda, D. M., Scott, D. C., Borg, L. A., Neale, G., Murray, P. J. & Roussel, M. F. E2-RING expansion of the NEDD8 cascade confers specificity to cullin modification. *Mol Cell* **33,** 483–495 (2009).

67. Kurz, T., Özlü, N., Rudolf, F., O'Rourke, S. M., Luke, B., Hofmann, K., Hyman, A. A., Bowerman, B. & Peter, M. The conserved protein DCN-1/Dcn1p is required for cullin neddylation in C. elegans and S. cerevisiae. *Nature* **435,** 1257–1261 (2005).

68. Zhou, L., Jiang, Y., Luo, Q., Li, L. & Jia, L. Neddylation: a novel modulator of the tumor microenvironment. *Mol Cancer* **18,** 1–11 (2019).

69. Enchev, R. I., Schulman, B. A. & Peter, M. Protein neddylation: beyond cullin – RING ligases. *Nat Rev Mol Cell Biol* **16,** 30–44 (2015).

70. Liu, X., Reitsma, J. M., Mamrosh, J. L., Zhang, Y., Straube, R. & Deshaies, R. J. Cand1-mediated adaptive exchange mechanism enables variation in F-box protein expression. *Mol Cell* **69,** 773–786. e6 (2018).

71. Franciosini, A., Serino, G. & Deng, X.-W. in *Molecular Biology* (ed Howell, S. H.) 313–332 (Springer New York, New York, NY, 2014). ISBN: 978-1-4614-7570-5.

72. Lingaraju, G. M., Bunker, R. D., Cavadini, S., Hess, D., Hassiepen, U., Renatus, M., Fischer, E. S. & Thomä, N. H. Crystal structure of the human COP9 signalosome. *Nature* **512,** 161–165 (2014).

73. Kapelari, B., Bech-Otschir, D., Hegerl, R., Schade, R., Dumdey, R. & Dubiel, W. Electron microscopy and subunit-subunit interaction studies reveal a first architecture of COP9 signalosome. *J Mol Biol* **300,** 1169–1178 (2000).

74. Sharon, M., Mao, H., Erba, E. B., Stephens, E., Zheng, N. & Robinson, C. V. Symmetrical modularity of the COP9 signalosome complex suggests its multi-functionality. *Structure* **17,** 31–40 (2009).

75. Deshaies, R. J. Corralling a protein-degradation regulator. *Nature* **512,** 145–146 (2014).

76. Mosadeghi, R., Reichermeier, K. M., Winkler, M., Schreiber, A., Reitsma, J. M., Zhang, Y., Stengel, F., Cao, J., Kim, M. & Sweredoski, M. J. Structural and kinetic analysis of the COP9-Signalosome activation and the cullin-RING ubiquitin ligase deneddylation cycle. *Elife* **5,** e12102 (2016).

77. Cavadini, S., Fischer, E. S., Bunker, R. D., Potenza, A., Lingaraju, G. M., Goldie, K. N., Mohamed, W. I., Faty, M., Petzold, G. & Beckwith, R. E. Cullin – RING ubiquitin E3 ligase regulation by the COP9 signalosome. *Nature* **531,** 598–603 (2016).

78. Faull, S. V., Lau, A. M., Martens, C., Ahdash, Z., Hansen, K., Yebenes, H., Schmidt, C., Beuron, F., Cronin, N. B. & Morris, E. P. Structural basis of Cullin 2 RING E3 ligase regulation by the COP9 signalosome. *Nat Commun* **10,** 1–13 (2019).

79. Qin, N., Xu, D., Li, J. & Deng, X. W. COP9 signalosome: discovery, conservation, activity, and function. *J Integr Plant Biol* **62,** 90–103 (2020).

80. Wee, S., Geyer, R. K., Toda, T. & Wolf, D. A. CSN facilitates Cullin – RING ubiquitin ligase function by counteracting autocatalytic adapter instability. *Nat Cell Biol* **7,** 387–391 (2005).

81. Hetfeld, B. K., Helfrich, A., Kapelari, B., Scheel, H., Hofmann, K., Guterman, A., Glickman, M., Schade, R., Kloetzel, P.-M. & Dubiel, W. The zinc finger of the CSN-associated deubiquitinating enzyme USP15 is essential to rescue the E3 ligase Rbx1. *Curr Biol* **15,** 1217–1221 (2005).

82. Schweitzer, K. & Naumann, M. CSN-associated USP48 confers stability to nuclear NF- $\varkappa$ B/RelA by trimming K48-linked Ub-chains. *Biochim Biophys Acta* **1853,** 453–469 (2015).

83. Schweitzer, K., Bozko, P. M., Dubiel, W. & Naumann, M. CSN controls NF - kappaB by deubiquitinylation of IkappaBα. *EMBO J* **26,** 1532–1541 (2007).

84. Schweitzer, K. & Naumann, M. Control of NF-kappaB activation by the COP9 signalosome. *Biochem Soc Trans* **38,** 156–161 (2010).

85. Asare, Y., Shagdarsuren, E., Schmid, J. A., Tilstam, P. V., Grommes, J., El Bounkari, O., Schütz, A. K., Weber, C., de Winther, M. P. & Noels, H. Endothelial CSN5 impairs NF-κB activation and monocyte adhesion to endothelial cells and is highly expressed in human atherosclerotic lesions. *Thromb Haemost* **110,** 141–152 (2013).

86. Ghanem, A., Schweitzer, K. & Naumann, M. Catalytic domain of deubiquitinylase USP48 directs interaction with Rel homology domain of nuclear factor kappaB transcription factor RelA. *Mol Biol Rep* **46,** 1369–1375 (2019).

87. Maine, G. N., Mao, X., Komarck, C. M. & Burstein, E. COMMD1 promotes the ubiquitination of NF - κB subunits through a cullin - containing ubiquitin ligase. *EMBO J* **26,** 436–447 (2007).

88. Dubiel, W., Chaithongyot, S., Dubiel, D. & Naumann, M. The COP9 Signalosome: A Multi-DUB Complex. *Biomolecules* **10** (2020).

89. Bech - Otschir, D., Kraft, R., Huang, X., Henklein, P., Kapelari, B., Pollmann, C. & Dubiel, W. COP9 signalosome - specific phosphorylation targets p53 to degradation by the ubiquitin system. *EMBO J* **20,** 1630–1639 (2001).

90. Wilson, M. P., Sun, Y., Cao, L. & Majerus, P. W. Inositol 1, 3, 4-trisphosphate 5/6-kinase is a protein kinase that phosphorylates the transcription factors c-Jun and ATF-2. *J Biol Chem* **276,** 40998–41004 (2001).

91. Jurenka, J. S. Anti-inflammatory properties of curcumin, a major constituent of Curcuma longa: a review of preclinical and clinical research. *Altern Med Rev* **14** (2009).

92. Meir, M., Galanty, Y., Kashani, L., Blank, M., Khosravi, R., Fernández-Ávila, M. J., Cruz-García, A., Star, A., Shochot, L. & Thomas, Y. The COP9 signalosome is vital for timely repair of DNA double-strand breaks. *Nucleic Acids Res* **43,** 4517–4530 (2015).

93. Huang, X., Wagner, E., Dumdey, R., Peth, A., Berse, M., Dubiel, W. & Berndt, C. Phosphorylation by COP9 Signalosome - Associated CK2 Promotes Degradation of p27 during the G1 Cell Cycle Phase. *Isr J Chem* **46,** 231–238 (2006).

94. Uhle, S., Medalia, O., Waldron, R., Dumdey, R., Henklein, P., Bech - Otschir, D., Huang, X., Berse, M., Sperling, J. & Schade, R. Protein kinase CK2 and protein kinase D are associated with the COP9 signalosome. *EMBO J* **22,** 1302–1312 (2003).

95. Dubiel, D., Rockel, B., Naumann, M. & Dubiel, W. Diversity of COP9 signalosome structures and functional consequences. *FEBS Lett* **589,** 2507–2513 (2015).

96. Weber, C. & Noels, H. Atherosclerosis: current pathogenesis and therapeutic options. *Nat Med* **17,** 1410–1422 (2011).

97. Kwon, G. P., Schroeder, J. L., Amar, M. J., Remaley, A. T. & Balaban, R. S. Contribution of macromolecular structure to the retention of low-density lipoprotein at arterial branch points. *Circulation* **117,** 2919–2927 (2008).

98. Ylä-Herttuala, S., Bentzon, J. F., Daemen, M., Falk, E., Garcia-Garcia, H. M., Herrmann, J., Hoefer, I., Jukema, J. W., Krams, R., Kwak, B. R., Marx, N., Naruszewicz, M., Newby, A., Pasterkamp, G., Serruys, P., Waltenberger, J., Weber, C. & Tokgözoglu, L. Stabilisation of atherosclerotic plaques. *Thromb Haemost* **106,** 1–19 (2011).

99. Russell, R. & Glomset, J. A. The pathogenesis of atherosclerosis. *N Engl J Med* **314,** 488–497 (1986).

100. Peter Libby, M. D. History of discovery: inflammation in atherosclerosis. *Arterioscler Thromb Vasc Biol* **32,** 2045–2051 (2012).

101. Tabas, I., García-Cardeña, G. & Owens, G. K. Recent insights into the cellular biology of atherosclerosis. *J Cell Biol* **209,** 13–22 (2015).

102. Orel, L., Neumeier, H., Hochrainer, K., Binder, B. R. & Schmid, J. A. Crosstalk between the NF - κB activating IKK - complex and the CSN signalosome. *J Cell Mol Med* **14,** 1555–1568 (2010).

103. Asare, Y., Ommer, M., Azombo, F. A., Alampour-Rajabi, S., Sternkopf, M., Sanati, M., Gijbels, M. J., Schmitz, C., Sinitski, D. & Tilstam, P. V. Inhibition of atherogenesis by the COP9 signalosome subunit 5 in vivo. *Proc Natl Acad Sci U S A* **114,** E2766–E2775 (2017).

104. Nishimoto, A., Lu, L., Hayashi, M., Nishiya, T., Horinouchi, T. & Miwa, S. Jab1 regulates levels of endothelin type A and B receptors by promoting ubiquitination and degradation. *Biochem Biophys Res Commun* **391,** 1616–1622 (2010).

105. Swirski, F. K., Nahrendorf, M. & Libby, P. Mechanisms of myeloid cell modulation of atherosclerosis. *Microbiol Spectr* **4,** 4.4. 60 (2016).

106. Medzhitov, R. Origin and physiological roles of inflammation. *Nature* **454,** 428–35 (2008).

107. Auffray, C., Sieweke, M. H. & Geissmann, F. Blood monocytes: development, heterogeneity, and relationship with dendritic cells. *Annu Rev Immunol* **27,** 669–92 (2009).

108. Robbins, C. S., Chudnovskiy, A., Rauch, P. J., Figueiredo, J. L., Iwamoto, Y., Gorbatov, R., Etzrodt, M., Weber, G. F., Ueno, T., van Rooijen, N., Mulligan-Kehoe, M. J., Libby, P., Nahrendorf, M., Pittet, M. J., Weissleder, R. & Swirski, F. K. Extramedullary hematopoiesis generates Ly-6C(high) monocytes that infiltrate atherosclerotic lesions. *Circulation* **125,** 364–74 (2012).

109. Murphy, A. J., Akhtari, M., Tolani, S., Pagler, T., Bijl, N., Kuo, C. L., Wang, M., Sanson, M., Abramowicz, S., Welch, C., Bochem, A. E., Kuivenhoven, J. A., Yvan-Charvet, L. & Tall, A. R. ApoE regulates hematopoietic stem cell proliferation, monocytosis, and monocyte accumulation in atherosclerotic lesions in mice. *J Clin Invest* **121,** 4138–49 (2011).

110. Hilgendorf, I., Swirski, F. K. & Robbins, C. S. Monocyte fate in atherosclerosis. *Arterioscler Thromb Vasc Biol* **35,** 272–9 (2015).

111. Tacke, F., Alvarez, D., Kaplan, T. J., Jakubzick, C., Spanbroek, R., Llodra, J., Garin, A., Liu, J., Mack, M., van Rooijen, N., Lira, S. A., Habenicht, A. J. & Randolph, G. J. Monocyte subsets differentially employ CCR2, CCR5, and CX3CR1 to accumulate within atherosclerotic plaques. *J Clin Invest* **117,** 185–94 (2007).

112. Boring, L., Gosling, J., Cleary, M. & Charo, I. F. Decreased lesion formation in CCR2-/- mice reveals a role for chemokines in the initiation of atherosclerosis. *Nature* **394,** 894–7 (1998).

113. Combadière, C., Potteaux, S., Rodero, M., Simon, T., Pezard, A., Esposito, B., Merval, R., Proudfoot, A., Tedgui, A. & Mallat, Z. Combined inhibition of CCL2, CX3CR1, and CCR5 abrogates Ly6C(hi) and Ly6C(lo) monocytosis and almost abolishes atherosclerosis in hypercholesterolemic mice. *Circulation* **117,** 1649–57 (2008).

114. Bernhagen, J., Krohn, R., Lue, H., Gregory, J. L., Zernecke, A., Koenen, R. R., Dewor, M., Georgiev, I., Schober, A., Leng, L., Kooistra, T., Fingerle-Rowson, G., Ghezzi, P., Kleemann, R., McColl, S. R., Bucala, R., Hickey, M. J. & Weber, C. MIF is a noncognate ligand of CXC chemokine receptors in inflammatory and atherogenic cell recruitment. *Nat Med* **13,** 587–96 (2007).

115. Kleemann, R., Hausser, A., Geiger, G., Mischke, R., Burger-Kentischer, A., Flieger, O., Johannes, F.-J., Roger, T., Calandra, T., Kapurniotu, A., Grell, M., Finkelmeier, D. & Bernhagen, J. Intracellular action of the cytokine MIF to modulate AP-1 activity and the cell cycle through Jab1. *Nature* **408,** 211–216 (2000).

116. Lue, H., Thiele, M., Franz, J., Dahl, E., Speckgens, S., Leng, L., Fingerle-Rowson, G., Bucala, R., Lüscher, B. & Bernhagen, J. Macrophage migration inhibitory factor (MIF) promotes cell survival by activation of the Akt pathway and role for CSN5/JAB1 in the control of autocrine MIF activity. *Oncogene* **26,** 5046–59 (2007).

117. Akhtar, S., Hartmann, P., Karshovska, E., Rinderknecht, F. A., Subramanian, P., Gremse, F., Grommes, J., Jacobs, M., Kiessling, F., Weber, C., Steffens, S. & Schober, A. Endothelial Hypoxia-Inducible Factor-1 α Promotes Atherosclerosis and Monocyte Recruitment by Upregulating MicroRNA-19a. *Hypertension* **66,** 1220–6 (2015).

118. Vink, A., Schoneveld, A. H., Lamers, D., Houben, A. J., van der Groep, P., van Diest, P. J. & Pasterkamp, G. HIF-1 alpha expression is associated with an atheromatous inflammatory plaque phenotype and upregulated in activated macrophages. *Atherosclerosis* **195,** e69–75 (2007).

119. Sluimer, J. C., Gasc, J. M., van Wanroij, J. L., Kisters, N., Groeneweg, M., Sollewijn Gelpke, M. D., Cleutjens, J. P., van den Akker, L. H., Corvol, P., Wouters, B. G., Daemen, M. J. & Bijnens, A. P. Hypoxia, hypoxia-inducible transcription factor, and macrophages in human atherosclerotic plaques are correlated with intraplaque angiogenesis. *J Am Coll Cardiol* **51,** 1258–65 (2008).

120. Parathath, S., Yang, Y., Mick, S. & Fisher, E. A. Hypoxia in murine atherosclerotic plaques and its adverse effects on macrophages. *Trends Cardiovasc Med* **23,** 80–4 (2013).

121. Bemis, L., Chan, D. A., Finkielstein, C. V., Qi, L., Sutphin, P. D., Chen, X., Stenmark, K., Giaccia, A. J. & Zundel, W. Distinct aerobic and hypoxic mechanisms of HIF-alpha regulation by CSN5. *Genes Dev* **18,** 739–44 (2004).

122. Bae, M. K., Ahn, M. Y., Jeong, J. W., Bae, M. H., Lee, Y. M., Bae, S. K., Park, J. W., Kim, K. R. & Kim, K. W. Jab1 interacts directly with HIF-1alpha and regulates its stability. *J Biol Chem* **277,** 9–12 (2002).

123. Ryu, J. H., Li, S. H., Park, H. S., Park, J. W., Lee, B. & Chun, Y. S. Hypoxia-inducible factor α subunit stabilization by NEDD8 conjugation is reactive oxygen species-dependent. *J Biol Chem* **286,** 6963–70 (Mar. 4, 2011).

124. Moore, K. J., Sheedy, F. J. & Fisher, E. A. Macrophages in atherosclerosis: a dynamic balance. *Nat Rev Immunol* **13,** 709–21 (Oct. 2013).

125. Moore, K. J. & Freeman, M. W. Scavenger receptors in atherosclerosis: beyond lipid uptake. *Arterioscler Thromb Vasc Biol* **26,** 1702–11 (Aug. 2006).

126. Moore, K. J. & Tabas, I. Macrophages in the pathogenesis of atherosclerosis. *Cell* **145,** 341–55 (Apr. 29, 2011).

127. Meurs, I., Out, R., Van Berkel, T. J. & Eck, M. v. Role of the ABC transporters ABCA1 and ABCG1 in foam cell formation and atherosclerosis. *Future Lipidology* **3,** 675–687 (2008).

128. Zhang, M., Li, L., Xie, W., Wu, J. F., Yao, F., Tan, Y. L., Xia, X. D., Liu, X. Y., Liu, D., Lan, G., Zeng, M. Y., Gong, D., Cheng, H. P., Huang, C., Zhao, Z. W., Zheng, X. L. & Tang, C. K. Apolipoprotein A-1 binding protein promotes macrophage cholesterol efflux by facilitating apolipoprotein A-1 binding to ABCA1 and preventing ABCA1 degradation. *Atherosclerosis* **248,** 149–59 (May 2016).

129. Yokoyama, S., Arakawa, R., Wu, C. A., Iwamoto, N., Lu, R., Tsujita, M. & Abe-Dohmae, S. Calpain-mediated ABCA1 degradation: post-translational regulation of ABCA1 for HDL biogenesis. *Biochim Biophys Acta* **1821,** 547–51 (Mar. 2012).

130. Mizuno, T., Hayashi, H. & Kusuhara, H. Cellular Cholesterol Accumulation Facilitates Ubiquitination and Lysosomal Degradation of Cell Surface-Resident ABCA1. *Arterioscler Thromb Vasc Biol* **35,** 1347–56 (June 2015).

131. Stoffel, W. & Demant, T. Selective removal of apolipoprotein B-containing serum lipoproteins from blood plasma. *Proc Natl Acad Sci U S A* **78,** 611–5 (Jan. 1981).

132. Azuma, Y., Takada, M., Maeda, M., Kioka, N. & Ueda, K. The COP9 signalosome controls ubiquitinylation of ABCA1. *Biochem Biophys Res Commun* **382,** 145–8 (Apr. 24, 2009).

133. Boro, M., Govatati, S., Kumar, R., Singh, N. K., Pichavaram, P., Traylor, J. G., Orr, A. W. & Rao, G. N. Thrombin-Par1 signaling axis disrupts COP9 signalosome subunit 3-mediated ABCA1 stabilization in inducing foam cell formation and atherogenesis. *Cell Death Differ* **28,** 780–798 (2021).

134. Willis, M. S., Townley-Tilson, W. H., Kang, E. Y., Homeister, J. W. & Patterson, C. Sent to destroy: the ubiquitin proteasome system regulates cell signaling and protein quality control in cardiovascular development and disease. *Circ Res* **106,** 463–78 (Feb. 19, 2010).

135. Day, S. M., Divald, A., Wang, P., Davis, F., Bartolone, S., Jones, R. & Powell, S. R. Impaired assembly and post-translational regulation of 26S proteasome in human end-stage heart failure. *Circ Heart Fail* **6,** 544–9 (2013).

136. Mearini, G., Schlossarek, S., Willis, M. S. & Carrier, L. The ubiquitin-proteasome system in cardiac dysfunction. *Biochim Biophys Acta* **1782,** 749–63 (2008).

137. Wang, X. & Robbins, J. Heart failure and protein quality control. *Circ Res* **99,** 1315–28 (2006).

138. Lykke-Andersen, K., Schaefer, L., Menon, S., Deng, X. W., Miller, J. B. & Wei, N. Disruption of the COP9 signalosome Csn2 subunit in mice causes deficient cell proliferation, accumulation of p53 and cyclin E, and early embryonic death. *Mol Cell Biol* **23,** 6790–7 (2003).

139. Yan, J., Walz, K., Nakamura, H., Carattini-Rivera, S., Zhao, Q., Vogel, H., Wei, N., Justice, M. J., Bradley, A. & Lupski, J. R. COP9 signalosome subunit 3 is essential for maintenance of cell proliferation in the mouse embryonic epiblast. *Mol Cell Biol* **23** (2003).

140. Menon, S., Chi, H., Zhang, H., Deng, X. W., Flavell, R. A. & Wei, N. COP9 signalosome subunit 8 is essential for peripheral T cell homeostasis and antigen receptor-induced entry into the cell cycle from quiescence. *Nat Immunol* **8,** 1236–45 (2007).

141. Tomoda, K., Yoneda-Kato, N., Fukumoto, A., Yamanaka, S. & Kato, J. Y. Multiple functions of Jab1 are required for early embryonic development and growth potential in mice. *J Biol Chem* **279,** 43013–8 (2004).

142. Hunter, C., Evans, J. & Valencik, M. L. Subunit 3 of the COP9 signalosome is poised to facilitate communication between the extracellular matrix and the nucleus through the muscle-specific beta1D integrin. *Cell Commun Adhes* **15,** 247–60 (2008).

143. Sheng, Z., Xu, Y., Li, F., Wang, S., Huang, T. & Lu, P. CSN5 attenuates Ang II-induced cardiac hypertrophy through stabilizing LKB1. *Exp Cell Res* **376,** 11–17 (2019).

144. Su, H., Li, J., Menon, S., Liu, J., Kumarapeli, A. R., Wei, N. & Wang, X. Perturbation of cullin deneddylation via conditional Csn8 ablation impairs the ubiquitin-proteasome system and causes cardiomyocyte necrosis and dilated cardiomyopathy in mice. *Circ Res* **108,** 40–50 (2011).

145. Su, H., Li, J., Zhang, H., Ma, W., Wei, N., Liu, J. & Wang, X. COP9 signalosome controls the degradation of cytosolic misfolded proteins and protects against cardiac proteotoxicity. *Circ Res* **117,** 956–66 (2015).

146. McLendon, P. M. & Robbins, J. Desmin-related cardiomyopathy: an unfolding story. *Am J Physiol Heart Circ Physiol* **301,** H1220–8 (2011).

147. Wang, X., Osinska, H., Klevitsky, R., Gerdes, A. M., Nieman, M., Lorenz, J., Hewett, T. & Robbins, J. Expression of R120G-alphaB-crystallin causes aberrant desmin and alphaB-crystallin aggregation and cardiomyopathy in mice. *Circ Res* **89,** 84–91 (2001).

148. Su, H., Li, F., Ranek, M. J., Wei, N. & Wang, X. COP9 signalosome regulates autophagosome maturation. *Circulation* **124,** 2117–28 (2011).

149. Su, H., Li, J., Osinska, H., Li, F., Robbins, J., Liu, J., Wei, N. & Wang, X. The COP9 signalosome is required for autophagy, proteasome-mediated proteolysis, and cardiomyocyte survival in adult mice. *Circ Heart Fail* **6,** 1049–57 (2013).

150. Abdullah, A., Eyster, K. M., Bjordahl, T., Xiao, P., Zeng, E. & Wang, X. Murine Myocardial Transcriptome Analysis Reveals a Critical Role of COPS8 in the Gene Expression of Cullin-RING Ligase Substrate Receptors and Redox and Vesicle Trafficking Pathways. *Front Physiol* **8,** 594 (2017).

151. Su, H., Huang, W. & Wang, X. The COP9 signalosome negatively regulates proteasome proteolytic function and is essential to transcription. *Int J Biochem Cell Biol* **41,** 615–24 (2009).

152. Oron, E., Tuller, T., Li, L., Rozovsky, N., Yekutieli, D., Rencus-Lazar, S., Segal, D., Chor, B., Edgar, B. A. & Chamovitz, D. A. Genomic analysis of COP9 signalosome function in Drosophila melanogaster reveals a role in temporal regulation of gene expression. *Mol Syst Biol* **3,** 108 (2007).

153. Ullah, Z., Buckley, M. S., Arnosti, D. N. & Henry, R. W. Retinoblastoma protein regulation by the COP9 signalosome. *Mol Biol Cell* **18,** 1179–86 (2007).

154. Ponikowski, P., Voors, A. A., Anker, S. D., Bueno, H., Cleland, J. G. F., Coats, A. J. S., Falk, V., González-Juanatey, J. R., Harjola, V. P., Jankowska, E. A., Jessup, M., Linde, C., Nihoyannopoulos, P., Parissis, J. T., Pieske, B., Riley, J. P., Rosano, G. M. C., Ruilope, L. M., Ruschitzka, F., Rutten, F. H. & van der Meer, P. 2016 ESC Guidelines for the diagnosis and treatment of acute and chronic heart failure: The Task Force for the diagnosis and treatment of acute and chronic heart failure of the European Society of Cardiology (ESC)Developed with the special contribution of the Heart Failure Association (HFA) of the ESC. *Eur Heart J* **37,** 2129–2200 (2016).

155. Yusuf, S., Rangarajan, S., Teo, K., Islam, S., Li, W., Liu, L., Bo, J., Lou, Q., Lu, F., Liu, T., Yu, L., Zhang, S., Mony, P., Swaminathan, S., Mohan, V., Gupta, R., Kumar, R., Vijayakumar, K., Lear, S., Anand, S., Wielgosz, A., Diaz, R., Avezum, A., Lopez-Jaramillo, P., Lanas, F., Yusoff, K., Ismail, N., Iqbal, R., Rahman, O., Rosengren, A., Yusufali, A., Kelishadi, R., Kruger, A., Puoane, T., Szuba, A., Chifamba, J., Oguz, A., McQueen, M., McKee, M. & Dagenais, G. Cardiovascular risk and events in 17 low-, middle-, and high-income countries. *N Engl J Med* **371,** 818–27 (2014).

156. Wang, X. & Wang, H. Priming the proteasome to protect against proteotoxicity. *Trends Mol Med* **26,** 639–648 (2020).

157. Wang, X. & Cui, T. Autophagy modulation: a potential therapeutic approach in cardiac hypertrophy. *Am J Physiol Heart Circ Physiol* **313,** H304–H319 (2017).

158. Del Re, D. P., Amgalan, D., Linkermann, A., Liu, Q. & Kitsis, R. N. Fundamental mechanisms of regulated cell death and implications for heart disease. *Physiol Rev* **99,** 1765–1817 (2019).

159. Choi, M. E., Price, D. R., Ryter, S. W. & Choi, A. M. Necroptosis: a crucial pathogenic mediator of human disease. *JCI Insight* **4** (2019).

160. Xiao, P., Wang, C., Li, J., Su, H., Yang, L., Wu, P., Lewno, M. T., Liu, J. & Wang, X. COP9 Signalosome Suppresses RIPK1-RIPK3-Mediated Cardiomyocyte Necroptosis in Mice. *Circ Heart Fail* **13,** e006996 (2020).

161. Kameda, K., Fukao, M., Kobayashi, T., Tsutsuura, M., Nagashima, M., Yamada, Y., Yamashita, T. & Tohse, N. CSN5/Jab1 inhibits cardiac L-type Ca2+ channel activity through protein-protein interactions. *J Mol Cell Cardiol* **40,** 562–9 (Apr. 2006).

162. Walweel, K. & Laver, D. R. Mechanisms of SR calcium release in healthy and failing human hearts. *Biophys Rev* **7,** 33–41 (2015).

163. Chen, C., Li, R., Ross, R. S. & Manso, A. M. Integrins and integrin-related proteins in cardiac fibrosis. *J Mol Cell Cardiol* **93,** 162–74 (2016).

164. Bianchi, E., Denti, S., Granata, A., Bossi, G., Geginat, J., Villa, A., Rogge, L. & Pardi, R. Integrin LFA-1 interacts with the transcriptional co-activator JAB1 to modulate AP-1 activity. *Nature* **404,** 617–21 (2000).

165. Levinson, H., Sil, A. K., Conwell, J. E., Hopper, J. E. & Ehrlich, H. P. Alpha V integrin prolongs collagenase production through Jun activation binding protein 1. *Ann Plast Surg* **53,** 155–61 (2004).

166. O'Donnell, M. J., Xavier, D., Liu, L., Zhang, H., Chin, S. L., Rao-Melacini, P., Rangarajan, S., Islam, S., Pais, P., McQueen, M. J., Mondo, C., Damasceno, A., Lopez-Jaramillo, P., Hankey, G. J., Dans, A. L., Yusoff, K., Truelsen, T., Diener, H. C., Sacco, R. L., Ryglewicz, D., Czlonkowska, A., Weimar, C., Wang, X. & Yusuf, S. Risk factors for ischaemic and intracerebral haemorrhagic stroke in 22 countries (the INTERSTROKE study): a case-control study. *Lancet* **376,** 112–23 (2010).

167. Frangogiannis, N. G. Pathophysiology of Myocardial Infarction. *Compr Physiol* **5,** 1841–75 (2015).

168. Turtzo, L. C., Li, J., Persky, R., Benashski, S., Weston, G., Bucala, R., Venna, V. R. & McCullough, L. D. Deletion of macrophage migration inhibitory factor worsens stroke outcome in female mice. *Neurobiol Dis* **54,** 421–31 (2013).

169. Bernhagen, J., Calandra, T., Mitchell, R. A., Martin, S. B., Tracey, K. J., Voelter, W., Manogue, K. R., Cerami, A. & Bucala, R. MIF is a pituitary-derived cytokine that potentiates lethal endotoxaemia. *Nature* **365,** 756–9 (1993).

170. Schmitz, C., Noels, H., El Bounkari, O., Straussfeld, E., Megens, R. T. A., Sternkopf, M., Alampour-Rajabi, S., Krammer, C., Tilstam, P. V., Gerdes, N., Bürger, C., Kapurniotu, A., Bucala, R., Jankowski, J., Weber, C. & Bernhagen, J. Mif-deficiency favors an atheroprotective autoantibody phenotype in atherosclerosis. *FASEB J* **32,** 4428–4443 (2018).

171. Ritzel, R. M., Capozzi, L. A. & McCullough, L. D. Sex, stroke, and inflammation: the potential for estrogen-mediated immunoprotection in stroke. *Horm Behav* **63,** 238–53 (2013).

172. Chauchereau, A., Georgiakaki, M., Perrin-Wolff, M., Milgrom, E. & Loosfelt, H. JAB1 interacts with both the progesterone receptor and SRC-1. *J Biol Chem* **275,** 8540–8 (2000).

173. Hallstrom, T. C. & Nevins, J. R. Jab1 is a specificity factor for E2F1-induced apoptosis. *Genes Dev* **20,** 613–23 (2006).

174. Liu, X., Pan, Z., Zhang, L., Sun, Q., Wan, J., Tian, C., Xing, G., Yang, J., Liu, X., Jiang, J. & He, F. JAB1 accelerates mitochondrial apoptosis by interaction with proapoptotic BclGs. *Cell Signal* **20,** 230–40 (2008).

175. Wacker, B. K., Perfater, J. L. & Gidday, J. M. Hypoxic preconditioning induces stroke tolerance in mice via a cascading HIF, sphingosine kinase, and CCL2 signaling pathway. *J Neurochem* **123,** 954–62 (Dec. 2012).

176. Khoury, J., Ibla, J. C., Neish, A. S. & Colgan, S. P. Antiinflammatory adaptation to hypoxia through adenosine-mediated cullin-1 deneddylation. *J Clin Invest* **117,** 703–11 (2007).

177. Zhang, J., Cui, J., Zhao, F., Yang, L., Xu, X., Shi, Y. & Wei, B. Cardioprotective effect of MLN4924 on ameliorating autophagic flux impairment in myocardial ischemia-reperfusion injury by Sirt1. *Redox Biol* **46,** 102114 (Oct. 2021).

178. Andérica-Romero, A. C., Hernández-Damián, J., Vázquez-Cervantes, G. I., Torres, I. & Pedraza-Chaverri, J. The MLN4924 inhibitor exerts a neuroprotective effect against oxidative stress injury via Nrf2 protein accumulation. *Redox Biol* **8,** 341–347 (2016).

179. Yu, H., Luo, H., Chang, L., Kang, L., Cao, Y., Wang, R., Yang, X., Zhu, Y., Shi, M.-J., Hu, Y., Liu, Z., Yin, X., Ran, Y., Yang, H., Fan, W. & Zhao, B. Neddylation inhibition protects against ischemic brain injury. *Proc Natl Acad Sci U S A* **119** (2022).

180. Ehrentraut, S. F., Kominsky, D. J., Glover, L. E., Campbell, E. L., Kelly, C. J., Bowers, B. E., Bayless, A. J. & Colgan, S. P. Central role for endothelial human deneddylase-1/SENP8 in fine-tuning the vascular inflammatory response. *J Immunol* **190,** 392–400 (2013).

181. Williams, A. J., Dave, J. R. & Tortella, F. C. Neuroprotection with the proteasome inhibitor MLN519 in focal ischemic brain injury: relation to nuclear factor κB (NF-κB), inflammatory gene expression, and leukocyte infiltration. *Neurochem Int* **49,** 106–112 (2006).

182. Williams, A. J., Myers, T. M., Cohn, S. I., Sharrow, K. M., Lu, X.-C. M. & Tortella, F. C. Recovery from ischemic brain injury in the rat following a 10 h delayed injection with MLN519. *Pharmacol Biochem Behav* **81,** 182–189 (2005).

183. Williams, A. J., Hale, S. L., Moffett, J. R., Dave, J. R., Elliott, P. J., Adams, J. & Tortella, F. C. Delayed treatment with MLN519 reduces infarction and associated neurologic deficit caused by focal ischemic brain injury in rats via antiinflammatory mechanisms involving nuclear factor-κB activation, gliosis, and leukocyte infiltration. *J Cereb Blood Flow Metab* **23,** 75–87 (2003).

184. Phillips, J. B., Williams, A. J., Adams, J., Elliott, P. J. & Tortella, F. C. Proteasome inhibitor PS519 reduces infarction and attenuates leukocyte infiltration in a rat model of focal cerebral ischemia. *Stroke* **31,** 1686–1693 (2000).

185. Berti, R., Williams, A., Velarde, L., Moffett, J., Elliott, P., Adams, J., Yao, C., Dave, J. & Tortella, F. Effect of the proteasome inhibitor MLN519 on the expression of inflammatory molecules following middle cerebral artery occlusion and reperfusion in the rat. *Neurotox Res* **5,** 505–514 (2003).

186. Milic, J., Tian, Y. & Bernhagen, J. Role of the COP9 Signalosome (CSN) in cardiovascular diseases. *Biomolecules* **9,** 217 (2019).

187. Wimo, A., Winblad, B. & Jönsson, L. The worldwide societal costs of dementia: Estimates for 2009. *Alzheimers Dement* **6,** 98–103 (2010).

188. Selkoe, D. J. Alzheimer's disease is a synaptic failure. *Science* **298,** 789–791 (2002).

189. Haass, C., Kaether, C., Thinakaran, G. & Sisodia, S. Trafficking and proteolytic processing of APP. *Cold Spring Harb Perspect Med* **2,** a006270 (2012).

190. Wang, H., Dey, D., Carrera, I., Minond, D., Bianchi, E., Xu, S. & Lakshmana, M. K. COPS5 (Jab1) protein increases β site processing of amyloid precursor protein and amyloid β peptide generation by stabilizing RanBP9 protein levels. *J Biol Chem* **288,** 26668–26677 (2013).

191. Wang, R., Wang, H., Carrera, I., Xu, S. & Lakshmana, M. K. COPS5 protein overexpression increases amyloid plaque burden, decreases Spinophilin-immunoreactive Puncta, and exacerbates learning and memory deficits in the mouse brain. *J Biol Chem* **290,** 9299–9309 (2015).

192. Oono, K., Yoneda, T., Manabe, T., Yamagishi, S., Matsuda, S., Hitomi, J., Miyata, S., Mizuno, T., Imaizumi, K., Katayama, T. & Tohyama, M. JAB1 participates in unfolded protein responses by association and dissociation with IRE1. *Neurochem Int* **45,** 765–772 (2004).

193. Paschen, W. Endoplasmic reticulum: a primary target in various acute disorders and degenerative diseases of the brain. *Cell Calcium* **34,** 365–383 (2003).

194. Huang, Y.-T., Iwamoto, K., Kurosaki, T., Nasu, M. & Ueda, S. The neuronal POU transcription factor Brn-2 interacts with Jab1, a gene involved in the onset of neurodegenerative diseases. *Neurosci Lett* **382,** 175–178 (2005).

195. Oddo, S. The ubiquitin-proteasome system in Alzheimer's disease. *J Cell Mol Med* **12,** 363–373 (2008).

196. Chen, Y., Neve, R. L. & Liu, H. Neddylation dysfunction in Alzheimer's disease. *J Cell Mol Med* **16,** 2583–2591 (2012).

197. Stoppini, L., Buchs, P.-A. & Muller, D. A simple method for organotypic cultures of nervous tissue. *J Neurosci Methods* **37,** 173–182 (1991).

198. Safaiyan, S., Besson-Girard, S., Kaya, T., Cantuti-Castelvetri, L., Liu, L., Ji, H., Schifferer, M., Gouna, G., Usifo, F., Kannaiyan, N., Fitzner, D., Xiang, X., Rossner, M., Brendel, M., Gokce, O. & Simons, M. White matter aging drives microglial diversity. *Neuron* **109,** 1100–1117 (2021).

199. Loo, L., Simon, J. M., Xing, L., McCoy, E. S., Niehaus, J. K., Guo, J., Anton, E. & Zylka, M. J. Single-cell transcriptomic analysis of mouse neocortical development. *Nat Commun* **10,** 1–11 (2019).

200. Van Hove, H., Martens, L., Scheyltjens, I., De Vlaminck, K., Antunes, A. R. P., De Prijck, S., Vandamme, N., De Schepper, S., Van Isterdael, G., Scott, C. L., Aerts, J., Berx, G., Boeckxstaens, G., Vandenbroucke, R., Vereecke, L., Moechars, D., Guilliams, M., Van Ginderachter, J., Saeys, Y. & Movahedi, K. A single-cell atlas of mouse brain macrophages reveals unique transcriptional identities shaped by ontogeny and tissue environment. *Nat Neurosci* **22,** 1021–1035 (2019).

201. Shemer, A., Scheyltjens, I., Frumer, G. R., Kim, J.-S., Grozovski, J., Ayanaw, S., Dassa, B., Van Hove, H., Chappell-Maor, L., Boura-Halfon, S., Leshkowitz, D., Mueller, W., Maggio, N., Movahedi, K. & Jung, S. Interleukin-10 prevents pathological microglia hyperactivation following peripheral endotoxin challenge. *Immunity* **53,** 1033–1049 (2020).

202. Brown, G. C. & Neher, J. J. Microglial phagocytosis of live neurons. *Nat Rev Neurosci* **15,** 209–216 (2014).

203. Neniskyte, U., Vilalta, A. & Brown, G. C. Tumour necrosis factor alpha-induced neuronal loss is mediated by microglial phagocytosis. *FEBS Lett* **588,** 2952–2956 (2014).

204. Neumann, H., Kotter, M. & Franklin, R. Debris clearance by microglia: an essential link between degeneration and regeneration. *Brain* **132,** 288–295 (2009).

205. Enchev, R. I., Schulman, B. A. & Peter, M. Protein neddylation: beyond cullin–RING ligases. *Nat Rev Mol Cell Biol* **16,** 30–44 (2015).

206. Soucy, T. A., Smith, P. G., Milhollen, M. A., Berger, A. J., Gavin, J. M., Adhikari, S., Brownell, J. E., Burke, K. E., Cardin, D. P., Critchley, S., Cullis, C., Doucette, A., Garnsey, J., Gaulin, J., Gershman, R., Lublinsky, A., McDonald, A., Mizutani, H., Narayanan, U., Olhava, E., Peluso, S., Rezaei, M., Sintchak, M., Talreja, T., Thomas, M., Traore, T., Vyskocil, S., Weatherhead, G., Yu, J., Zhang, J., Dick, L., Claiborne, C., Rolfe, M., Bolen, J. & SP, L. An inhibitor of NEDD8-activating enzyme as a new approach to treat cancer. *Nature* **458,** 732–736 (2009).

207. Zhou, L., Zhang, W., Sun, Y. & Jia, L. Protein neddylation and its alterations in human cancers for targeted therapy. *Cell Signal* **44,** 92–102 (2018).

208. Swords, R. T., Coutre, S., Maris, M. B., Zeidner, J. F., Foran, J. M., Cruz, J., Erba, H. P., Berdeja, J. G., Tam, W., Vardhanabhuti, S., Pawlikowska-Dobler, I., Faessel, H., Dash, A., Sedarati, F., Dezube, B., Faller, D. & Savona, M. Pevonedistat, a first-in-class NEDD8-activating enzyme inhibitor, combined with azacitidine in patients with AML. *Blood* **131,** 1415–1424 (2018).

209. Rangaraju, S., Raza, S. A., Li, N. X., Betarbet, R., Dammer, E. B., Duong, D., Lah, J. J., Seyfried, N. T. & Levey, A. I. Differential phagocytic properties of CD45low microglia and CD45high brain mononuclear phagocytes—activation and age-related effects. *Front Immunol* **9,** 405 (2018).

210. Karin, M. & Ben-Neriah, Y. Phosphorylation meets ubiquitination: the control of NF-κB activity. *Annu Rev Immunol* **18,** 621–663 (2000).

211. Liu, T., Zhang, L., Joo, D. & Sun, S.-C. NF-κB signaling in inflammation. *Signal Transduct Target Ther* **2,** 1–9 (2017).

212. Bonizzi, G. & Karin, M. The two NF-κB activation pathways and their role in innate and adaptive immunity. *Trends Immunol* **25,** 280–288 (2004).

213. Bachstetter, A. D., Xing, B., de Almeida, L., Dimayuga, E. R., Watterson, D. M. & Van Eldik, L. J. Microglial p38α MAPK is a key regulator of proinflammatory cytokine up-regulation induced by toll-like receptor (TLR) ligands or beta-amyloid (Aβ). *J Neuroinflammation* **8,** 1–12 (2011).

214. Kim, S. H., Smith, C. J. & Van Eldik, L. J. Importance of MAPK pathways for microglial pro-inflammatory cytokine IL-1β production. *Neurobiol Aging* **25,** 431–439 (2004).

215. Saponaro, C., Cianciulli, A., Calvello, R., Dragone, T., Iacobazzi, F. & Panaro, M. A. The PI3K/Akt pathway is required for LPS activation of microglial cells. *Immunopharmacol Immunotoxicol* **34,** 858–865 (2012).

216. Cianciulli, A., Porro, C., Calvello, R., Trotta, T., Lofrumento, D. D. & Panaro, M. A. Microglia mediated neuroinflammation: Focus on PI3K modulation. *Biomolecules* **10,** 137 (2020).

217. Boyle, D. L., Jones, T. L., Hammaker, D., Svensson, C. I., Rosengren, S., Albani, S., Sorkin, L. & Firestein, G. S. Regulation of peripheral inflammation by spinal p38 MAP kinase in rats. *PLoS Med* **3,** e338 (2006).

218. Chin, Y. R. & Toker, A. Function of Akt/PKB signaling to cell motility, invasion and the tumor stroma in cancer. *Cell Signal* **21,** 470–476 (2009).

219. Madry, C. & Attwell, D. Receptors, ion channels, and signaling mechanisms underlying microglial dynamics. *J Biol Chem* **290,** 12443–12450 (2015).

220. Jiang, X., Andjelkovic, A. V., Zhu, L., Yang, T., Bennett, M. V., Chen, J., Keep, R. F. & Shi, Y. Blood-brain barrier dysfunction and recovery after ischemic stroke. *Prog Neurobiol* **163,** 144–171 (2018).

221. Cai, Z., Hussain, M. D. & Yan, L.-J. Microglia, neuroinflammation, and beta-amyloid protein in Alzheimer's disease. *Int J Neurosci* **124,** 307–321 (2014).

222. Scott, D. C., Hammill, J. T., Min, J., Rhee, D. Y., Connelly, M., Sviderskiy, V. O., Bhasin, D., Chen, Y., Ong, S.-S., Chai, S. C., Goktug, A., Huang, G., Monda, J., Low, J., Kim, H., Paulo, J., Cannon, J., Shelat, A., Chen, T., Kelsall, I., Alpi, A., Pagala, V., Wang, X., Peng, J., Singh, B., Harper, J., Schulman, B. & Guy, R. Blocking an N-terminal acetylation–dependent protein interaction inhibits an E3 ligase. *Nat Chem Biol* **13,** 850–857 (2017).

223. Lykke-Andersen, K., Schaefer, L., Menon, S., Deng, X.-W., Miller, J. B. & Wei, N. Disruption of the COP9 signalosome Csn2 subunit in mice causes deficient cell proliferation, accumulation of p53 and cyclin E, and early embryonic death. *Mol Cell Biol* **23,** 6790–6797 (2003).

224. Yan, J., Walz, K., Nakamura, H., Carattini-Rivera, S., Zhao, Q., Vogel, H., Wei, N., Justice, M. J., Bradley, A. & Lupski, J. R. COP9 signalosome subunit 3 is essential for maintenance of cell proliferation in the mouse embryonic epiblast. *Mol Cell Biol* **23,** 6798–6808 (2003).

225. Tomoda, K., Yoneda-Kato, N., Fukumoto, A., Yamanaka, S. & Kato, J.-y. Multiple functions of Jab1 are required for early embryonic development and growth potential in mice. *J Biol Chem* **279,** 43013–43018 (2004).

226. Menon, S., Chi, H., Zhang, H., Deng, X. W., Flavell, R. A. & Wei, N. COP9 signalosome subunit 8 is essential for peripheral T cell homeostasis and antigen receptor–induced entry into the cell cycle from quiescence. *Nat Immunol* **8,** 1236–1245 (2007).

227. Lykke-Andersen, K. & Wei, N. Gene structure and embryonic expression of mouse COP9 signalosome subunit 8 (Csn8). *Gene* **321,** 65–72 (2003).

228. Forozan, F., Mahlamäki, E. H., Monni, O., Chen, Y., Veldman, R., Jiang, Y., Gooden, G. C., Ethier, S. P., Kallioniemi, A. & Kallioniemi, O.-P. Comparative genomic hybridization analysis of 38 breast cancer cell lines: a basis for interpreting complementary DNA microarray data. *Cancer Res* **60,** 4519–4525 (2000).

229. Hou, J., Deng, Q., Zhou, J., Zou, J., Zhang, Y., Tan, P., Zhang, W. & Cui, H. CSN6 controls the proliferation and metastasis of glioblastoma by CHIP-mediated degradation of EGFR. *Oncogene* **36,** 1134–1144 (2017).

230. Lee, Y.-H., Judge, A., Seo, D., Kitade, M., Gomez-Quiroz, L., Ishikawa, T., Andersen, J. B., Kim, B., Marquardt, J., Raggi, C., Avital, I., Conner, E., MacLachlan, I., Factor, V. & Thorgeirsson, S. Molecular targeting of CSN5 in human hepatocellular carcinoma: a mechanism of therapeutic response. *Oncogene* **30,** 4175–4184 (2011).

231. Sui, L., Dong, Y., Ohno, M., Watanabe, Y., Sugimoto, K., Tai, Y. & Tokuda, M. Jab1 expression is associated with inverse expression of p27kip1 and poor prognosis in epithelial ovarian tumors. *Clin Cancer Res* **7,** 4130–4135 (2001).

232. Solinas-Toldo, S., Wallrapp, C., Müller-Pillasch, F., Bentz, M., Gress, T. & Lichter, P. Mapping of chromosomal imbalances in pancreatic carcinoma by comparative genomic hybridization. *Cancer Res* **56,** 3803–3807 (1996).

233. Koussounadis, A., Langdon, S. P., Um, I. H., Harrison, D. J. & Smith, V. A. Relationship between differentially expressed mRNA and mRNA-protein correlations in a xenograft model system. *Sci Rep* **5,** 1–9 (2015).

234. Vogel, C. & Marcotte, E. M. Insights into the regulation of protein abundance from proteomic and transcriptomic analyses. *Nat Rev Genet* **13,** 227–232 (2012).

235. Richardson, K. S. & Zundel, W. The emerging role of the COP9 signalosome in cancer. *Mol Cancer Res* **3,** 645–653 (2005).

236. Lee, M.-H., Zhao, R., Phan, L. & Yeung, S.-C. J. Roles of COP9 signalosome in cancer. *Cell Cycle* **10,** 3057–3066 (2011).

237. Liu, G., Claret, F. X., Zhou, F. & Pan, Y. Jab1/COPS5 as a novel biomarker for diagnosis, prognosis, therapy prediction and therapeutic tools for human cancer. *Front Pharmacol* **9,** 135 (2018).

238. Oladghaffari, M., Islamian, J. P., Baradaran, B. & Monfared, A. S. MLN4924 therapy as a novel approach in cancer treatment modalities. *J Chemother* **28,** 74–82 (2016).

239. Schlierf, A., Altmann, E., Quancard, J., Jefferson, A. B., Assenberg, R., Renatus, M., Jones, M., Hassiepen, U., Schaefer, M., Kiffe, M., Weiss, A., Wiesmann, C., Sedrani, R., Eder, J. & Martoglio, B. Targeted inhibition of the COP9 signalosome for treatment of cancer. *Nat Commun* **7,** 1–10 (2016).

240. Su, H., Li, J., Menon, S., Liu, J., Kumarapeli, A. R., Wei, N. & Wang, X. Perturbation of cullin deneddylation via conditional Csn8 ablation impairs the ubiquitin–proteasome system and causes cardiomyocyte necrosis and dilated cardiomyopathy in mice. *Circ Res* **108,** 40–50 (2011).

241. Galloway, D. A., Phillips, A. E., Owen, D. R. & Moore, C. S. Phagocytosis in the brain: homeostasis and disease. *Front Immunol* **10,** 790 (2019).

242. Lambertsen, K. L., Biber, K. & Finsen, B. Inflammatory cytokines in experimental and human stroke. *J Cereb Blood Flow Metab* **32,** 1677–1698 (2012).

243. Shi, J., Li, W., Zhang, F., Park, J. H., An, H., Guo, S., Duan, Y., Wu, D., Hayakawa, K., Lo, E. H. & Ji, X. CCL2 (CC Motif Chemokine Ligand 2) Biomarker Responses in Central Versus Peripheral Compartments After Focal Cerebral Ischemia. *Stroke* **52,** 3670–3679 (2021).

244. Kinsner, A., Pilotto, V., Deininger, S., Brown, G. C., Coecke, S., Hartung, T. & Bal-Price, A. Inflammatory neurodegeneration induced by lipoteichoic acid from Staphylococcus aureus is mediated by glia activation, nitrosative and oxidative stress, and caspase activation. *J Neurochem* **95,** 1132–1143 (2005).

245. Neher, J. J., Neniskyte, U., Zhao, J.-W., Bal-Price, A., Tolkovsky, A. M. & Brown, G. C. Inhibition of microglial phagocytosis is sufficient to prevent inflammatory neuronal death. *J Immunol* **186,** 4973–4983 (2011).

246. Silva, E., Au-Yeung, H. W., Van Goethem, E., Burden, J. & Franc, N. C. Requirement for a Drosophila E3-ubiquitin ligase in phagocytosis of apoptotic cells. *Immunity* **27,** 585–596 (2007).

247. Stansley, B., Post, J. & Hensley, K. A comparative review of cell culture systems for the study of microglial biology in Alzheimer's disease. *J Neuroinflammation* **9,** 1–8 (2012).

248. Giulian, D. & Baker, T. J. Characterization of ameboid microglia isolated from developing mammalian brain. *J Neurosci* **6,** 2163–2178 (1986).

249. Takata, K., Kitamura, Y., Saeki, M., Terada, M., Kagitani, S., Kitamura, R., Fujikawa, Y., Maelicke, A., Tomimoto, H., Taniguchi, T. & Shimohama, S. Galantamine-induced amyloid-β clearance mediated via stimulation of microglial nicotinic acetylcholine receptors. *J Biol Chem* **285,** 40180–40191 (2010).

250. Henkel, J. S., Beers, D. R., Zhao, W. & Appel, S. H. Microglia in ALS: the good, the bad, and the resting. *J Neuroimmune Pharmacol* **4,** 389–398 (2009).

251. Blasi, E., Barluzzi, R., Bocchini, V., Mazzolla, R. & Bistoni, F. Immortalization of murine microglial cells by a v-raf/v-myc carrying retrovirus. *J Neuroimmunol* **27,** 229–237 (1990).

252. Henn, A., Lund, S., Hedtjärn, M., Schrattenholz, A., Pörzgen, P. & Leist, M. The suitability of BV2 cells as alternative model system for primary microglia cultures or for animal experiments examining brain inflammation. *ALTEX* **26,** 83–94 (2009).

253. Zhang, H., Jia, L. & Jia, J. Oxiracetam offers neuroprotection by reducing amyloid β-induced microglial activation and inflammation in alzheimer's disease. *Front Neurol,* 623 (2020).

254. Xu, J., Yu, T., Pietronigro, E. C., Yuan, J., Arioli, J., Pei, Y., Luo, X., Ye, J., Constantin, G., Mao, C. & Xiao, Y. Peli1 impairs microglial Aβ phagocytosis through promoting C/EBPβ degradation. *PLoS Biol* **18,** e3000837 (2020).

255. Yli-Karjanmaa, M., Clausen, B. H., Degn, M., Novrup, H. G., Ellman, D. G., Toft-Jensen, P., Szymkowski, D. E., Stensballe, A., Meyer, M., Brambilla, R. & Lambertsen, K. Topical administration of a soluble TNF inhibitor reduces infarct volume after focal cerebral ischemia in mice. *Front Neurosci,* 781 (2019).

256. Oeckinghaus, A. & Ghosh, S. The NF-κB family of transcription factors and its regulation. *Cold Spring Harb Perspect Biol* **1,** a000034 (2009).

257. Liu, T., Zhang, L., Joo, D. & Sun, S.-C. NF- $\varkappa$ B signaling in inflammation. *Signal Transduct Target Ther* **2,** 17023 (2017).

258. Panattoni, M., Sanvito, F., Basso, V., Doglioni, C., Casorati, G., Montini, E., Bender, J. R., Mondino, A. & Pardi, R. Targeted inactivation of the COP9 signalosome impairs multiple stagesof T cell development. *J Exp Med* **205,** 465–477 (2008).

259. Terai, K., Matsuo, A., McGeer, E. G. & McGeer, P. L. Enhancement of immunoreactivity for NF-κB in human cerebral infarctions. *Brain Res* **739,** 343–349 (1996).

260. Cho, I.-H., Hong, J., Suh, E. C., Kim, J. H., Lee, H., Lee, J. E., Lee, S., Kim, C.-H., Kim, D. W., Jo, E.-K., Lee, K., Karin, M. & Lee, S. Role of microglial IKKβ in kainic acid-induced hippocampal neuronal cell death. *Brain* **131,** 3019–3033 (2008).

261. Schweitzer, K., Bozko, P. M., Dubiel, W. & Naumann, M. CSN controls NF-κB by deubiquitinylation of IκBα. *EMBO J* **26,** 1532–1541 (2007).

262. Deng, Q., Zhang, J., Gao, Y., She, X., Wang, Y., Wang, Y. & Ge, X. MLN4924 protects against bleomycin-induced pulmonary fibrosis by inhibiting the early inflammatory process. *Am J Transl Res* **9,** 1810 (2017).

263. Mao, H., Tang, Z., Li, H., Sun, B., Tan, M., Fan, S., Zhu, Y. & Sun, Y. Neddylation inhibitor MLN4924 suppresses cilia formation by modulating AKT1. *Protein Cell* **10,** 726–744 (2019).

264. Zhao, Y., Xiong, X., Jia, L. & Sun, Y. Targeting Cullin-RING ligases by MLN4924 induces autophagy via modulating the HIF1-REDD1-TSC1-mTORC1-DEPTOR axis. *Cell Death Dis* **3,** e386–e386 (2012).

265. Zhou, X., Tan, M., Nyati, M. K., Zhao, Y., Wang, G. & Sun, Y. Blockage of neddylation modification stimulates tumor sphere formation in vitro and stem cell differentiation and wound healing in vivo. *Proc Natl Acad Sci U S A* **113,** E2935–E2944 (2016).

266. Zhou, Q., Li, H., Li, Y., Tan, M., Fan, S., Cao, C., Meng, F., Zhu, L., Zhao, L., Guan, M.-X., Jin, H. & Sun, Y. Inhibiting neddylation modification alters mitochondrial morphology and reprograms energy metabolism in cancer cells. *JCI Insight* **4** (2019).

267. Hao, R., Song, Y., Li, R., Wu, Y., Yang, X., Li, X., Qian, F., Ye, R. D. & Sun, L. MLN4924 protects against interleukin-17A-induced pulmonary inflammation by disrupting ACT1-mediated signaling. *Am J Physiol Lung Cell Mol Physiol* **316,** L1070–L1080 (2019).

268. Song, H., Huai, W., Yu, Z., Wang, W., Zhao, J., Zhang, L. & Zhao, W. MLN4924, a first-in-class NEDD8-activating enzyme inhibitor, attenuates IFN-β production. *J Immunol* **196,** 3117–3123 (2016).

269. Zhao, L., Yue, P., Lonial, S., Khuri, F. R. & Sun, S.-Y. The NEDD8-activating enzyme inhibitor, MLN4924, cooperates with TRAIL to augment apoptosis through facilitating c-FLIP degradation in head and neck cancer cells. *Mol Cancer Ther* **10,** 2415–2425 (2011).

270. Lo, E. H., Dalkara, T. & Moskowitz, M. A. Mechanisms, challenges and opportunities in stroke. *Nat Rev Neurosci* **4,** 399–414 (2003).

271. Weksler, B., Subileau, E., Perriere, N., Charneau, P., Holloway, K., Leveque, M., Tricoire-Leignel, H., Nicotra, A., Bourdoulous, S., Turowski, P., Male, D., Roux, F., Greenwood, J., Romero, I. & Couraud, P. Blood-brain barrier-specific properties of a human adult brain endothelial cell line. *FASEB J* **19,** 1872–1874 (2005).

272. Weksler, B., Romero, I. A. & Couraud, P.-O. The hCMEC/D3 cell line as a model of the human blood brain barrier. *Fluids Barriers CNS* **10,** 1–10 (2013).

273. Poller, B., Gutmann, H., Krähenbühl, S., Weksler, B., Romero, I., Couraud, P.-O., Tuffin, G., Drewe, J. & Huwyler, J. The human brain endothelial cell line hCMEC/D3 as a human blood-brain barrier model for drug transport studies. *J Neurochem* **107,** 1358–1368 (2008).

274. Butt, A. M., Jones, H. C. & Abbott, N. J. Electrical resistance across the blood-brain barrier in anaesthetized rats: a developmental study. *J Physiol* **429,** 47–62 (1990).

275. Kovačević, I., Sakaue, T., Majoleé, J., Pronk, M. C., Maekawa, M., Geerts, D., Fernandez-Borja, M., Higashiyama, S. & Hordijk, P. L. The Cullin-3–Rbx1–KCTD10 complex controls endothelial barrier function via K63 ubiquitination of RhoB. *J Cell Biol* **217,** 1015–1032 (2018).

276. Sakaue, T., Fujisaki, A., Nakayama, H., Maekawa, M., Hiyoshi, H., Kubota, E., Joh, T., Izutani, H. & Higashiyama, S. Neddylated Cullin 3 is required for vascular endothelial-cadherin-mediated endothelial barrier function. *Cancer Sci* **108,** 208–215 (2017).

277. Xu, J., Li, L., Yu, G., Ying, W., Gao, Q., Zhang, W., Li, X., Ding, C., Jiang, Y., Wei, D., Duan, S., Lei, Q., Li, P., Shi, T., Qian, X., Qin, J. & Jia, L. The Neddylation-Cullin 2-RBX1 E3 Ligase Axis Targets Tumor Suppressor RhoB for Degradation in Liver Cancer. *Mol Cell Proteomics* **14,** 499–509 (2015).

278. Pandey, D., Hori, D., Kim, J. H., Bergman, Y., Berkowitz, D. E. & Romer, L. H. NEDDylation promotes endothelial dysfunction: a role for HDAC2. *J Mol Cell Cardiol* **81,** 18–22 (2015).

279. Khatri, R., McKinney, A. M., Swenson, B. & Janardhan, V. Blood–brain barrier, reperfusion injury, and hemorrhagic transformation in acute ischemic stroke. *Neurology* **79,** S52–S57 (2012).

280. Shi, Y., Zhang, L., Pu, H., Mao, L., Hu, X., Jiang, X., Xu, N., Stetler, R. A., Zhang, F., Liu, X., Leak, R., Keep, R., Ji, X. & Chen, J. Rapid endothelial cytoskeletal reorganization enables early blood–brain barrier disruption and long-term ischaemic reperfusion brain injury. *Nat Commun* **7,** 1–18 (2016).

281. Sahu, M. P., Nikkilä, O., Lågas, S., Kolehmainen, S. & Castrén, E. Culturing primary neurons from rat hippocampus and cortex. *Neuronal Signal* **3** (2019).

282. Gordon, J. & Amini, S. General overview of neuronal cell culture. *Methods Mol Biol,* 1–8 (2021).

283. Allen, C. L. & Bayraktutan, U. Oxidative stress and its role in the pathogenesis of ischaemic stroke. *Int J Stroke* **4,** 461–470 (2009).

284. Zhao, L.-P., Ji, C., Lu, P.-H., Li, C., Xu, B. & Gao, H. Oxygen glucose deprivation (OGD)/re-oxygenation-induced in vitro neuronal cell death involves mitochondrial cyclophilin-D/P53 signaling axis. *Neurochem Res* **38,** 705–713 (2013).

285. Xu, S., Li, Y., Chen, J.-p., Li, D.-Z., Jiang, Q., Wu, T. & Zhou, X.-z. Oxygen glucose deprivation/re-oxygenation-induced neuronal cell death is associated with Lnc-D63785 m6A methylation and miR-422a accumulation. *Cell Death Dis* **11,** 1–12 (2020).

286. Niture, S. K., Khatri, R. & Jaiswal, A. K. Regulation of Nrf2—an update. *Free Radic Biol Med* **66,** 36–44 (2014).

287. Zhang, R., Xu, M., Wang, Y., Xie, F., Zhang, G. & Qin, X. Nrf2—a promising therapeutic target for defensing against oxidative stress in stroke. *Mol Neurobiol* **54,** 6006–6017 (2017).

288. Rada, P., Rojo, A. I., Chowdhry, S., McMahon, M., Hayes, J. D. & Cuadrado, A. SCF/β-TrCP promotes glycogen synthase kinase 3-dependent degradation of the Nrf2 transcription factor in a Keap1-independent manner. *Mol Cell Biol* **31,** 1121–1133 (2011).

289. Baird, L. & Yamamoto, M. The molecular mechanisms regulating the KEAP1-NRF2 pathway. *Mol Cell Biol* **40,** e00099–20 (2020).

290. Cho, S., Wood, A. & Bowlby, M. R. Brain slices as models for neurodegenerative disease and screening platforms to identify novel therapeutics. *Curr Neuropharmacol* **5,** 19–33 (2007).

291. Cho, S., Liu, D., Fairman, D., Li, P., Jenkins, L., McGonigle, P. & Wood, A. Spatiotemporal evidence of apoptosis-mediated ischemic injury in organotypic hippocampal slice cultures. *Neurochem Int* **45,** 117–127 (2004).

292. Ray, A. M., Owen, D. E., Evans, M. L., Davis, J. B. & Benham, C. D. Caspase inhibitors are functionally neuroprotective against oxygen glucose deprivation induced CA1 death in rat organotypic hippocampal slices. *Brain Res* **867,** 62–69 (2000).

293. Hua, W., Li, C., Yang, Z., Li, L., Jiang, Y., Yu, G., Zhu, W., Liu, Z., Duan, S., Chu, Y., Yang, M., Zhang, Y., Mao, Y. & Jia, L. Suppression of glioblastoma by targeting the overactivated protein neddylation pathway. *Neuro Oncol* **17,** 1333–1343 (2015).

294. Pardridge, W. M. Drug transport across the blood–brain barrier. *J Cereb Blood Flow Metab* **32,** 1959–1972 (2012).

295. Liang, E., Li, X., Fu, W., Zhao, C., Yang, B. & Yang, Z. COP9 Signalosome Subunit 3 Restricts Neuroinflammatory Responses During Cerebral Ischemia/Reperfusion Injury Through Stabilizing Suppressor of Cytokine Signaling 3 Protein. *Neuropsychiatr Dis Treat* **17,** 1217 (2021).

296. Bongartz, T., Sutton, A. J., Sweeting, M. J., Buchan, I., Matteson, E. L. & Montori, V. Anti-TNF antibody therapy in rheumatoid arthritis and the risk of serious infections and malignancies: systematic review and meta-analysis of rare harmful effects in randomized controlled trials. *Jama* **295,** 2275–2285 (2006).

297. Aggarwal, B. B. Signalling pathways of the TNF superfamily: a double-edged sword. *Nat Rev Immunol* **3,** 745–756 (2003).

298. Mpofu, S., Fatima, F. & Moots, R. Anti-TNF-α therapies: they are all the same (aren't they?) *Rheumatology* **44,** 271–273 (2005).

299. Scallon, B., Cai, A., Solowski, N., Rosenberg, A., Song, X.-Y., Shealy, D. & Wagner, C. Binding and functional comparisons of two types of tumor necrosis factor antagonists. *J Pharmacol Exp Ther* **301,** 418–426 (2002).

300. Banner, D. W., D'Arcy, A., Janes, W., Gentz, R., Schoenfeld, H.-J., Broger, C., Loetscher, H. & Lesslauer, W. Crystal structure of the soluble human 55 kd TNF receptor-human TNFβ complex: implications for TNF receptor activation. *Cell* **73,** 431–445 (1993).

301. Mohler, K. M., Torrance, D., Smith, C., Goodwin, R., Stremler, K., Fung, V., Madani, H. & Widmer, M. Soluble tumor necrosis factor (TNF) receptors are effective therapeutic agents in lethal endotoxemia and function simultaneously as both TNF carriers and TNF antagonists. *J Immunol* **151,** 1548–1561 (1993).

302. Scallon, B. J., Moore, M. A., Trinh, H., Knight, D. M. & Ghrayeb, J. Chimeric anti-TNF-α monoclonal antibody cA2 binds recombinant transmembrane TNF-α and activates immune effector functions. *Cytokine* **7,** 251–259 (1995).

303. Bonetti, N., Diaz-Canestro, C., Liberale, L., Crucet, M., Akhmedov, A., Merlini, M., Reiner, M., Gobbato, S., Stivala, S., Kollias, G., Ruschitzka, F., Lüscher, T., Beer, J. & Camici, G. Tumour necrosis factor-α inhibition improves stroke outcome in a mouse model of rheumatoid arthritis. *Sci Rep* **9,** 1–11 (2019).

304. Clausen, B. H., Degn, M., Martin, N. A., Couch, Y., Karimi, L., Ormhøj, M., Mortensen, M.-L. B., Gredal, H. B., Gardiner, C., Sargent, I. I., Szymkowski, D., Petit, G., Deierborg, T., Finsen, B., Anthony, D. & Lambertsen, K. Systemically administered anti-TNF therapy ameliorates functional outcomes after focal cerebral ischemia. *J Neuroinflammation* **11,** 1–17 (2014).

305. Ravetch, J. Fcgamma receptors as regulators of immune responses. *Nat Rev Immunol* **8,** 34–47 (2008).

306. Zhang, S. Microglial activation after ischaemic stroke. *Stroke Vasc Neurol* **4** (2019).

307. Colonna, M. & Butovsky, O. Microglia function in the central nervous system during health and neurodegeneration. *Annu Rev Immunol* **35,** 441–468 (2017).

308. Nimmerjahn, A., Kirchhoff, F. & Helmchen, F. Resting microglial cells are highly dynamic surveillants of brain parenchyma in vivo. *Science* **308,** 1314–1318 (2005).

309. Heindl, S., Gesierich, B., Benakis, C., Llovera, G., Duering, M. & Liesz, A. Automated morphological analysis of microglia after stroke. *Front Cell Neurosci* **12,** 106 (2018).

Acknowledgements

Undertaking this Ph.D. has truly changed my life, and without all the support I have received from my supervisors, colleagues, friends and family, it would not be close to toward obtaining the degree successfully. I am extremely excited typing down the acknowledgements and have a huge debt of gratitude to express.

First and foremost, I would like to thank my direct supervisor Prof. Bernhagen for offering me the opportunity to pursue a Ph.D. in Germany, opening me the access to the world of research, and following this project with great interest while offering valuable ideas which guided me all over these four and a half years. His enthusiasm and genuinely love for science is and will always be an inspiration for me in the present and future. I am truly appreciate the incredible experiences I could not have imagined before starting to work here. The ”ZOMES” conference in the ancient fortresses with novel topics allowed me to meet all the best scientists in the field, ”Ubiquitin, Autophagy and Disease (virtual)” meeting lighted me up in the difficult lonely Covid-19 pandemic time.

I am sincerely grateful to my thesis advisory committee members Dr. Alpi and Prof. Behrends, for their continuous interest in the project, steering my work with constructive discussions. Not only the advice they offered, but also the novel DCN-1 inhibitors and antibodies which Prof. Schulman and Dr. Alpi provided me. Thank you so much for improving my project.

I am very much indebted to Dr. Tahirovic and Dr. Sebastian for their outstanding collaboration. Training me organotypic slice culture skills and sharing their passion for science made this thesis possible. Thank you for the help and discussions.

I also appreciate the working institute, Institute for Stroke and Dementia Research (ISD), LMU University Hospital. The director, Prof. Dichgans and other professors organize our ISD retreat and Christmas Party every year and Happy Hour every season, not only for sharing the scientific expertise abut also for organizing fun activities and building bridges between groups.
Many thanks to the MMRS team for selecting me for in an individual Ph.D. program, offering workshop advice and technical support.
I would also like to acknowledge the China Scholarship Council(CSC) and LMU-CSC for providing the three years financial support, offering a platform to meet compatriots as well as the fun and useful orientation program. Special thanks to Dr. Zhang from the international office for supporting, introducing and sharing experiences in Munich to us.

A warm thank you to all the members and former members in Prof. Bernhagen's lab and Dr. Özgün's lab. To Sabrina, for helping me with paper work, Visa and life advice. A big thanks to Markus, for introducing and trouble shooting programming problems of Latex, as well as offer the help with German summary of this thesis. To Omar, Priscila, Jelena, Dzmitry, Lisa, Christine, Marlies, Laura, Simon, Fumi, Buket for helping with the start of the Ph.D. and teaching me new methods. Special thanks to Sijia, for teaching me the neuronal culture and always sharing home-like-taste food with me. Without you, I would not have adapt to the life here that fast. To Chunfang, for being a great source of energy to encourage the writing this thesis. To Ying, Bishan, Lin, Hao and Lu, for our "China town corner" friendship. To all the colleagues, I really appreciate the Oktorbefest and nice evenings. You showed the lab is not only about professional collaborations, but also real friendship and fun.

Last but not least, I want to express my gratitude to my family and friends, for being patient and remaining understanding during these years over this far too far distance. To my friends in China, Shiyi Gao, Nan Yang, Guangning Fan, and others, for the friendship

and moral support oversea. Especially, thanks to them who crossed 8000km to visit me and delivered me masks when covid-19 broken down in Europe. To Lingyun Guo, for accompanying all the way along this Ph.D. in Germany, starting together, hopefully finishing together as well.

I am very grateful to Andreas Lüchinger, for enduring some stressful periods, enduring complaints and his trust in me. I would like to express my deepest and most heartfelt gratitude to my grandparents who inspired me to study medicine, and to my parents who always supported me on every perspective. Their love encouraged me to finish this thesis.

感谢所有家人对我的支持与鼓励。